Seismic vibration produced by wind turbines in the Eskdalemuir region

Release 2.0 of Substantial Research Project

Presented to FMB

Issue Date: 15/05/2014

Document No: FMB_203_FINAL_V5R

This report has been prepared by Xi Engineering Consultants Ltd with full cooperation and significant input from the Ministry of Defence. It has been prepared on behalf of, and under the guidance of, the Eskdalemuir Working Group, whose members are the Scottish Government (chair), the Ministry of Defence, UK Government's Department for Energy and Climate Change, Renewable UK, Scottish Renewables and the Aviation Investment Fund Company Ltd.

Xi Engineering Consultants Conference House, 152 Morrison Street, Edinburgh, EH3 8EB
T +44 (0)131 200 6170 **E** enquiries@xiengineering.com **xiengineering.com**

Registered address: Xi Engineering Consultants Ltd, 5th Floor, 125 Princes Street, Edinburgh, EH2 4AD, Company no. SC386913

Document Summary

Xi Engineering Consultants Ltd has conducted substantial analysis of the mechanisms and underlying physics of wind turbine seismic vibration propagation in line with the 'Eskdalemuir Working Group agreed scope for the substantial research Stage One - dated 16 August 2013'. The aim of this research is to re-examine the Styles Model which is used by the Ministry of Defence to safeguard the detection capabilities of the Eskdalemuir seismic array with respect to seismic vibration produced by wind turbines.

The research presented here builds on initial Phase 0 work (reported in Doc Ref FMB_102_TRP0_V6) which found that based on studies of Nordex N80 wind turbines there was the prospect for head room in the Eskdalemuir budget. This report supersedes Release 1.0 of Substantial Research Project (Final version released on 3/3/2014).

The work presented in this document is valid for a three bladed, up-wind, horizontal axis wind turbine mounted on a tubular steel tower with a gearbox transmission under normal operating conditions. On-tower and far-field seismic vibration data has been analysed from four turbine types, which vary in maximum production capacity from 0.66 MW to 2.5 MW systems. In analysing these turbines it has become apparent that the Nordex N80 is not representative of all the turbines within the Eskdalemuir Consultation zone. As the Phase 0 work calculated the budget headroom based on N80 turbines it can be confirmed that the Phase 0 calculated headroom no longer remains valid.

It has been found that the seismic vibrations produced by certain turbines are dominated by vibrations related to blade pass frequencies, whilst other turbines produce seismic vibrations related to their structural resonances. A physics-based algorithm was developed which was based on the conservation of energy approach in which seismic amplitude varied linearly with the swept area of the rotor and the cube of wind speed. The physics-based algorithm was fitted to empirical data from Craig, Clyde and Dun Law wind farms using a very conservative approach.

The utilisation factor used from the 2005 Styles model has been re-analysed using recent concurrent wind data sets for an 80 m hub height from 14 locations across the consultation zone. Based on the same principles as the 2005 budget, the analysis of this more recent data provides a revised utilisation factor of 82%. However as the approach to the algorithm has changed a utilisation factor of unity has been used until, and if, further work is conducted in this area.

The MoD released revised tables with all wind turbines which have been allocated budget and those subject to MoD objection up to and including the end of December 2013. The cumulative rms amplitude of the December 2013 MoD tables was calculated with the physics-based algorithm, frequency-distance weighting function and utilisation factor and found to be 0.1938325 nm. This figure is significantly less than the 0.336 nm threshold.

An assessment has been made of the developable land for wind turbines between 10 km and 50 km from the array. A method for understanding the physical implications of an exclusion zone has been developed, and different scenarios investigated.

Xi Engineering Consultants Ltd recommend that the 2005 model currently used by the MOD to safeguard Eskdalemuir seismic array be replaced by the physics-based algorithm presented in this report.

Matters relating to this document should be directed to:

Dr Mark-Paul Buckingham
Managing Director

E: mp@xiengineering.com
T: 0131 200 6171

Principal contacts at client's organisation

Tim French
Chair of Eskdalemuir Engineering Group, Fund Management Board subgroup

E: tim.french@res-ltd.com

Contents

1 Introduction 8
2 Technical background 9
2.1 Eskdalemuir seismic array 9
2.2 Previous studies 11
2.3 Ground vibration produced by wind turbines 13
3 Field survey 14
3.1 Introduction 14
3.2 Methodology 14
3.2.1 Dun Law wind farm 14
3.2.2 Craig wind farm 16
3.2.3 Clyde wind farm 18
3.2.4 St Seine-l'Abbaye wind farm 20
3.3 Data processing 22
3.3.1 Variations to the primary processing methodology 22
3.4 Statistical analysis 27
3.5 Results 28
3.5.1 Dunlaw 28
3.5.2 Craig wind farm 30
3.5.3 Clyde wind farm 36
3.5.4 St Seine-l'Abbaye 40
3.6 Azimuth effect 41
3.6.1 Dun Law 41
3.6.2 Craig wind farm 43
3.6.3 Clyde 44
3.7 Discussion 48
3.7.1 Comparison of far-field spectra from different wind turbines 48
3.7.2 Characterisation of far-field seismic vibrations 49
3.7.3 Relationship between on-tower and far-field seismic vibrations 49
3.7.4 Azimuth effect interpretation 50
4 Broadband operational noise 51
4.1 Introduction 51
4.2 Methodology 51
4.2.1 Craig wind farm 51
4.2.2 Clyde wind farm 53

4.3 Conclusion 55
5 Finite Element Analysis of seismic vibration produced by wind turbines 56
5.1 Introduction 56
5.2 Methodology 56
5.2.1 Geometry 56
5.2.2 Material properties 58
5.2.3 Meshing and time step optimisation 59
5.2.4 boundary conditions and loads 59
5.2.5 Variance model 61
5.3 Results 62
5.3.1 Near-field calibration 62
5.3.2 Far-field amplitude 63
5.3.3 Characterisation of ground waves 65
5.3.4 Variance models 67
5.4 Discussion 70
6 Utilisation factor 71
6.1 Revised utilisation factor 71
7 Conservation of energy approach 73
7.1 Introduction 73
7.2 Hypothesis 73
7.3 Test 73
7.4 Method 73
7.5 Results 74
7.6 Conclusion 76
8 A physics-based algorithm 77
8.1 Introduction 77
8.2 Methodology 77
8.2.1 Optimisation of reference worst-case turbine spectrum 77
8.3 The physics-based algorithm 79
8.3.1 Wind speed at hub height 79
8.3.2 Rotor speed variation with blade length 80
8.3.3 Frequency-distance weighting function for EKA 81
8.3.4 Sensitivity of calculated amplitude to site-specific parameters 81
8.4 Application of the physics-based algorithm 82
8.4.1 Calculation of cumulative seismic vibration at EKA 86
9 Analysis for size of exclusion zone 89
9.1 Introduction 89

9.2 Approach 89
9.3 Results and Worked Example 91
9.4 Discussion 93
10 Discussion 94
10.1 Generation of seismic vibrations by wind turbines 94
10.2 Conservatism in the physics-based algorithm 95
10.3 Implication of physics-based algorithms 95
10.4 Further work 96
11 Conclusions 96
12 Bibliography 98

Appendix A Sensor Calibrations 99
A.1 Dun Law Calibrations 99
A.2 Craig Calibrations 99
A.3 Clyde Calibrations 106
A.4 St Seine-L'Abbaye Equipment Specifications 114
A.4.1 Blue Geophone Calibration: 6073152 116
A.4.2 Green Geophone Calibration: 8020010 117
Appendix B Seismic Sensor Data 118
B.1 Dun Law Alpha vs. Wind Speed 118
B.2 Dun Law Beta vs. Wind Speed 121
B.3 Dun Law Gamma vs. Wind Speed 124
B.4 Dun Law Alpha, Beta, Gamma at 12 ms^{-1} Wind Speed 128
B.5 Craig Far-Field Alpha vs. Wind Speed 131
B.6 Craig Far-Field Beta vs. Wind Speed 134
B.7 Craig Far-Field Gamma vs. Wind Speed 137
B.8 Craig Far-Field Alpha, Beta, Gamma at 12 ms^{-1} Wind Speed 140
B.9 Craig Near-Field East vs. Wind Speed 143
B.10 Craig Near-Field North vs. Wind Speed 144
B.11 Craig Near-Field Vertical vs. Wind Speed 145
B.12 Craig Near-Field East, North, Vertical at 12 ms^{-1} Wind Speed 146
B.13 Clyde East vs. Wind Speed 148
B.14 Clyde North vs. Wind Speed 150
B.15 Clyde Vertical vs. Wind Speed 152
B.16 Clyde East, North, Vertical at 12 ms^{-1} Wind Speed 154
Appendix C Filtering Investigation for Seismic estimation 156

Appendix D Variance Modelling 160
D.1 Variation of Seismic amplitude with turbine parameter in the variance models 160
D.2 Variance Model Spectra 163
Appendix E Utilisation Investigation 166
Appendix F A Physics Base Algorithm 184
F.1 Fit of algorithm to empirical data 184
F.2 Tip speed for a variety of wind turbines 193
F.3 Hub heights and rotor diameters 196
Appendix G Turbine Distances to Sensor 4443 at Clyde Wind Farm 198
Appendix H MATLAB Script, FDWF 199

1 INTRODUCTION

The seismometer array at Eskdalemuir (EKA) in the southern uplands of Scotland is part of the UK's contribution to the 321 stations in the International Monitoring System (IMS) network. The IMS is part of the Comprehensive Nuclear-test-Ban Treaty (CTBT) verification regime, and the UK is required by the treaty to safeguard its IMS stations. To safeguard EKA from interference from seismic vibration due to wind turbines, a consultation zone for wind farm development has been defined between 10 and 50 km from the cross-over point of the two arms of EKA. The safeguards were recommended by the original Eskdalemuir Working Group (EWG) in 2005, relying on commissioned research (Styles, et al. 2005), utilising measurement of the vertical component of seismic vibration in 2004 at Dun Law wind farm, which at that time comprised 26 stall-regulated turbines with rated-power of 0.66 megawatt (MW). The 2005 model (Styles, et al. 2005) is used to predict the seismic vibration from wind turbines in the zone. The 2005 model is a narrow-frequency approximation around 4.5 Hz, with a source term that depends on the turbine rated-power, and a propagation term that depends on the distance of the turbine from the EKA cross-over. Under the safeguards the cumulative seismic vibration of permitted wind turbines in the zone is not allowed to exceed a threshold of root-mean square (rms) displacement of 0.336 nanometres (nm) — the value taken as the seismic vibration at EKA at windy times (Styles, et al. 2005). The MoD's wind farm safeguarding approach is to not object to wind farm development on a first-come, first-served basis until the threshold is reached. That threshold was reached (see Table 1 of document FMB_102_TRP0_V4) by the Wind Energy project Earlshaugh. This approach provisionally allocates a proportion of the seismic vibration threshold to a wind farm development, calculated using the 2005 model, considering the contribution from each individual turbine in the development. A development is not objected to if the cumulative seismic vibration is less than the threshold.

In 2012, analysis of seismic data collected near the Dun Law and Craig wind farms has shown that errors were made in the calculations and assumptions used to construct a predictive tool for the seismic vibration made by wind turbines and its effect on the Eskdalemuir seismic array (EKA). Implicit in the predictive tool is the assumption that the frequency produced by wind turbines that is most harmful to EKA is 4.5 Hz. Data gathered near Dun Law wind farm was used to calibrate the predictive tool at 4.5 Hz. However, the data used was processed incorrectly and over estimates the seismic vibration produced by wind turbines at this frequency. Furthermore, data gathered near Craig wind farm in the summer of 2011 showed the turbines generated far-field seismic vibration with multiple spectral peaks at frequencies lower than 4 Hz, each peak with larger power than the spectral peaks in the 4-5 Hz band. These lower amplitude peaks may have a detrimental effect on the detection capabilities of EKA and invalidate the assumption that the most harmful seismic vibration produced by wind turbines occurs at 4.5 Hz. In order to safeguard the detection capabilities of EKA these lower frequency peaks must be considered.

On 27 February 2012 a reconvened EWG, chaired by the Scottish Government, considered a staged approach to the technical work required to re-examine the 2005 model. The EWG agreed a "Stage Zero" of the technical work "for an initial piece of work which would inform the fuller research stages referred to at the meeting". This research was conducted in 2013 and reported in "Initial study of ground vibration data recorded near Craig Wind Farm" (Doc ref. *FMB_102_TRPO_V6*) issued to the EWG on 30th July 2013. The work substantiated parallel work conducted by Dr David Bowers (of AWE) which was reported in his *Initial study of seismic ground vibration data from mega-watt class wind turbines: Interim Technical Report* of June 2013. Both reports used seismic vibration data collected at Craig wind farm to determine whether there is prospect for "head room" in the budget that would allow the building of wind farms without breaching the 0.336 nm threshold. The key finding of the Phase 0 research was that provided the Nordex N80 wind turbines at Craig wind farm are representative of turbines in the Southern Uplands then it is likely that there will be significant head room in the Eskdalemuir budget.

A substantive research programme was agreed by the EWG ("Stage 1") that would build on the research conducted in Phase 0, specifically in regards to how representative Nordex N80 turbines are of other wind turbines in, or to be built in, the Eskdalemuir consultation zone. The nature of the research project has required on going modifications of scope as new material, data and their related interpretation have come to light.

A First Release Report (Release 1 of 2) of work conducted for this substantive research programme was submitted to the EWG on the 22nd January 2014 detailing empirical measurements of Siemens 2.3 MW turbines, Nordex N80 turbines and Vestas V47 and V90 turbines, the quantification of an utilisation factor and an initial worst-case turbine spectrum. The First Release Report provided EWG members with an insight into the development of the research project and an opportunity to offer guidance on its final scope of work. The authors have found the input from all stakeholders extremely helpful in finalising the research which is presented here in this Second Release (Release 2 of 2) of the substantive research programme.

The goal of this research has been to produce an algorithm that will better predict the amplitude of seismic vibrations produced by wind turbines in the 0.5 to 8 Hz passband, which might allow the exploitation of wind resource in the Southern Uplands while maintaining protection of the detection capabilities of EKA. A physics-based algorithm has been constructed based on empirical results from a number of wind farms with different turbines. This report details the empirical measurements of Siemens 2.3 MW turbines, Nordex N80 turbines and Vestas V47 and V90 turbines. The 2005 model includes an utilisation factor that reflects that not all turbines are operational at the same time; this utilisation factor has been reassessed based on empirical data. A series of finite element analysis (FEA) models of wind turbines have been constructed and tested against empirical data to help better understand how wind turbines generate far-field seismic vibrations. The models have also been used to determine which parameters should be included in an algorithm for the prediction of seismic amplitude. A conservation of energy approach has been tested against empirical data and shows that far-field seismic amplitude varies with the swept area of wind turbine rotors and the cube of wind speed. These analyses have been used to construct a physics-based algorithm that predicts the worst-case seismic amplitude produced by any wind turbine based on its rotor diameter, hub height and distance from EKA. The physics-based algorithm has been used to determine the cumulative amplitude of all wind turbines in the Eskdalemuir consultation zone that are either allocated budget or the subject to objection. The physics-based algorithm is also used to determine how close to EKA wind turbines can be built while optimising the generating capacity within the consultation zone; this work could be used to inform policy on the radius of a wind turbine exclusion zone from EKA.

2 TECHNICAL BACKGROUND

2.1 Eskdalemuir seismic array

The high topography and wind conditions found in the Southern Uplands of Scotland offer a prime source of on-shore wind energy. The value of the wind energy resource is further increased by the region's proximity to grid connection between Scotland and England and to the population and industrial centres of the Scottish central belt including Glasgow and Edinburgh. However, the Southern Uplands is also the site of the Eskdalemuir seismic array for which the detection capabilities could be adversely affected by the ground vibrations produced by wind turbines (Schofield 2001).

The Eskdalemuir seismic array (EKA) is a component of the United Kingdom's contribution to the International Monitoring System for the Comprehensive Nuclear-Test Ban Treaty. The seismic array has been operational

since 1962 and is composed of 20 seismic sensors in seismic pits arranged in 2 straight lines (10 sensors in each line) that intersect at right angles (Figure 1). The two lines of sensors makes it possible to calculate the direction of the seismic wave travel and therefore to determine the direction of the likely source relative to the array. The array was located near Eskdalemuir because it is a region with very low seismic back-ground noise (Styles, et al. 2005) making it ideal for sensing earthquakes and covert nuclear weapons tests.

The array detects seismic vibrations at low frequencies (< 8 Hz). The work of Schofield (2001) at Stateline wind farm in Washington, USA, showed that wind turbines produce seimic vibration at low frequencies raising concern that wind farm development in the Southern Uplands may raise background seismic levels and reduce the detection capabilities of EKA. The United Kingdom is bound by the Comprehensive Nuclear-Test Ban Treaty not to compromise the detection capabilities of EKA leading the Ministry of Defence (MoD) to place a cautionary ban on all wind turbine development within 80 km of EKA. In 2004 the Eskdalemuir Working Group (EWG) formed and commissioned research to be carried out by the Applied and Environmental Geophysics Group at Keele University led by Professor Styles to establish the interference that wind turbine development in the Southern Uplands may have on EKA.

Based on the research carried out by the Keele University group a ban was placed on development of any wind turbines within 10 km of EKA and a statutory consultation zone was fixed at a radius of 50 km (Styles, et al. 2005). A budget was set that represents the acceptable upper limit to the amount of ground vibration produced by all wind turbines within the statutory consultation zone that could be detected (at EKA) without impairing its detection capabilities. The budget threshold was set at 0.336 nm which is the same as the average noise amplitude measured at EKA at *windy times* in the 1.5 to 4.5 Hz band. An algorithm was designed to estimate the cumulative ground vibration amplitude from all wind turbines within the statutory consultation zone. The algorithm used the amplitude produced by a reference wind farm to estimate the ground vibration produced by any other wind farm based on its distance from EKA, the rated power of the wind turbines in the farm and the number of turbines. On-going research following the submission and acceptance of the report of Styles, et al., (2005) indicates that the amplitude of the reference wind farm used in the algorithm is significantly greater than that produced by wind turbines and that the algorithm has systematically over-estimated the cumulative seismic vibration produced by all wind turbines within the statutory consultation zone.

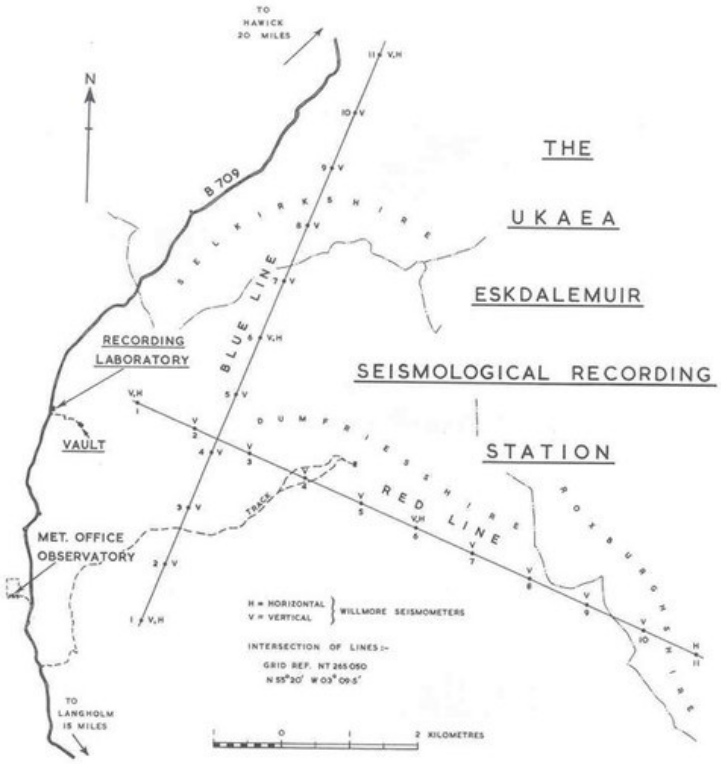

Figure 1 – The Eskdalemuir seismic array (Guralp Systems 2002)

2.2 Previous studies

Measurements at distances of 25, 50 and 100 m from the St Breock's Down wind farm, Cornwall, found discrete seismic vibrations could be detected at 0.5 Hz and multiples of 0.5 Hz, specifically 3.0, 4.5, 6.0 and 7.5 Hz (Legerton, et al. 1996, Snow and Styles 1997). Using turbine shut down sequences it was shown that the discrete vibrations were produced by the wind turbines and it was inferred that 0.5 Hz multiples were related to multiples of the blade pass frequency. It was also shown that the amplitude of seismic vibration increased with wind speed.

Seismic measurements near the Stateline wind farm, Washington, USA found seismic signals that could be attributed to the wind farm up to 18 km from the closest wind turbine (Schofield 2001). The geology of the survey site is dominated by the Touchet bed of the Walla Walla Valley consisting of gravel, fine sediment and rhythmites which are up to 100 m thick (Baker 1978) which have slow ground wave propagation velocities of ~ 500 ms^{-1} (Schofield 2001). Schofield (2001) deployed seismometers at 10 sites ranging from 24 m to 18,270 m from the wind farm and found discrete signals at 1.47, 2.95, 4.34, 5.88 and 7.35 Hz that were attributed to multiples of the frequency at which the blade passes the turbine tower, the *blade pass frequency*. Stable peaks with respect to time and wind speed were found and interpreted as being due to the resonance of the tower topped by the nacelle and rotor. Schofield (2001) found that amplitude of seismic vibation reduced with the inverse of distance (1/r) and postulated that this indicated that seismic path propogated partly through air as infrasound, before being coupled with the earth to form seismic waves.

The work commissioned by the EWG and reported in Styles, et al. (2005), P. Styles (2005) and England (2006) took infrasound and seismic measurements of the Dun Law, Crystal Rig and Ardrossan wind farms. The geology of the measurement site stretching between the Dun Law and Crystal Rig wind farms is similar to the

EKA site and is dominated by greywacke and conglomerates with high ground wave propagation velocities ~ 2000 ms^{-1} (Styles, et al. 2005). The seismic and infrasound measurement showed that seimic vibration produced by wind turbines propagated through the ground via a direct mechanical coupling at the base of the turbine and did not involve propagation through the air as postulated by Schofield (2001). Using turbine shut down sequences it was shown that the seismic amplitude varied as a quadrature sum of the number of turbines running confirming the theory proposed by Schofield (2001). Using comparisons between seismic measurements conducted at Dun Law and Ardrossan wind farms it was shown that the seismic amplitude increased linearly with the rated power of the wind turbines. Discrete vibrations at multiples of the blade pass frequency were found confirming the observation of Schofield (2001), with particularly prominant peaks at 2.8, 4.3, 5.7, 7.1 and 8.5 Hz. Styles, et al. (2005) also proposed that a 1.4 Hz (blade pass frequency) vibration may have been present but was masked by high background noise which rose steeply below 2 Hz. Stable peaks were noted when the turbines were not running and these were interpreted as structural resonance of the tower and nacelle. Analysis of the principal axes of motion sensed while the turbines were running showed that seismic vibration was confined to the vertical and longitudinal (colinear with a line from the sensor and the wind farm) direction indicative of Rayleigh waves.

Wind turbine base, near-field and far-field measurements were conducted at Schliekum wind farm, Germany, in order to determine how wind turbine generated seismic vibration affects the GEO600 gravity wave detector and how the Vigro gravitational wave detector, Italy, may be affected by future wind turbine developments (Fiori, et al. 2009). The survey site consisted of 20-50 m thick soil deposits composed of lime and sand sediment, that have low ground wave propagation velocities of ~450 ms^{-1} for frequencies below 4 Hz and 260 ms^{-1} for frequencies between 4 and 10 Hz. The wind farm consisted of four different turbines; Nordex N90, Nordex S77, EnronWind 1.5s and EnronWind 1.5; allow the comparison of the seismic vibrations produced by different makes and models. Measurements of the foundations of different turbines showed slight variations in the frequency of peaks and more significant variation in the size and shape. Seismic vibration produced by wind turbines were detectable up to 2 km from the wind farm. Beyond 2 km it became difficult to detect wind turbine produced vibrations as they become masked by background noise (GEO006 is a seismically noisy site due to anthropogenic activity). Coherence tests were conducted between a sensor mounted on the foundation of a wind turbine and a second sensor placed between 25 m and 1130 m and good coherence was found between vibrations between 2 and 10 Hz. A strong signal at 0.3 Hz was found not to be coherant with vibration from the turbine. Horizontal motion produced by wind turbines was found to be significantly greater than the vertical motion indicating the waves propagated as Love waves (horizontally polorised shear waves). Fiori, et al. (2009) also found that the background seismic vibration propagated as Love waves.

Saccorotti, et al. (2011) conducted a seismic study of wind turbines near the Vigro gravitational wave observatory in Tuscany, Italy. The survey site consists of thick measures of unconsolidated conglomerates, fluvio-lacustrine muds and sands (at least 60 m deep) that overlay several hundred meters of marine and continental deposits that sits on a carbonate basement. Measurements close to the base of the wind turbine found 0.45 and 1.7 Hz peaks that were stable with respect to time, rotor speed and wind speed and were attributed to the structural resonances. Peaks at around 0.3, 0.6, 0.9, ... 20 Hz changed frequency with respect to time and were attributed to blade pass and its multiples. Far-field measurements taken in wind speeds of 11 ms^{-1} included several peaks (3.5 and 4.5 Hz) that were not noted at measurements taken at the base of the turbine in 3 ms^{-1}. Based on this lack of correlation, Saccorotti, et al. (2011) concluded that beneath-turbine measurements can not be taken as representative of the overall wind farm noise as observed in the far-field. A dense, two-dimensional array deployment 480 m from the closest turbine was used to determine the composition of the seismic wave field. Cross corelation of data obtained for the array deployment showed that vibration above 1 Hz propagated from the direction of the wind farm, while lower frequencies propagated from the direction of the coast and were most likely marine microseismic. The motion of the frequency with the greatest power (1.7 Hz) was predominantly in the horizontal direction acting perpendicular to the direction

of travel and was therefore a Love wave. The attenuation of seismic vibration with distance exhibited a complicated pattern which led Saccorotti, et al. (2011) to propose a complex vibration pathway whereby surface waves add to body waves reflected at depth by the boundary between the sedimentary sequence and underlying carbonate basement.

Styles, et al. (2011) conducted seismic vibration measurements at the Craig wind farm in the Scottish Borders to determine the effectiveness of a vibration mitigation system. The survey was combined with numerical modelling of the wind turbine using finite element methods to determine the nature of structural resonance in the blades and tower responsible for the observed seismic vibrations close to the base of the tower. The second bending mode of the tower was identified as producing a broad peak of seismic vibration in the 4 to 5 Hz band. This resonance amplifies the vibration caused by the fifth multiple of blade pass.

2.3 Ground vibration produced by wind turbines

Based on the research summarised above, and further research that will be presented below, it is apparent that vibrations in wind turbines move through their foundations into the surrounding rock where they radiate away as seismic waves referred to here as ground vibrations. Vibrations in wind turbines that eventually become ground vibrations have two sources; structural resonances and excitation frequencies related to rotational machinery. Structural resonances are the frequencies at which a structure naturally vibrates, akin to the note at which a bell rings when struck. In wind turbines at low frequencies (<10 Hz) these resonances are related to the flapping of blades and the rocking of the tower. The resonances of a wind turbine are excited by random fluctuations in wind speed due to turbulence resulting in the tower and blades vibrating at discrete frequencies.

Vibrations from excitation frequencies related to rotating machinery are produced by rotational imbalances in the rotating components, gear teeth meshing in the gearbox, electromagnetic interactions in the generator, the shadow and turbulence cast by the blade as it passes the turbine tower. The turbulence cast by the passage of the blade, referred to as the *blade pass frequency*, is particularly important in the generation of ground vibration based on field measurements at Stateline, Dun Law and Craig wind farms.

3 FIELD SURVEY

3.1 Introduction

Extensive seismic vibration data has been recorded from four wind farms. The aim being to empirically determine the low frequency (< 8 Hz) far-field seismic vibration produced by wind turbines so that a predictive algorithm can be developed. The measurement surveys investigated four different wind turbines and four different wind farms (Table 1). The experimental setup for each site survey is introduced in the following sections of this chapter. There are many similarities in the methodology used, however each will be presented individually as each survey has unique aspects be it sensors used, geometry of sensor deployment or region of interest - Near-field (on tower) or Far-Field. Table 1 presents a summary of the wind farms studied, the respective wind turbine and style of measurement undertaken, be it near- or far-field.

Location	Wind Turbine Type	Near-field	Far-Field
Dun Law, UK	Vestas V47		X
Craig, UK	Nordex N80	X	X
Clyde, UK	Siemens 2.3	X	X
St Seine-l'Abbaye, France	Vestas V90	X	

Table 1 – Summary of wind farm locations investigated. The type of wind turbine and near- or far-field measurement is indicated.

3.2 Methodology

3.2.1 DUN LAW WIND FARM

In 2004 ten CMG-6TD seismometers where deployed in shallow pits by Keele University, as reported by Styles et al. (2005), at distances ranging from 1 391m to 17 287 m from the closest wind turbine within the Dun Law wind farm. It should be noted that the distance should more accurately be taken to be the effective centre of the wind farm. Deployment techniques used are described in Styles et al. (2005). The geology of the measurement site is similar to that of EKA, where it is dominated by greywacke and conglomerates with high ground wave propagation velocities ~ 2000 ms^{-1}, (Styles, et al. 2005). The sensors were deployed in an approximately linear fashion, stretching from the Dun Law wind farm in an east-northeast direction towards the Crystal Rig wind farm (Figure 2 & Figure 3). The distance between the sensors and the Dun Law and Crystal Rig wind farms are shown in Table 2. The Dun Law wind farm was the target of the survey; however the sensors at Hope Hills 1, Hope Hills 2 and Johnscleugh could have received relatively high ground vibration from Crystal Rig. In addition, the sensor reference number is provided in Table 2, for which the corresponding calibration constants are provided in Appendix A.1, Dun Law Calibrations.

Dun Law wind farm consists of 26 Vestas V-47 wind turbines that are rated to produce 0.66 MW each. The turbines have a 40 m hub height and a 47 m diameter rotor. At the time of measurement, the Crystal Rig wind farm consisted of 20 Nordex N80 wind turbines rated to produce 2.5 MW each. The N80 turbines have a hub height of 60 m and a rotor diameter of 80 m. The data made available to Xi dated from the 29th July 2004 to the 31st October 2004. Wind speed and direction data was recorded during this period, logged as average values in 10 minute blocks. The wind speed was measured at hub height of the wind turbines and reported by the wind farm operators.

Sensor Name	Sensor Ref No.	Distance to (m)	
		Dun Law	Crystal Rig
Array 1	6087	5939	14368
Array 2	6179	6175	14156
Array 3	6132	5981	14364
Crib Law 1	6091	5286	15129
Crib Law 2	6083	4425	15964
Hope Hills 1	6124	8868	11662
Hope Hills 2	6047	10702	9619
Johnscleugh	6155	17287	2970
Kelphope 1	6123	2362	17953
Kelphope 2	6121	1391	18878

Table 2 – Distance of seismometers to the closest turbines in the Dun Law and Crystal Rig wind farms.

Figure 2 – Position of seismometers relative to Dun Law wind farm

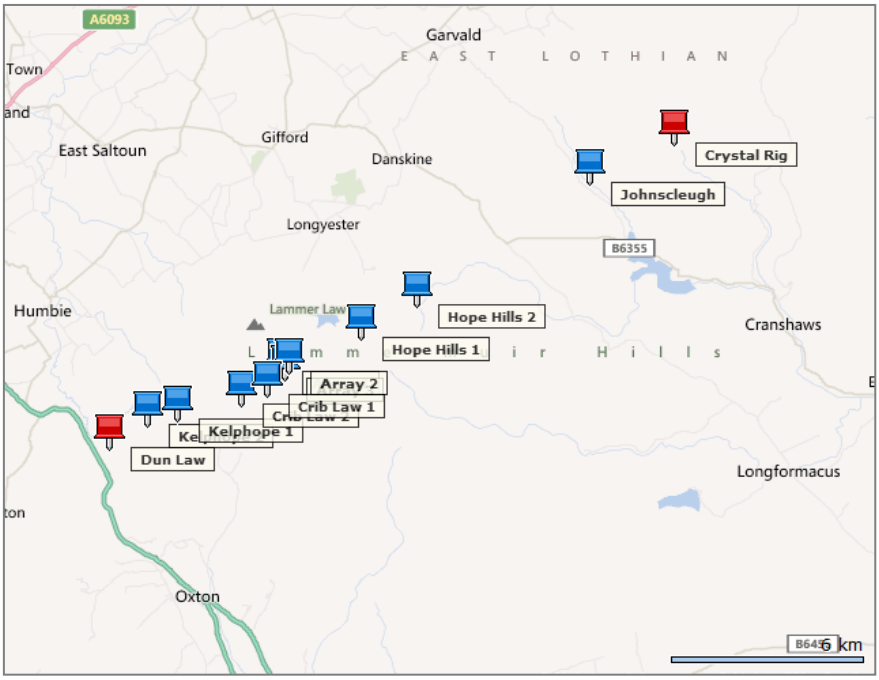

Figure 3 – Position of seismometers relative to Dun Law and Crystal Rig wind farms

3.2.2 CRAIG WIND FARM

3.2.2.1 Far-field

In the summer of 2011 a measurement of far-field seismic vibration was conducted at the Craig wind farm. Eight seismometers were positioned radially around the wind farm with distances between 308 m and 1016 m to the closest wind turbine in the farm (Figure 4). Six 6TD and two Guralp 40TD and one Guralp 3ESP seismometers were used. Measurements were recorded between 17th May and 25th July 2011. During this time site 6188 was decommissioned and 6099 deployed at a new location, Figure 4. Similarly to Dun Law and EKA, the underlying geology is dominated by greywacke. Craig wind farm (CWF) consists of 4 Nordex N80 wind turbines that are rated to produce 2.5 MW. Each turbine has a hub height of 60m and the rotor has a swept diameter of 80 m. Turbine 1 (T1) includes a Seismically Quiet Turbine (SQT) device designed to mitigate the amount of seismic vibration produced in the 4 to 5 Hz band. The position of each sensor and distance from each turbine are shown in Table 3. Calibration constants for each sensor are provided in Appendix A.2 Craig Calibrations.

Previous work produced by Xi on the Craig wind farm seismic survey used the sensor reference number to discuss results (Table 3). The Interim Technical Report of Dr Bowers uses site names. To avoid confusion both the sensor reference number and site name will be used here. Wind speed and direction data was recorded during this period, logged as average values in 10 minute blocks. The wind speed was measured at hub height of the wind turbines and reported along with rpm data by the wind farm operators.

The seismic amplitude produced by T1 and the effectiveness of the SQT is not discussed in this report. Rather, the data set gathered at CWF is used here to examine the seismic vibration produced by unmitigated N80 turbines and the presence of the SQT is ignored.

Turbine	OS East	OS North
T1	32451	85800
T2	32263	85978
T3	31983	86044
T4	31872	86238

					Distance between sensor and turbine (m)			
Sensor Ref No.	Site	OS East	OS North	Sensor Type	T1	T2	T3	T4
4421	GSL-2	31994	87247	40TD	1517	1297	1203	1016
6028	AEG-1	31395	86044	6TD	1084	871	588	515
6099	AEG-2b	32662	86419	6TD	654	595	776	810
6140	AEG-4	32946	85308	6TD	698	957	1212	1421
6159	AEG-3	33117	85535	6TD	717	962	1243	1430
6188	AEG-2a	32575	86521	6TD	732	626	760	758
6351	AEG-5	32302	87061	6TD	1270	1084	1066	929
3Y96	GSL-3	33143	86491	3ESP	977	1015	1239	1291
4T50	GSL-1	31704	86495	40TD	1021	762	532	308

Table 3 – Positions of turbines and sensors at Craig wind farm.

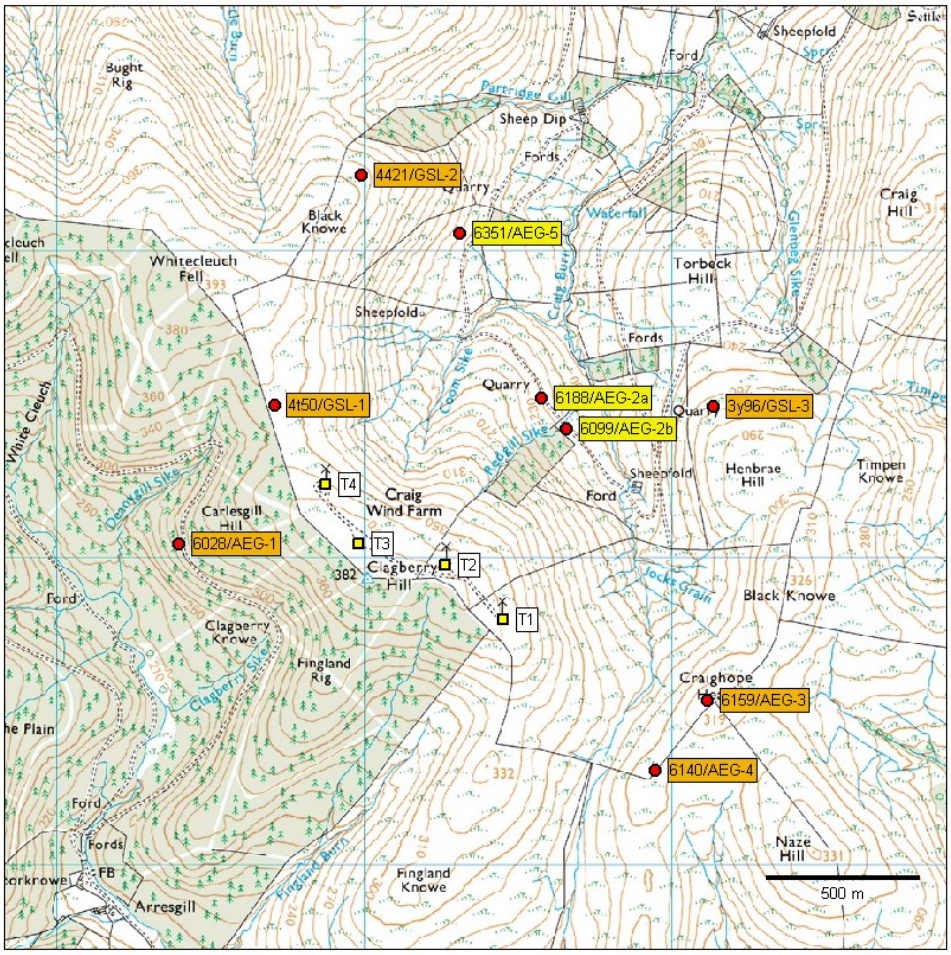

Figure 4 – Sensor placement at Craig wind farm. Turbines within Craig wind farm are labelled T1 to T4.

3.2.2.2 Near-field

There were two periods during which near-field measurements were conducted at Craig wind farm. The first coincided with the Far-Field survey outlined above. During this time a 5TD accelerometer was positioned centrally on the foundation of T1 (Figure 4).

The second was an independent measurement campaign consisting of three 6TD seismometers supplied through Keele University. The seismometers were deployed centrally on the foundations of turbines T1, T3 and T4 between the 18th January and the 9th February 2012. Again the wind speed and direction data was recorded during this period, logged as average values in 10 minute blocks. The wind speed was measured at hub height of the wind turbines and reported by the wind farm operators. Sensor details are shown in Table 4.

Sensor Ref No.	Location
6195	T1
6120	T3
6064	T4

Table 4 – Sensor locations for the near-field measurements taken at Craig wind farm in 2012.

3.2.3 CLYDE WIND FARM

3.2.3.1 Far-field and Near-field

A seismic vibration survey of Clyde wind farm was conducted by Grontmij from 14th June to 10th July 2013 and the data was kindly provided to Xi by SSE. The Clyde wind farm that consists of 152 Siemens 2.3 MW (S2.3) turbines was measured using four Guralp CMG-3T seismometers. The sensors were positioned approximately linearly from a single turbine, turbine T39, extending to a distance of 825 m. A site map is shown in Figure 5 with the position of the test turbine and the sensor locations. The closest seismometer was positioned on the hardstand of T39 providing near-field measures concurrent with those conducted in the far-field. The distance of each seismometer relative to turbine T39 is listed in Table 5. Calibration constants for each sensor are provided in Appendix A.3, Clyde Calibrations. The underlying geology of T39 and the sensors array is Ordovician greywacke; the same geological unit as EKA and Craig wind farm. The S2.3 turbines are rated to produce 2.3 MW with a hub height of 78.3 m and swept diameter of 93 m. Wind speed data was recorded during this period, logged as average values in 10 minute blocks. The wind speed was measured at hub height of the wind turbines and reported by the wind farm operators.

Sensor Ref No.	Distance to Tower T39 (m)
4442	Hardstand
4444	100
4445	500
4443	825

Table 5 – Sensor positions for the measurements taken at Clyde wind farm in 2013.

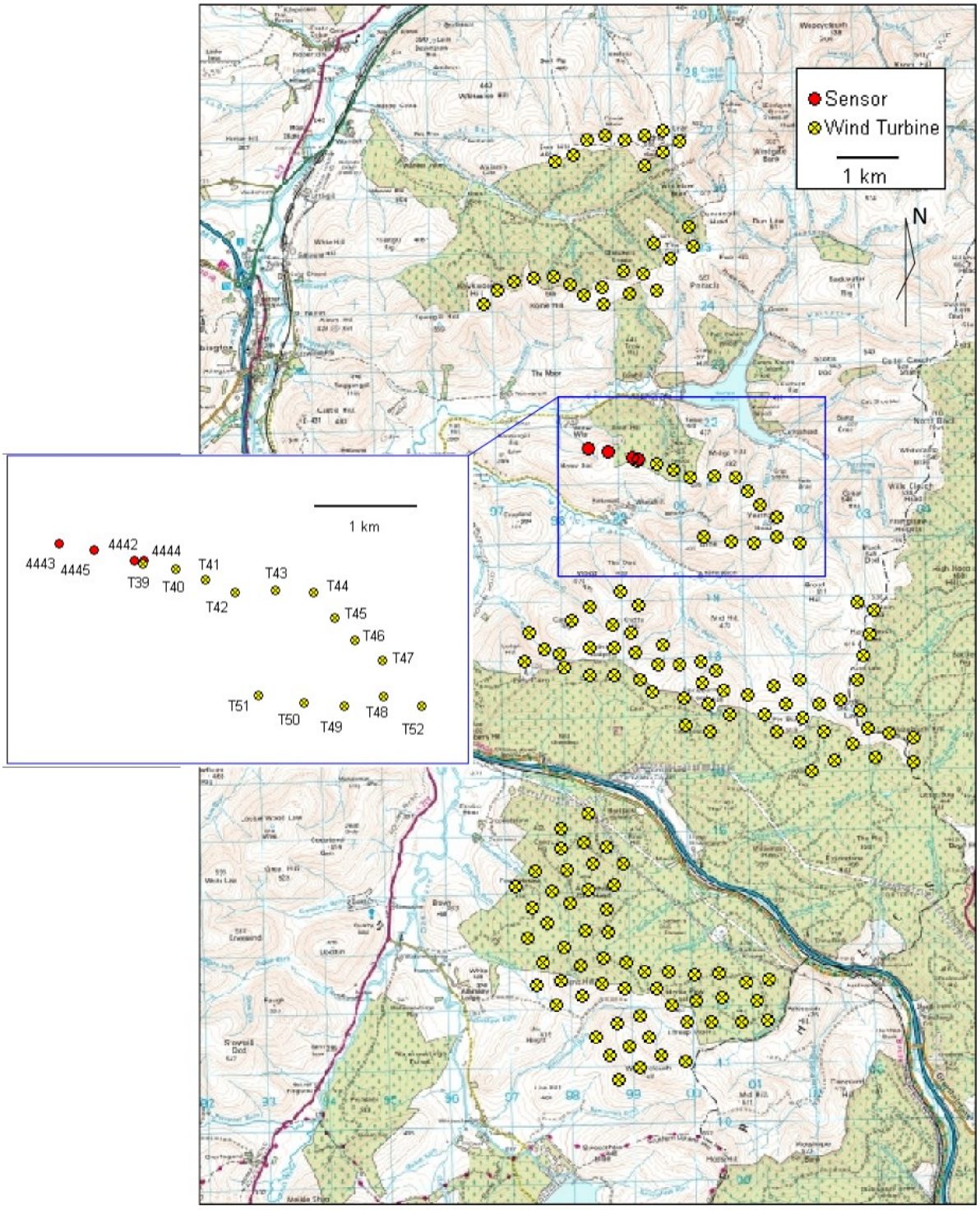

Figure 5 – Sensor placement at Clyde wind farm. The test Turbine T39 is highlighted. Sensor 4442 was positioned on the T39 hardstand. The remaining sensors positioned linearly out to a distance of 825 m.

3.2.4 ST SEINE-L'ABBAYE WIND FARM

3.2.4.1 Near-field

A Vestas V90 at St Seine-L'Abbaye, France, was used for conducting on tower vibration measurements on the 21st and 22nd of June 2012 (Figure 6). Permission to use the data was kindly provided to Xi by RES. The V90 turbine investigated here has a rated power of 2.0 MW with a hub height of 80m and a rotor diameter of 90 m. Xi engineering equipped the tower foundation with 2 Syscom tri-axial geophone sensors, selected for their accuracy and low frequency response characteristics. Details of the sensors with calibration certificates and typical frequency responses are provided in Appendix A.4, St Seine-L'Abbaye Equipment Specifications.

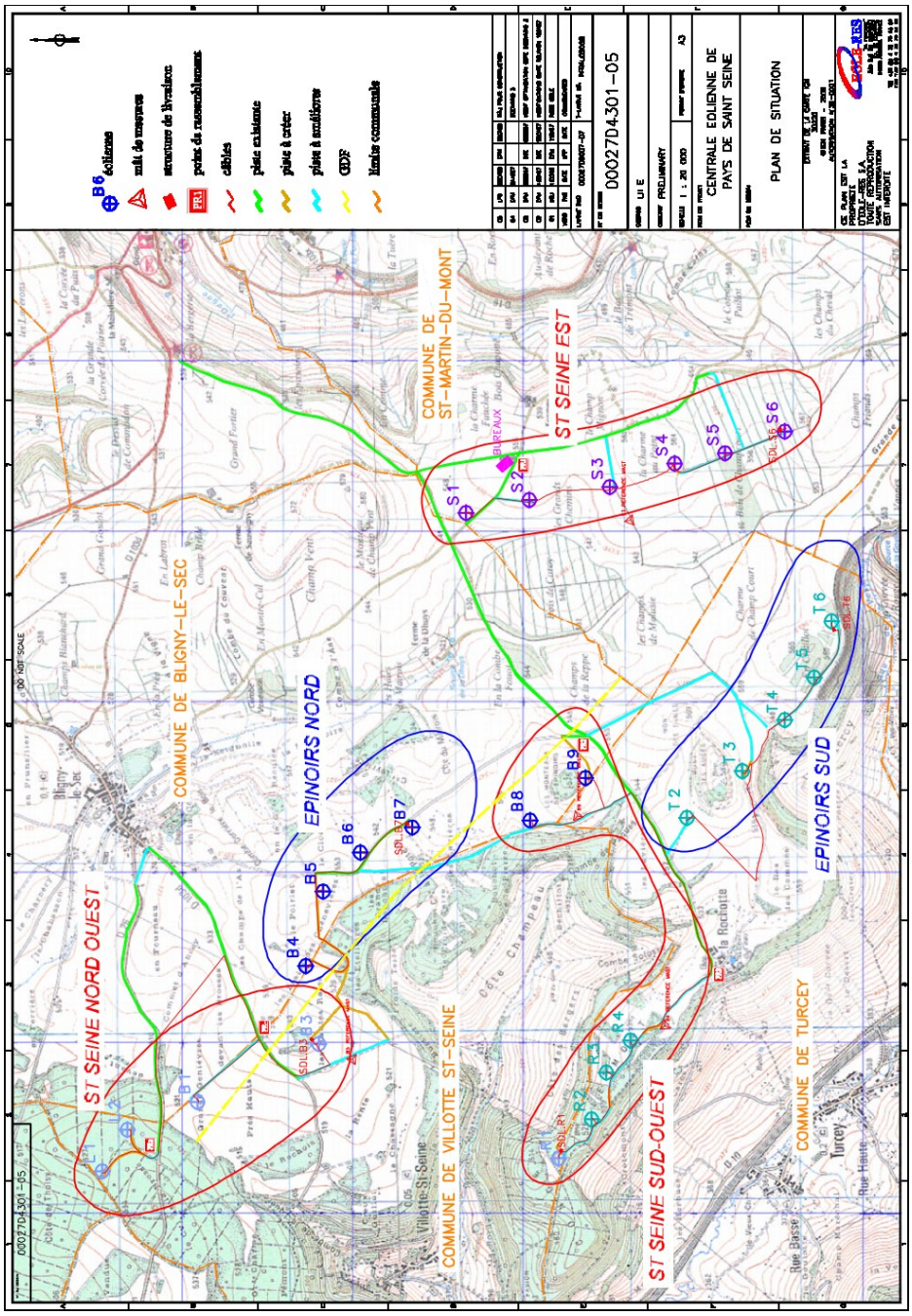

Figure 6 – Location of the test turbine, S6, at St Seine-l'Abbaye.

Figure 7 shows a simplified turbine layout with the relative locations of the key internal components. Also shown is the approximate wind direction experienced on both measurement days. The green geophone represented the primary sensor and was inline (vertically) below the wind turbine door. The blue geophone was a spare sensor and was wired to log z-axis motion only. It was positioned at 90 degrees on the west side of the tower. Initial tests during the equipment set-up showed it was possible to run the foundation geophones with their 50x gain mode activated without risk of the signal being clipped from high amplitude vibrations. The 50x gain mode enhances the geophone sensitivity and produces a clearer vibration signal. Figure 8 shows the sensor locations relative to the tower.

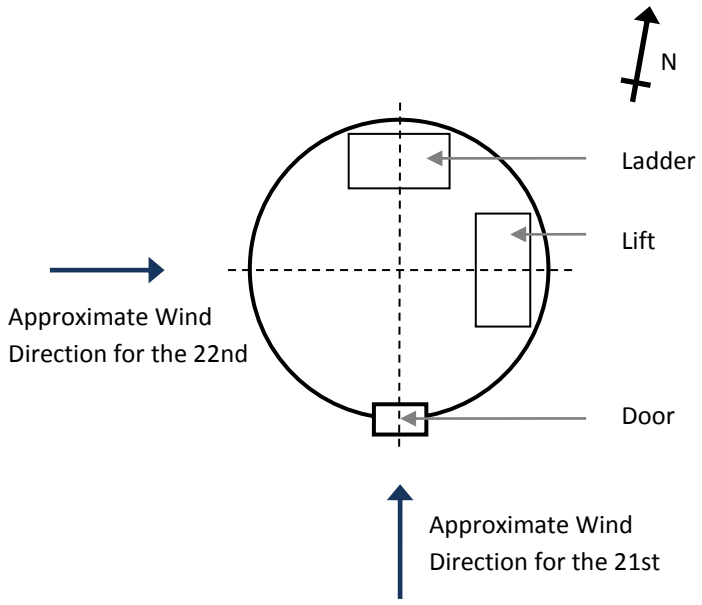

Figure 7 – Layout of major internal components of the V90 with the relative wind direction indicated for each of the days tested.

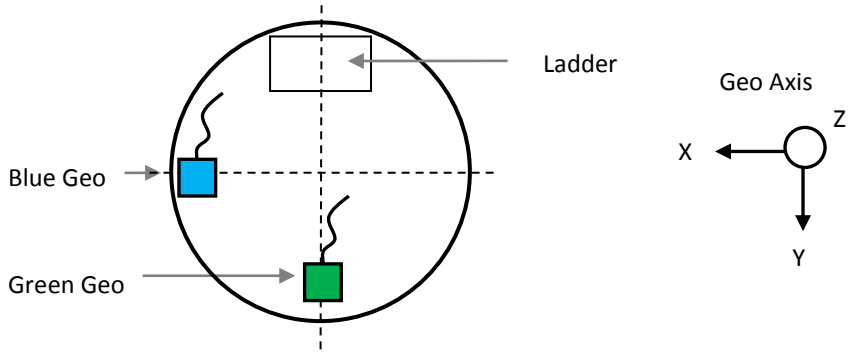

Figure 8 – Sensor locations in the wind turbine S6 basement.

3.3 Data processing

Where possible the data from all wind turbines surveyed was processed using the same methodology to allow for direct comparison. The post-processing methodology used is also consistent with work presented for Phase 0 (Doc ref. *FMB_102_TRPO_V6*) and is referred to as the Primary Processing Methodology (PPM). Variations to the PPM resulting from site measurement specifics are noted in Section 3.3.1 so that the displacement power spectral density (PSD) can be calculated for each site and compared accordingly. The PPM is as follows:

1. The data recorded at sensors was stored in hour-long files. The data was extracted in 10 minute intervals, corresponding to the wind speed data.
2. The sensor output was calibrated for each axis, including removal of any linear trend/mean, resulting in a measured velocity (†) (ms^{-1}) in the time domain. Calibration values are provided for each site in Appendix A.
3. The velocity data was down-sampled to 50 Hz using an 8^{th} order Chebyshev Type I Low Pass Filter.
4. Welch's method was applied to each of the data bins to produce velocity PSD. The Matlab function *pwelch* was applied using 28 sections with a 50 % overlap.
5. The resulting velocity data in the frequency domain was converted to displacement PSD (m^2/Hz) by dividing by a factor of $(2\pi f)^2$. (†)

(†) The primary processing methodology applies for seismometers recording velocity. Where accelerometers are used this is adjusted accordingly including a second integration for the conversion to displacement in Step 5).

3.3.1 VARIATIONS TO THE PRIMARY PROCESSING METHODOLOGY

3.3.1.1 Dun Law wind farm and Craig wind farm far-field processing variations

The Dun Law and Craig wind farm datasets had an additional processing step included to remove the effects of topography on the calculation of seismic amplitude (Figure 9 to Figure 12). This was not performed on the Clyde data due to the location of the seismometers at the centre of the wind farm. Rayleigh waves are polarised normal to the surface of the ground. At both Dun Law and Craig wind farms the steep topography means that the normal to the ground surface and the vertical upward direction are not co-linear. Once the far-field data for each axis had been converted to velocity in the compass coordinates of the sensors (East, North, Vertical) it underwent a further conversion to propagation coordinates. This required the topography of the sites to be digitised and the reference frame of the sensor to be rotated resulting in axis relevant to the travel of the ground waves - direction of travel (α), orthogonal to the direction of travel (β) and perpendicular to the surface (γ). The unit normals used to re-orient the Craig data is listed in Table 6 and for Dun Law they are listed in Table 7.

	α - unit normal			β - unit normal			γ - unit normal		
	x	y	z	x	y	z	x	y	z
3y96	0.8909	0.4533	-0.0293	-0.4515	0.8767	-0.1659	-0.0495	0.1610	0.9857
4t50	-0.6328	0.7713	0.0683	-0.7726	-0.6348	0.0108	0.0517	-0.0459	0.9976
4421	-0.1133	0.9834	-0.1418	-0.9822	-0.0893	0.1654	0.1500	0.1580	0.9760
6028	-0.9555	0.0929	-0.2800	-0.0797	-0.9951	-0.0581	-0.2841	-0.0332	0.9582
6188	0.6645	0.7097	-0.2341	-0.7094	0.6975	0.1011	0.2350	0.0989	0.9669
6140	0.7683	-0.6398	0.0211	0.6395	0.7686	0.0181	-0.0278	-0.0004	0.9996
6159	0.9112	-0.4010	0.0939	0.4062	0.9127	-0.0445	-0.0678	0.0787	0.9946
6099	0.7684	0.5961	-0.2328	-0.6091	0.7929	0.0198	0.1964	0.1266	0.9723
6351	0.2143	0.9761	0.0368	-0.9395	0.1957	0.2811	0.2671	-0.0948	0.9590

Table 6 – Unit normal at sensors used to re-orient Craig wind farm data. The x-axis is collinear with east, the y-axis is collinear with north and the z-axis is vertically upward.

	α - unit normal			β - unit normal			γ - unit normal		
	x	y	z	x	y	z	x	y	z
Array 1	0.8769	0.4480	-0.1743	-0.4470	0.8933	0.0472	0.1768	0.0365	0.9836
Array 2	0.9015	0.4329	0.0000	-0.4329	0.9015	0.0000	0.0000	0.0000	1.0000
Array 3	0.9126	0.4088	0.0000	-0.4088	0.9126	0.0000	0.0000	0.0000	1.0000
Crib Law 1	0.9115	0.3821	-0.1524	-0.3843	0.9231	0.0155	0.1466	0.0444	0.9882
Crib Law 2	0.9199	0.3920	-0.0144	-0.3838	0.9071	0.1730	0.0809	-0.1536	0.9848
Hope Hills 1	0.9040	0.4273	-0.0162	-0.4276	0.9033	-0.0353	-0.0005	0.0388	0.9992
Hope Hills 2	0.8979	0.4402	0.0000	-0.4402	0.8979	0.0000	0.0000	0.0000	1.0000
Johnsclough	0.8727	0.4883	0.0000	-0.4883	0.8727	0.0000	0.0000	0.0000	1.0000
Kelphope 1	0.8642	0.4984	-0.0685	-0.4961	0.8669	0.0478	0.0832	-0.0073	0.9965
Kelphope 2	0.7868	0.6126	0.0752	-0.6150	0.7885	0.0108	-0.0527	-0.0547	0.9971

Table 7 - Unit normal at sensors used to re-orient Dun Law data. The x-axis is collinear with east, the y-axis is collinear with north and the z-axis is vertically upward.

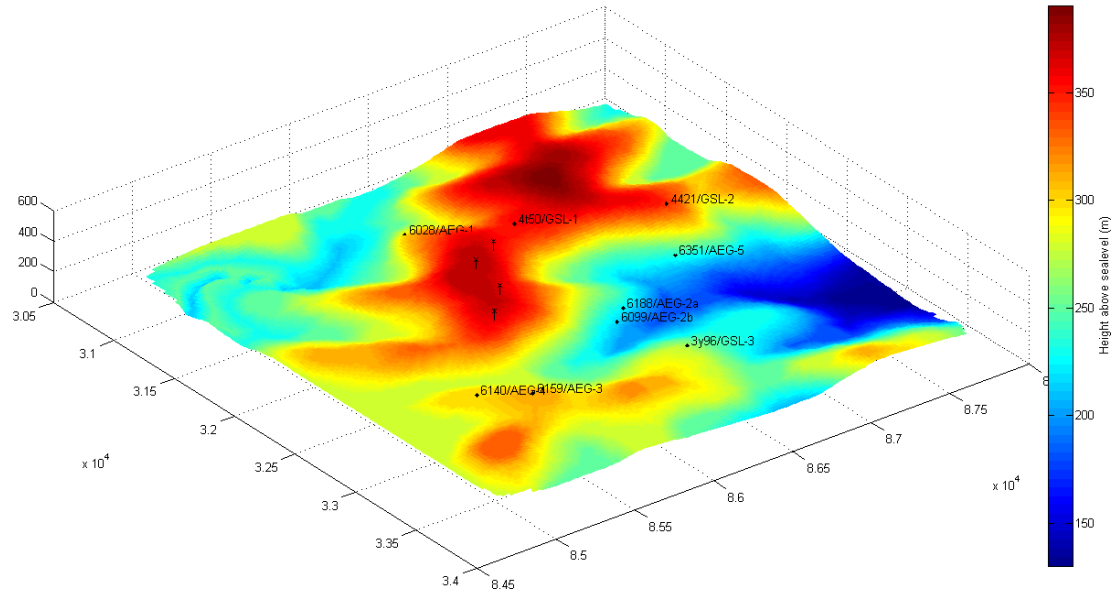

Figure 9 - Digitised topography at Craig wind farm with sensor positions and wind turbines. The digitised topography is used to calculate the unit normal to the ground surfaces.

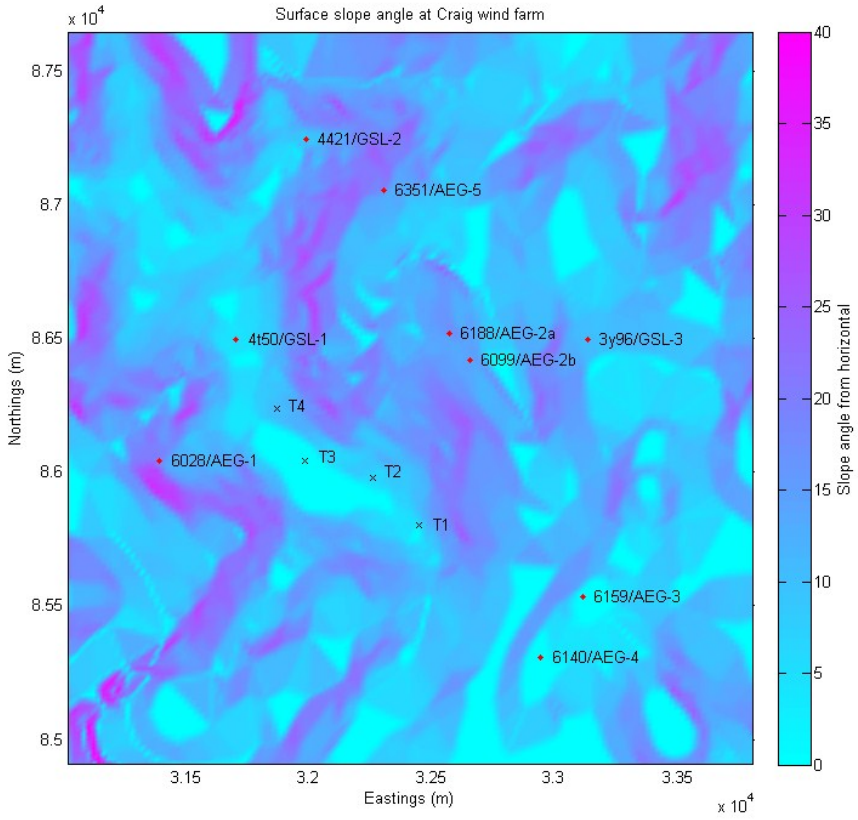

Figure 10 – The surface slope of topography at Craig wind farm with the sensors and turbines shown. The local unit normal to the ground surface at each sensor was used to re-orient measurements in to α-, β- and γ-axes.

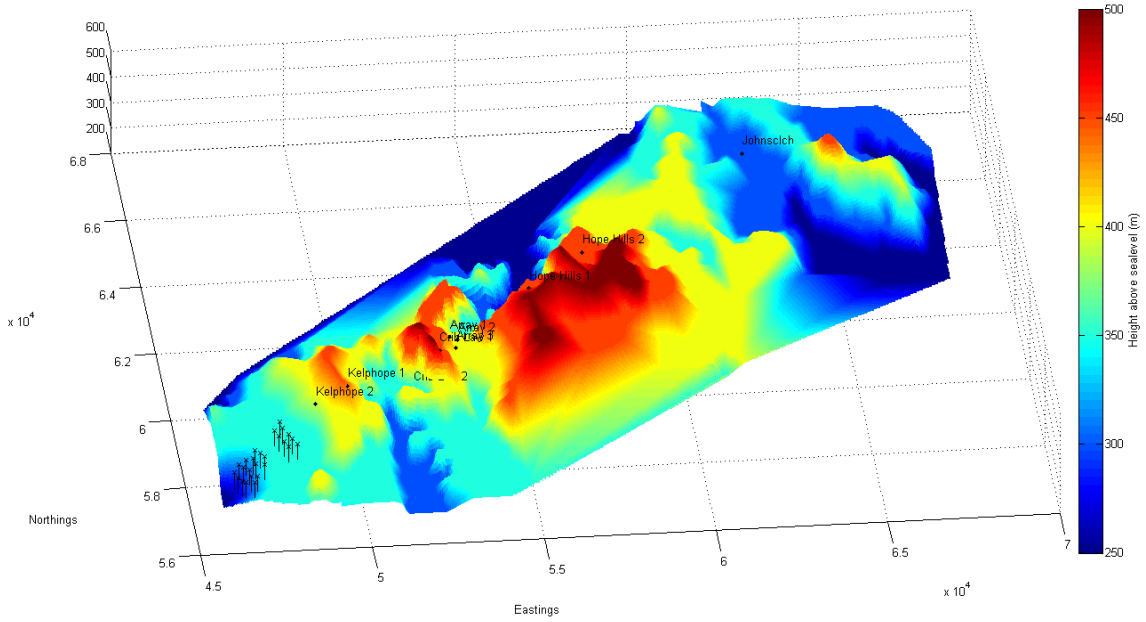

Figure 11 - Digitised topography at Dun Law wind farm with sensor positions and wind turbines. The digitised topography is used to calculate the unit normal to the ground surfaces.

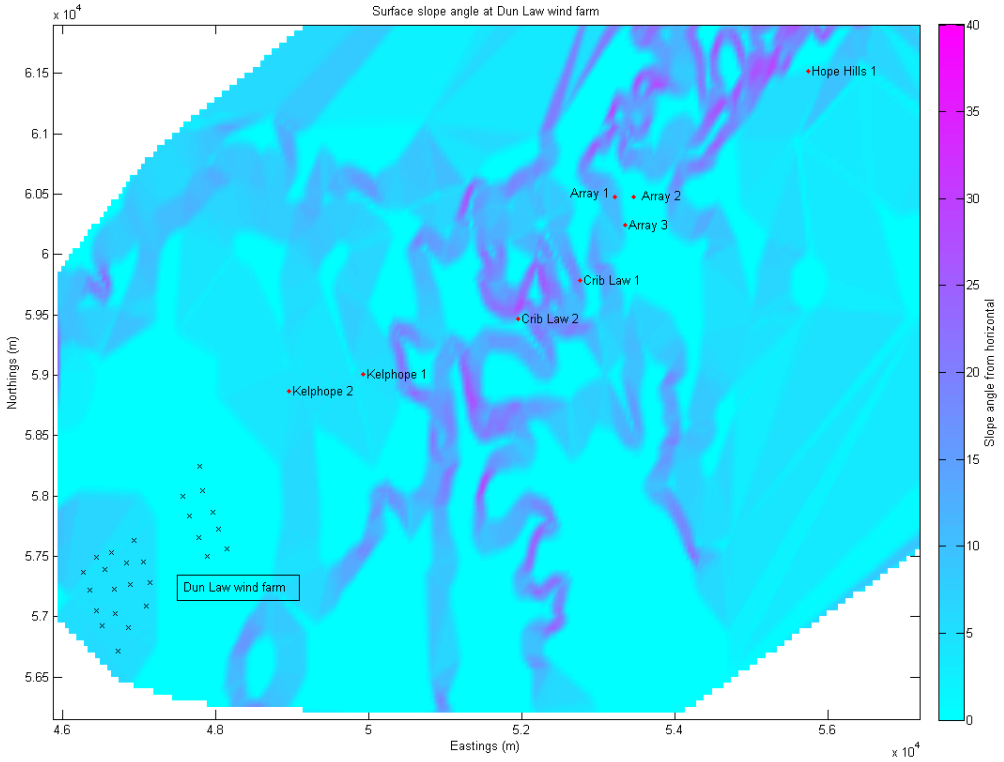

Figure 12 - The surface slope of topography at Dun Law wind farm with the sensors and turbines shown. The local unit normal to the ground surface at each sensor was used to re-orient measurements in to α-, β- and γ-axes.

3.3.1.2 St Seine-L'Abbaye near-field processing variations

The measurements conducted at St Seine L'Abbaye were shorter in duration due to the nature of the investigation. The measurements were a combination of turbine running, turbine off and bump tests ranging from 60-528 seconds in duration. The details of the tests carried out are presented in Table 8 and Table 9 for the dates 21st and 22nd June 2012 respectively. The sample rate was 2000 samples per second which was higher than the other measurements. Real time wind speed data was also available and so although these tests are less than the 10 minute duration of data sets recorded elsewhere the same PPM was used, excluding Step 1).

Test	Duration of Test (secs)	Wind Speed (m/s) Avg	Test Condition
001	62	4.5-4.6	Background
002	123	4.7-4.9	Foot Stomp at mid-level platform: 0, 30, 60s
003	84	4.7-4.9	Lift from mid to top level
004	93	4.9	Foot Stomp at top level platform: 5, 35, 65s
005	22	4.9	Tower wall hand slap at yaw room
006	224	4.9-4.8	Lift from yaw room to ground level
007	40	4.8-5.0	Tower wall hand slap at ground level
008	185	4.8-5.0	Background – 3mins
009	128.5	5.0	Turbine start: connected 80-90s
Break for Lunch			
010	342.5	3.4-3.5	Turbine Running – Very low wind
011	184.5	3.4-3.5	Turbine Running – Very low wind
012	154.5	3.4-3.5	Turbine Running to stop
013	307.5	3.5-3.8	Background (all stop)
014	528	3.8-3.1	Clockwise yaw (0.5deg per second)
015	25	3.8-3.1	Yawing to stop
016	450	3.1	Anti-clockwise yaw
017	308	3.1-3.0	Background
018	190	3.0-3.2	Background
019	223	3.0-3.2	Off to Start – Low wind 3m/s
020	323	3.2-3.0	Running – Low wind
021	60	3.0-3.4	Running L- Low wind 3.9 m/s
022	267	3.4-4.6	Running 4-5m/s

Table 8 - Log of tests run at turbine S6 on the 21st June 2012.

Test	Duration of Test (secs)	Wind Speed (m/s) Avg	Test Condition
001	308	5.9	Running
003	100	5.9-4.7	Turbine turned off
004	309	5.9-4.7	Background
005	205	4.7-5.5	Turbine started up (14s)
006	246	4.7-5.7	Running
007	314	5.7-5.6	Turbine stopping
008	185	5.7-5.6	Yaw clockwise
009	185	5.7-5.6	Yaw anti-clockwise
010	62	5.4-5.3	Background, short test

Table 9 - Log of tests run at turbine S6 on the 22nd June 2012.

3.4 Statistical analysis

Following the processing of each of the measurement surveys the data is subjected to statistical analysis. Over the duration of each measurement there will be results that are not indicative of the seismic vibration produced by wind turbines due to sensor interference by such events as animal ingress. Datasets were binned into 1 ms^{-1} wind speed bins and the interquartile mean calculated at each discrete frequency; this effectively removes outlying data falling outside of the interquartile range. Data collected at sensor AEG-2b/6099 for a wind speed of 12 ms^{-1} is shown in Figure 13. The mean, median, interquartile mean calculated at discrete frequencies and the interquartile mean calculated based on the -3dB peak gain of the frequency-distance weighting filter (1.71 to 5.76 Hz band) were calculated for the whole dataset. It can be seen in Figure 13 that the mean level is significantly higher than the median and interquartile mean indicating that the data is not symmetrically distributed and carries a high contribution from outliers in the dataset. The interquartile mean however is comparable to the median showing that the elimination of data sets outside of the interquartile range presents a stable dataset. Furthermore interquartile means calculated at discrete frequencies and across a frequency band produce similar results. The authors therefore believe that the interquartile mean calculated at discrete frequencies is a robust approach to calculating seismic vibration amplitude produced by wind turbines and this method is used in the following presentation of results. All interquartile amplitude reported below were based on data recorded when entire wind farms were active (i.e. all four turbines at Craig, 26 at Dun Law and 152 at Clyde).

In addition, the 25th and 75th percentile can also be seen in Figure 13 both exhibiting the characteristic shape observed by the median. This increases the robustness of the statistical analysis indicating the band between the 25th and 75th percentile produces data free from contribution due to outliers. The results shown in Figure 13 are representative of statistical analysis of the other datasets from the remaining sensors from Craig wind farm and those used at Clyde and Dun Law wind farms.

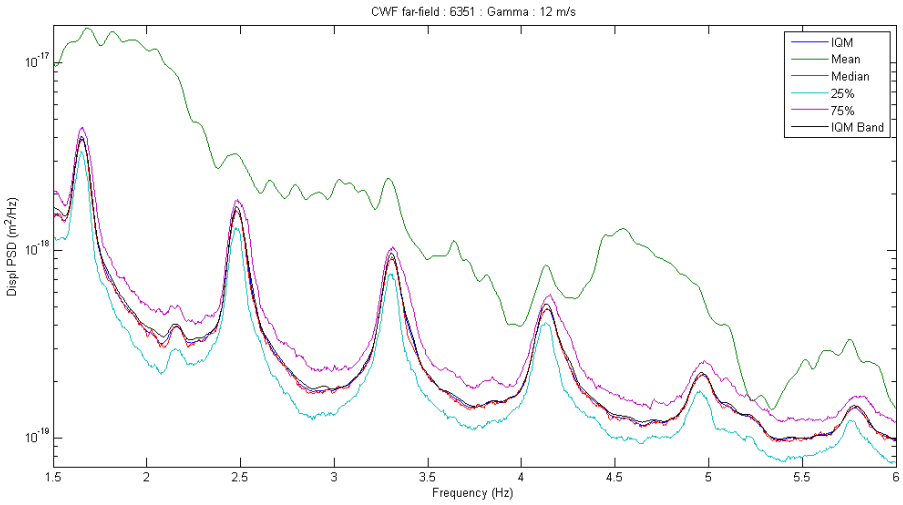

Figure 13 - Statistical analysis of data recorded from sensor AEG-5/6351 at Craig wind farm with a wind speed of 12ms^{-1}. The mean, median and interquartile mean calculated at discrete frequencies (IQM) and the interquartile mean calculated using rms amplitude across the 1.71 to 5.76 Hz band (IQM Band) are presented. The higher level mean is due to contribution from outliers in the data set. The similarity between the median and the interquartile mean indicates the outliers fall beyond the limits of the 25th and 75th percentiles, both of which are also shown and carry the same characteristic topology as the median and interquartile mean.

3.5 Results

The following sections present the seismic ground vibrations produced by wind turbines for each of the sites investigated. These are provided as plots of displacement PSD. The vertical axis, or perpendicular to ground surface for datasets that are converted to propagation coordinates, gamma (γ), is used to show the dependency of the resultant seismic vibration on wind speed. A comparison of the three axes from the sensor of interest is then shown for data recorded at a wind speed of 11.5 to 12.5 ms^{-1}. The wind speed at 11.5 to 12.5 ms^{-1} was determined to be the primary wind speed of interest as part of Phase 0 (Doc ref. *FMB_102_TRPO_V6*) due to the wind turbines investigated approaching rated power. At greater speeds the number of available data sets falls rapidly and the background noise increases. While key results from sensors of interest are presented in the following sections, results from the remaining sensors are provided in Appendix B.

3.5.1 DUNLAW

Of the ten sensors placed linearly for far-field measurements collected at Dun Law, the information recorded at Kelphope 2 (1391 m from the closest turbine) provided the dataset most representative of seismic vibrations produced by wind turbines (i.e. the sensor with the best turbine signal to background noise ratio). Results from Kelphope 1 also had high signal to noise ratio, however a problem with the digitiser used to record the seismic vibration made the data unusable. An attempt to remove the digitiser related signal from Kelphope 1 dataset using a linear interpolation of the frequency domain data proved to be unstable when applied to the whole dataset. Signal to noise ratios at the other Dun Law sensors were too low to provide useful wind turbine data. Results presented here are based on the Kelphope 2 dataset only.

The Dun Law data was processed in propagation coordinates. Figure 14 shows the interquartile of the displacement PSD from Kelphope 2 for the γ-axis at wind speeds of 4 - 17 ms^{-1} in 1 ms^{-1} increments. In general the spectra contain peaks that coincide with multiples of the blade pass frequency of the V47 wind turbines. The amplitudes of these peaks increase with wind speed and move to higher frequencies (related to the increase in rotor speed and related blade pass frequency at higher wind speed). As the wind speed approaches 17 ms-1 the peaks become less distinguishable as the background noise also rises with wind speed (Figure 14).

At 11.5 to 12.5 ms^{-1} a total of 231 10 minute interval datasets were used resulting in an interquartile mean with 5 distinct peaks visible up to a frequency of 8 Hz. The precise frequencies and magnitudes of displacement PSD reached are given in Table 10. The interquartile mean displacement PSD for each of the axes, in propagation coordinates, recorded at Kelphope 2 are shown in Figure 15. In general most power is contained in peaks of the spectra orthogonal to the ground surface (γ). Significant power is also noted in the axes parallel to the surface (α-direction of travel and β transverse direction) at 6 Hz (Figure 15).

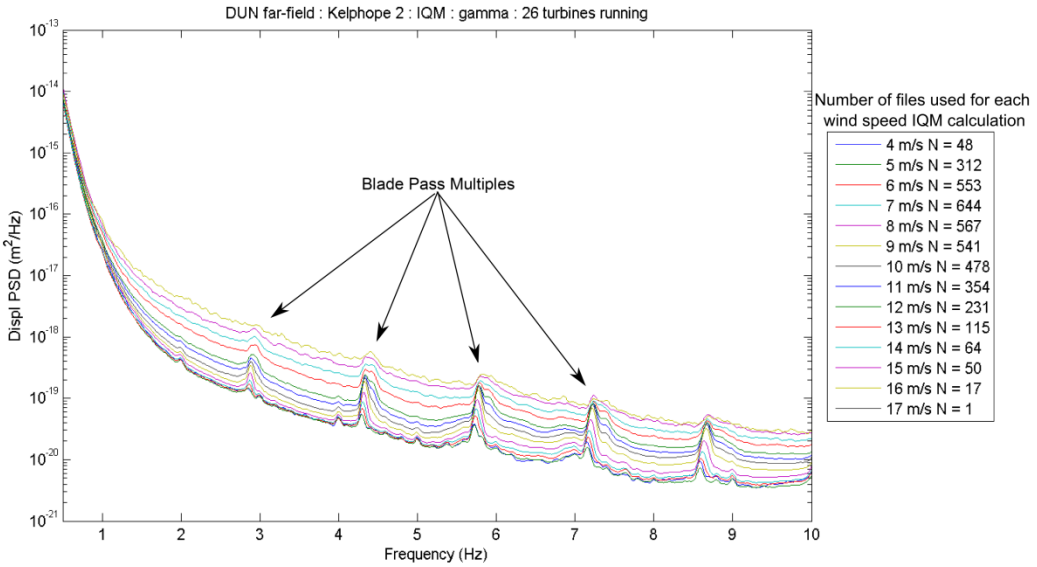

Figure 14 - Interquartile mean of displacement PSD data recorded at Kelphope 2 with all 26 turbines running. Data is presented in 1 m/s increments with the number of files used for each calculation noted. Peaks at regularly spaced intervals are attribued to multiples of the blade pass frequency

Dun Law : Kelphope 2	
Frequency (Hz)	Displ PSD (m^2/Hz)
2.91	5.19E-19
4.34	2.40E-19
5.79	1.61E-19
7.23	8.23E-20

Table 10 - Frequencies and magnitudes of peaks present in the interquartile mean displacement PSD at Kelphope 2, γ-axis and a wind speed of 11.5 to 12.5 ms^{-1}.

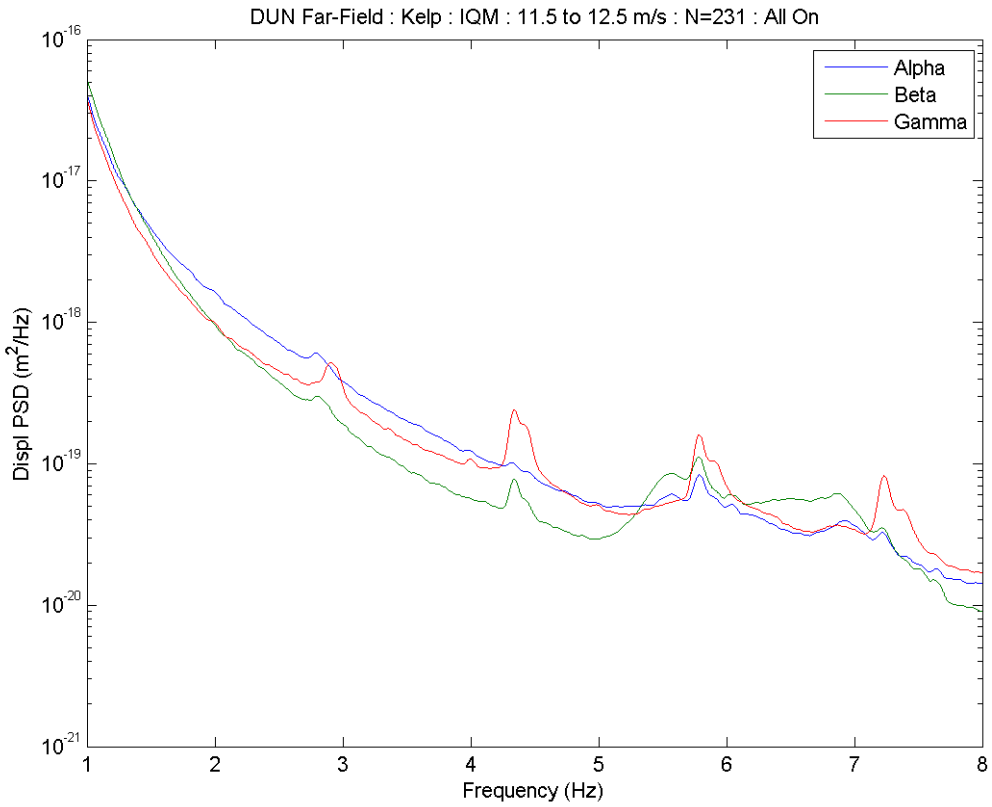

Figure 15 - Comparison of α,β,γ axes interquartile mean displacement PSD recorded at Kelphope 2, Dun Law wind farm and a wind speed of 11.5 to 12.5 ms^{-1}.

3.5.2 CRAIG WIND FARM

3.5.2.1 Far-field survey

Data from Craig wind farm was rotated into axes related to normal to ground surface (γ), direction of travel (α) and transverse direction (β). Of the eight sensors positioned radially around Craig wind farm, AEG-2b/6099 and AEG-5/6351 provided the dataset most representative of seismic vibrations produced by wind turbines datasets. This result was also found in Phase 0 of this project (Doc ref. *FMB_102_TRPO_V6*) where results were reported for axes that were vertical, east and north.

The seismic vibration produced increases with wind speed, Figure 16 and Figure 17 for sensors AEG-5/6351 and AEG-2b/6099 respectively. Peaks coincide with multiples of blade pass (denoted by black dots) and their amplitude increase with wind speed. The frequencies of these peaks also increase with wind speed reflecting the increased rotor speed and related blade pass frequency. A peak is noted at 2.1 Hz recorded at both AEG-2b/6099and AEG-5/6351 that does not increase frequency with wind speed and does not coincide with a multiple of the blade pass frequency (Figure 16 and Figure 17). This 2.1 Hz peak is interpreted as relating to a structural resonance in the N80 wind turbines.

It is sensor AEG-2b/6099that exhibits the most pronounced peaks, with 7 distinguishable peaks below 6 Hz up to a wind speed of 12 ms^{-1}. The frequencies and magnitudes of these peaks are given in Table 11 for AEG5/6351. Spectra of α-, β- and γ-directions for AEG-5/6351 and AEG-2b/6099 are shown in Figure 18 and

Figure 19 respectively. Generally, the direction orthogonal to the ground surface (γ) have seismic peaks with the greatest power, though there are strong vibrations at 4.7 Hz and 5.3 Hz that have no γ component (Figure 19). The strong vibrations at 4.7 Hz and 5.3Hz are seen on the β component.

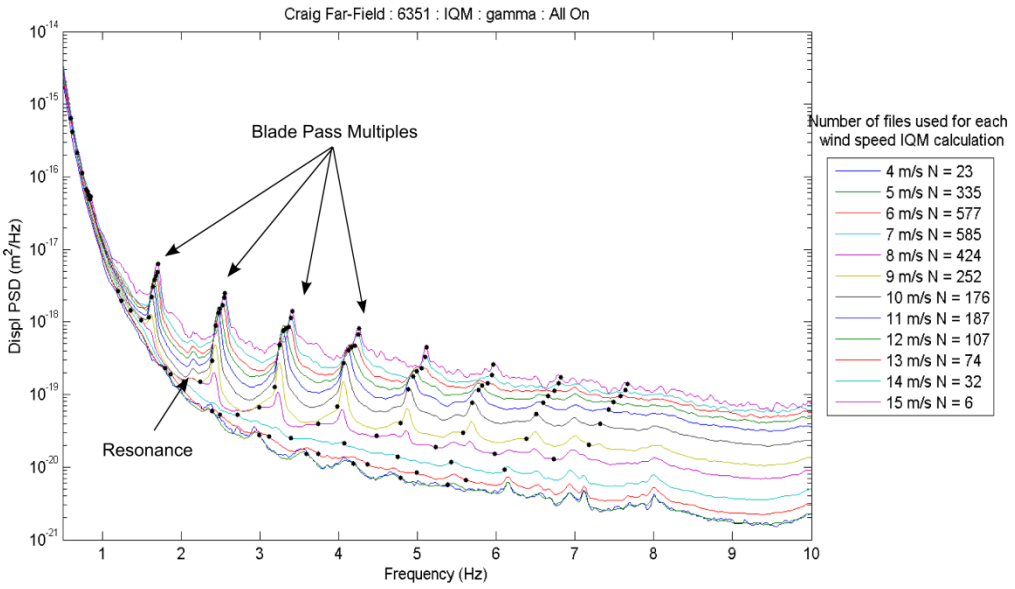

Figure 16 - Interquartile mean of displacement PSD data recorded at AEG-5/6351 with all 4 turbines running. Data is presented in 1 m/s increments with the number of files used for each calculation noted. Peaks at regularly spaced intervals are attribued to multiples of the blade pass frequency while the lower magnitude peak at 2.14 Hz is the result of a structural resonance. The black dots indicate multiples of blade pass frequency from the rpm data.

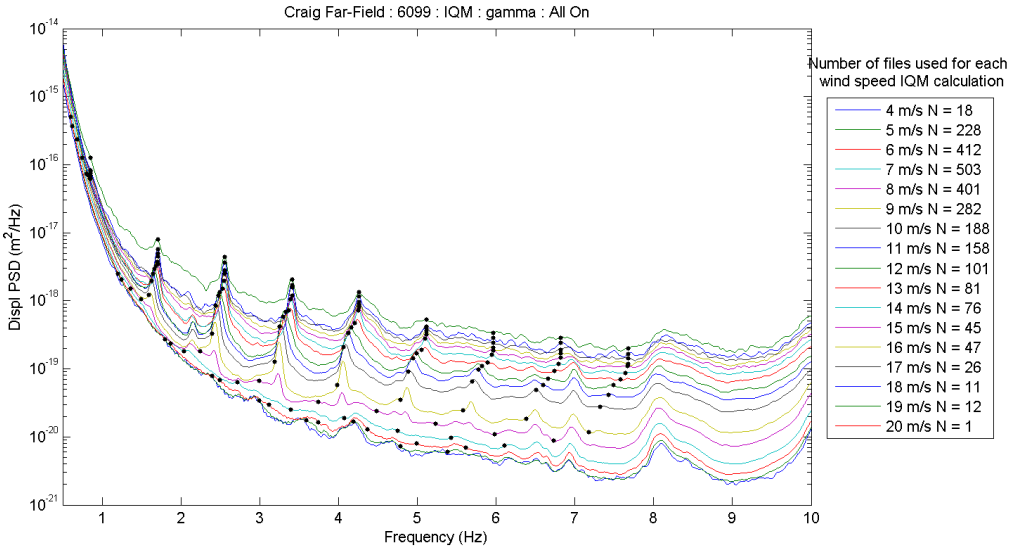

Figure 17 - Interquartile mean of displacement PSD data recorded at AEG-2b/6099 with all 4 turbines running. Data is presented in 1 m/s increments with the number of files used for each calculation noted. The black dots indicate multiples of blade pass frequency from the rpm data.

CWF : 6351	
Frequency (Hz)	Displ PSD (m^2/Hz)
1.65	3.93E-18
2.16	3.93E-19
2.48	1.62E-18
3.31	8.99E-19
4.14	4.85E-19
4.97	2.15E-19
5.78	1.44E-19

Table 11 - Frequencies and magnitudes of peaks present in the interquartile mean displacement PSD at AEG-5/6351, γ-axis at a wind speed of 11.5 to 12.5 ms^{-1}.

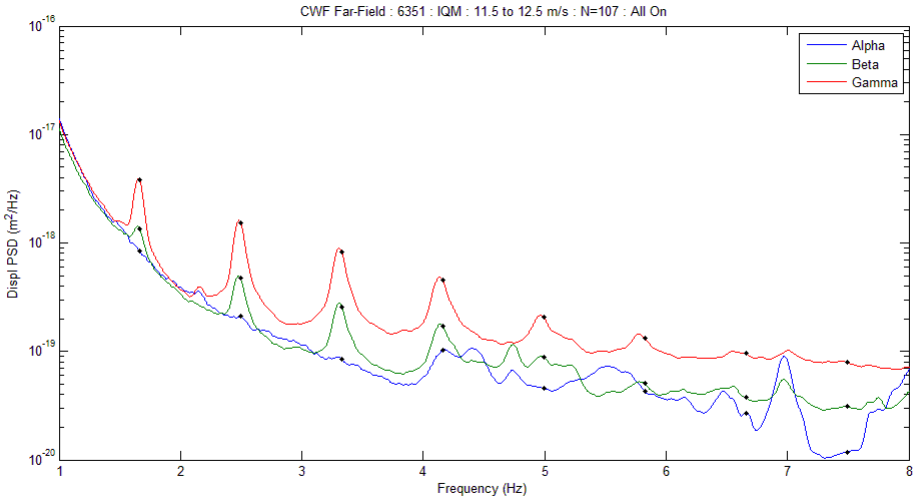

Figure 18 - Comparison of α,β,γ axes interquartile mean displacement PSD recorded at AEG-5/6351, Craig wind farm at a wind speed of 11.5 to 12.5 ms^{-1}. The black dots indicate multiples of blade pass frequency from the rpm data.

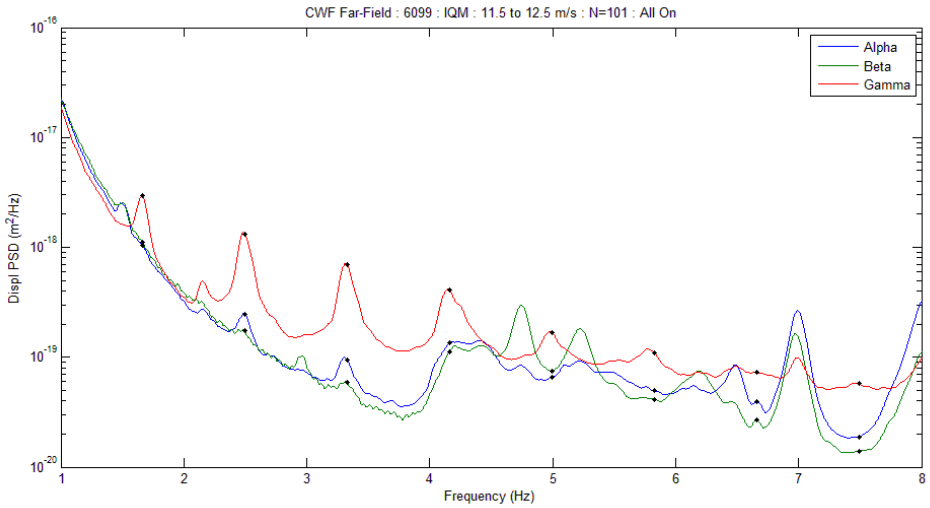

Figure 19 - Comparison of α,β,γ axes interquartile mean displacement PSD recorded at AEG-2b/6099, Craig wind farm at a wind speed of 11.5 to 12.5 ms^{-1}. The black dots indicate multiples of blade pass frequency from the rpm data.

3.5.2.2 On-tower survey

Craig wind farm had two periods in which on-tower measurements were carried out. The first period taking place in 2011, coinciding with the far-field measurements presented above. A sensor was positioned on the foundation of T1 which was fitted with a SQT device vibration mitigation device. The motivation of this survey was to correlate on tower measurements with far-field measurements. The results of the on-tower and far-field measurement will be discussed in Section 3.7.

The second on-tower survey was conducted in 2012 and involved the placement of sensors on the foundations of turbines T1, T3 and T4. The vibration of turbine T1 is not representative of a standard turbine as it includes an SQT vibration mitigation device that was targeted to reduce vibration in the 4-5 Hz band. The SQT moved vibration power out of this frequency band so that it vibrates in a very different way to T3 and T4 (Figure 20). Results from T3 which are more representative of standard N80 wind turbines will therefore be used to discuss on-tower vibrations measured at Craig wind farm.

Figure 21 shows the relationship between displacement PSD and wind speeds across 1 ms^{-1} wind speed bin from 5 to 15 ms^{-1} with peaks of interest identified and shown in Table 12. Generally the amplitudes of peak vibrations increase with wind speed, though this relationship is not as consistent as noted in the far-field (Figure 17). An example of this inconsistency is the peak at 1.3 Hz at 5ms^{-1} which reduces in amplitude and moved at 1.4 Hz at 6 ms^{-1}.

A fundamental difference between the on-tower vibration and that measured in the far-field is that the on-tower vibration has significantly more power in the horizontal direction than the vertical direction (Figure 22 and Figure 18). The power in the down-wind direction tends to be an order of magnitude greater than the cross-wind direction and two orders of magnitude greater than the vertical direction (Figure 22). The cross-wind vibrates with significant power at 4.7 and 5.3 Hz (Figure 22), which are frequencies noted in the far-field as having significant horizontal vibration on the β component.

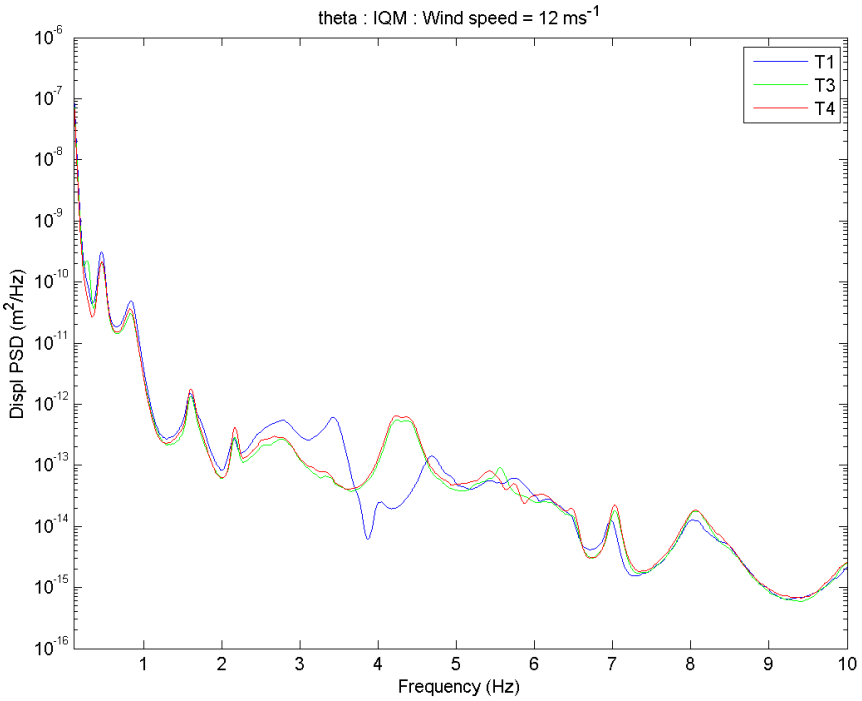

Figure 20 – Comparison of interquartile mean displacement PSD measured at the base of T1, T3 and T4 horizontal component parallel to wind direction at a wind speed of 11.5 to 12.5 ms^{-1}. The difference in spectra between Turbines T3 and T4 with that of T1 is due to the SQT device in T1 that was targeted to mitigate vibration 4 to 5 Hz band.

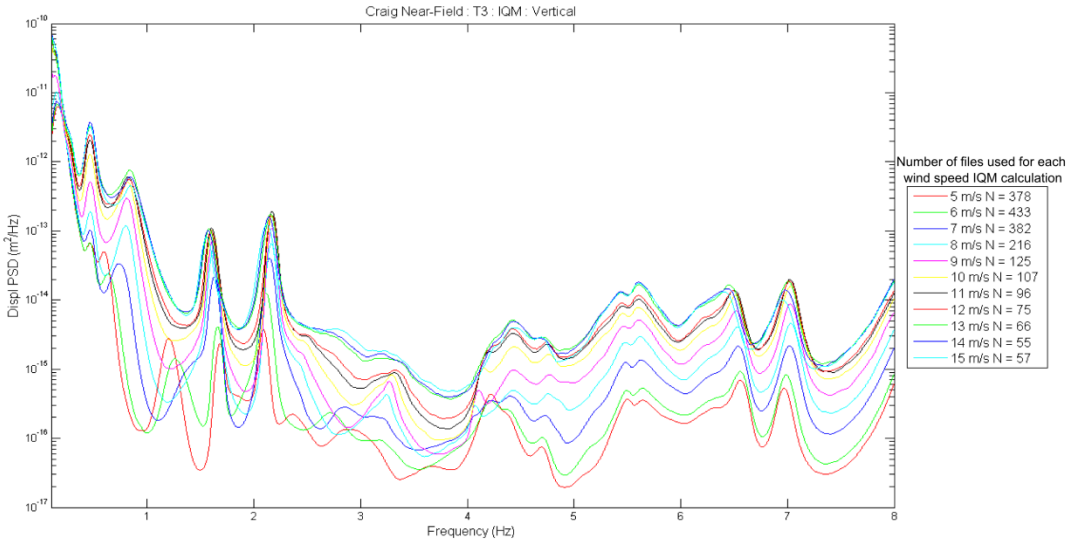

Figure 21 - Interquartile mean of displacement PSD data recorded at the foundation of T3. Data is presented in 1 m/s increments with the number of files used for each calculation noted.

CWF : T3 Foundation	
Frequency (Hz)	Displ PSD (m^2/Hz)
0.46	2.45E-12
0.83	5.56E-13
1.60	1.01E-13
2.17	1.73E-13
3.33	9.71E-16

Table 12 - Frequencies and magnitudes of peaks present in the interquartile mean displacement PSD at T3, vertical axis at a wind speed of 11.5 to 12.5 ms^{-1}.

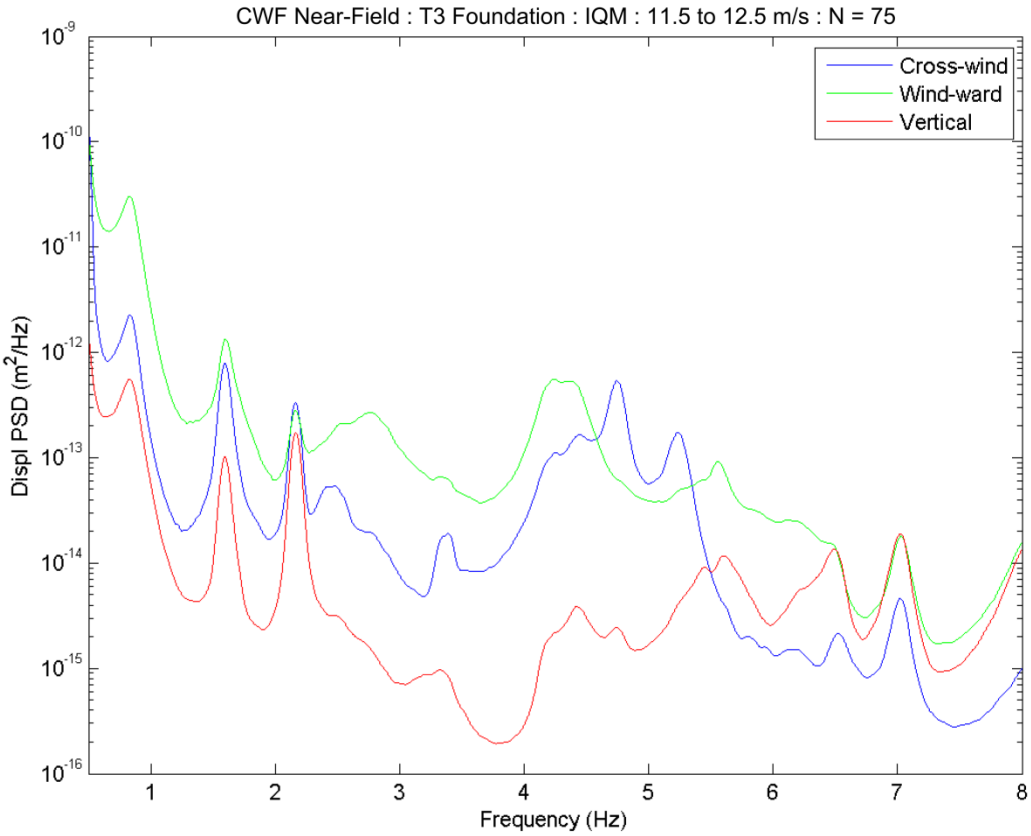

Figure 22 - Comparison of interquartile mean displacement PSD for all three axes recorded at the foundation of T3, Craig wind farm.

3.5.3 CLYDE WIND FARM

Four sensors were used to measure Clyde wind farm extending linearly from turbine T39 (Figure 5). While T39 was the target of the survey performed by Grontmij, the remainder of the wind farm was active so contributions from over 100 turbines were recorded at each sensor. The Clyde wind farm covers a vast geographic region that can experience a variety of wind speeds and directions in any 10 minute interval. To allow comparison of spectra from the Clyde wind farm to far-field spectra recorded at Craig and Dun Law, the Clyde dataset has been cut such that only 10 minute intervals where wind speeds across the wind farm where within 1 ms^{-1} of that recorded at T39 and when the turbines were rotating within +/- 1 rpm of T39 are used in statistical analysis.

The amplitude of seismic vibration measured at each sensor decreases with increasing distance from T39 (Figure 23). The topology of vertical seismic vibration at sensors 4444, 4445 and 4443 that are 100m, 500m and 825 m from T39 are very similar, while sensor 4442 measured on the hard stand T39 has and different topology.

Spectral peaks measured at sensor 4443 increase with wind speed (Figure 24). However, the increase in frequency at which these peaks occur with wind speed observed at Craig (Figure 16) and Dun Law (Figure 14) was not observed at Clyde wind farm. The Clyde spectra also contain peaks that do not occur on blade pass multiples, such as the peak at 2.8 Hz that contains significant power. Spectral peaks measured at Clyde wind farm have similar power in the vertical direction as the horizontal direction (Figure 25), though the peak at 2.39 Hz tends to be greatest in the vertical direction. A summary of spectral peaks recorded at sensor 4443 are listed in Table 13.

The data recorded on the hard stand of T39 using sensor 4442 (Figure 26) have peaks that generally increase with wind speed, though as for the Craig on-tower measurements, this relationship is inconsistent. The relationship between the peak at ~1.6 Hz and wind speed appears complex (Figure 26) and the frequency at which the peak at ~5.3 Hz occurs tend to decrease with increasing wind speed.

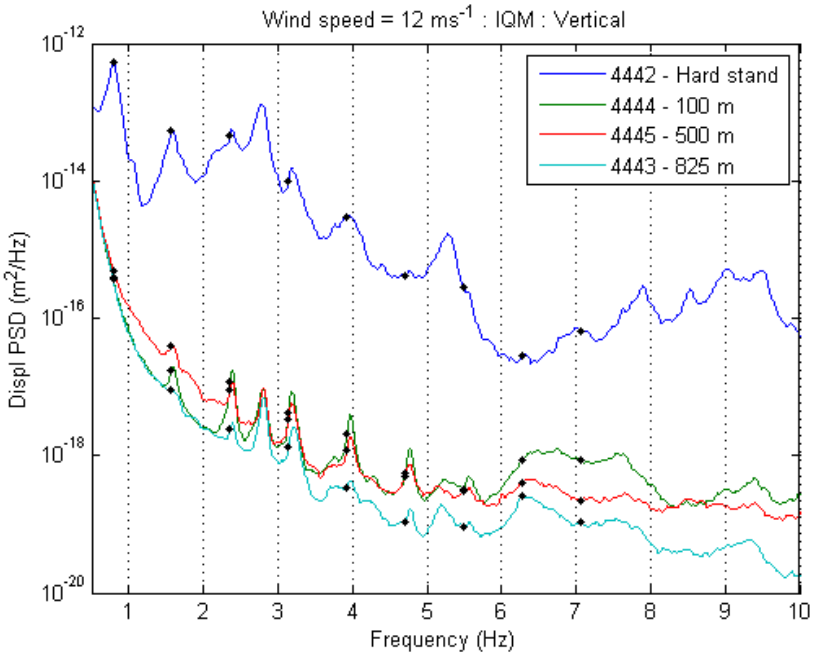

Figure 23 – Comparison of interquartile mean spectra at the four sensors used to measure Clyde wind farm at a wind speed of 11.5 to 12.5 ms^{-1}. The distances noted in the legend are from the closest wind turbine (T39). The black dots indicate multiples of blade pass frequency from rpm data at T39.

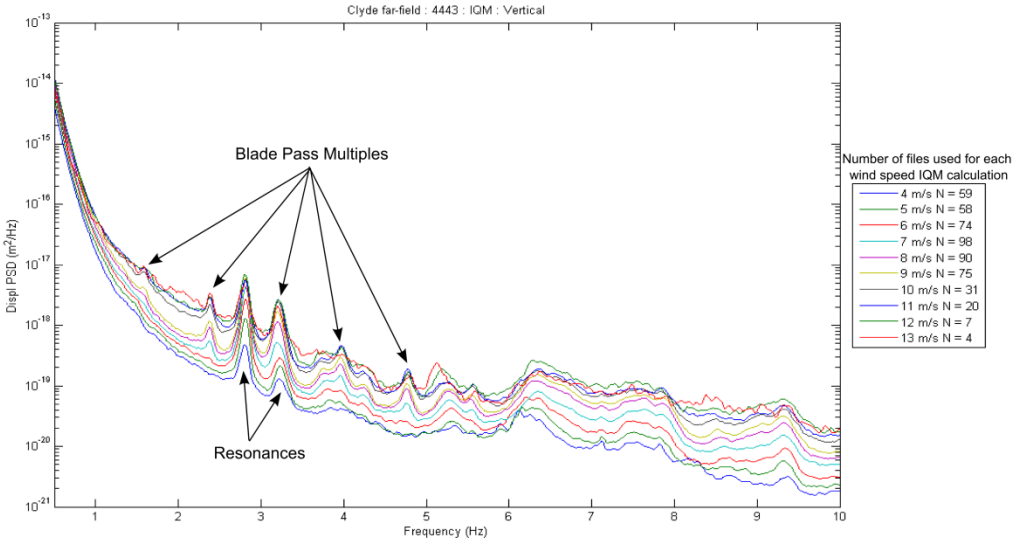

Figure 24 - Interquartile mean of displacement PSD data recorded at 825 m from T39 at Clyde Wind Farm. Data is presented in 1 m/s increments with the number of files used for each calculation noted. Peaks at regularly spaced intervals are attribued to multiples of the blade pass frequency while the lower magnitude peaks at 3.21 Hz and 3.98 are the result of structural resonances with the 3.98 Hz resonance coinciding with a blade pass multiple.

Clyde: 4443	
Frequency (Hz)	Displ PSD (m^2/Hz)
1.60	9.06E-18
2.39	2.97E-18
2.79	6.55E-18
3.21	2.57E-18
3.98	4.34E-19
4.78	1.68E-19
5.20	1.91E-19
5.57	1.07E-19

Table 13 - Frequencies and magnitudes of peaks present in the interquartile mean displacement PSD 825 m from T39, vertical axis at a wind speed of 11.5 to 12.5 ms^{-1}.

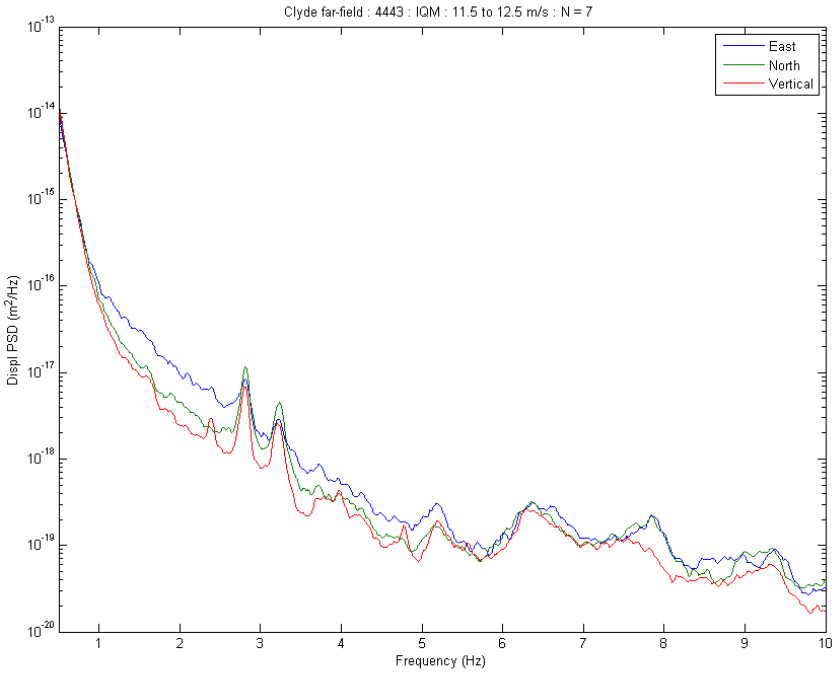

Figure 25 - Comparison of interquartile mean displacement PSD for all three axes 825 m from T39, Clyde wind farm at a wind speed of 11.5 to 12.5 ms^{-1}.

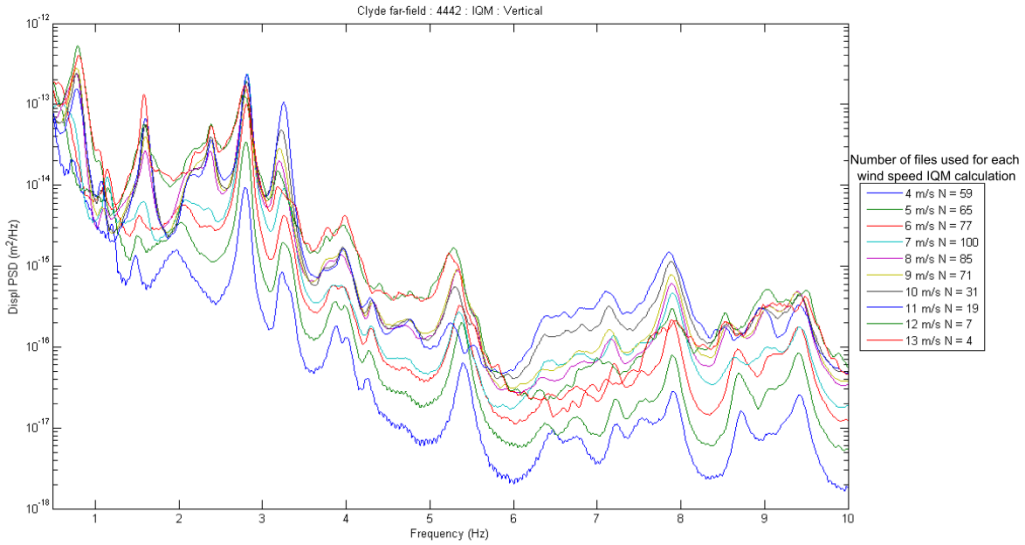

Figure 26 - Interquartile mean of displacement PSD data recorded at the hardstand of T39 at Clyde wind farm. Data is presented in 1 m/s increments with the number of files used for each calculation noted.

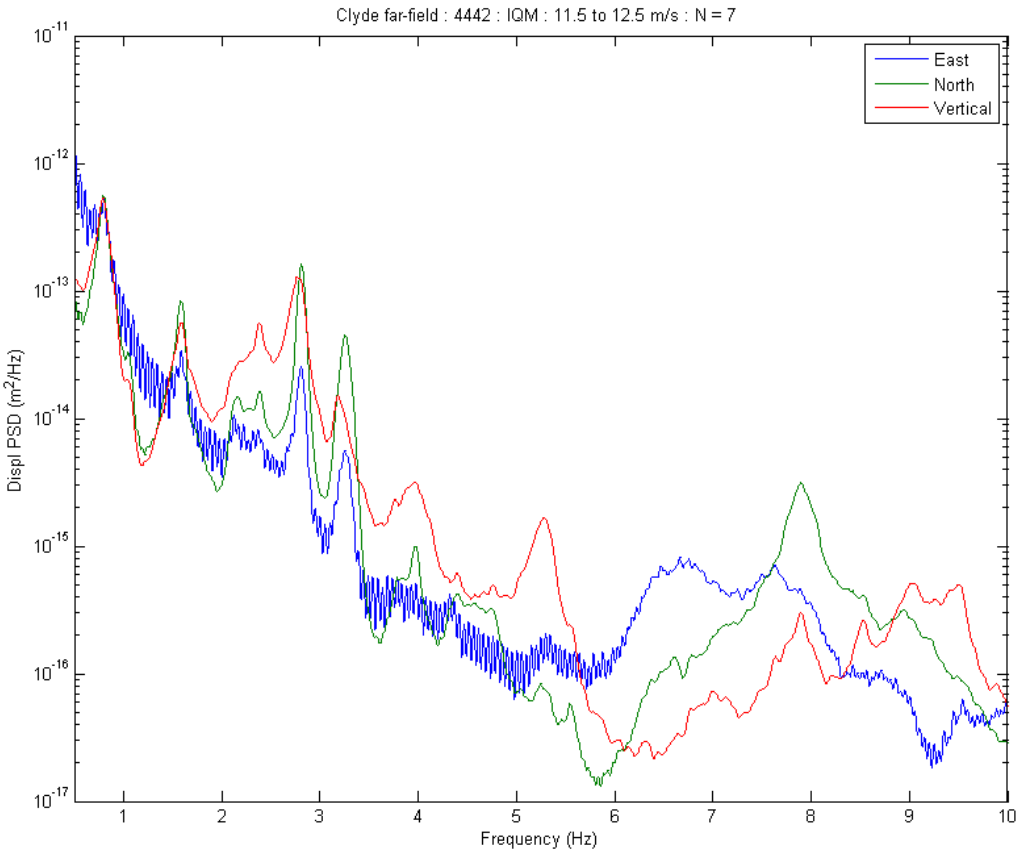

Figure 27 - Comparison of interquartile mean displacement PSD for all three axes at the hardstand of T39, Clyde wind farm at a wind speed of 11.5 to 12.5 ms^{-1}. It is apparent that the East axis experiences some interference. With the interference only being observed on the East axis indicates a faulty sensor output for this axis.

3.5.4 ST SEINE-L'ABBAYE

The measurements described above were carried out with similar experimental setups with measurement periods running continuously from 22 days at Craig wind farm on Tower survey up to 93 days at Dun Law far-field survey. The investigation at St Seine-l'Abbaye differed in both sensor type and measurement duration. The St Seine-l'Abbaye survey used Syscom geophones instead of the Guralp seismometers. As outlined in Section 3.3.1.2 the St Seine-l'Abbaye measurements were far shorter in duration (60-528 seconds) and spread over 2 days. The resulting data sets were captured during limited wind speeds, typically 3-6 ms^{-1}. It is therefore not possible to compare the dependency on wind speed of the near-field seismic vibration produced from the Vestas V90 turbines at St Seine-l'Abbaye. The resulting displacement PSD for each of the three axes is presented in Figure 28 for a wind speed of 4.7 to 5.7 ms^{-1}.

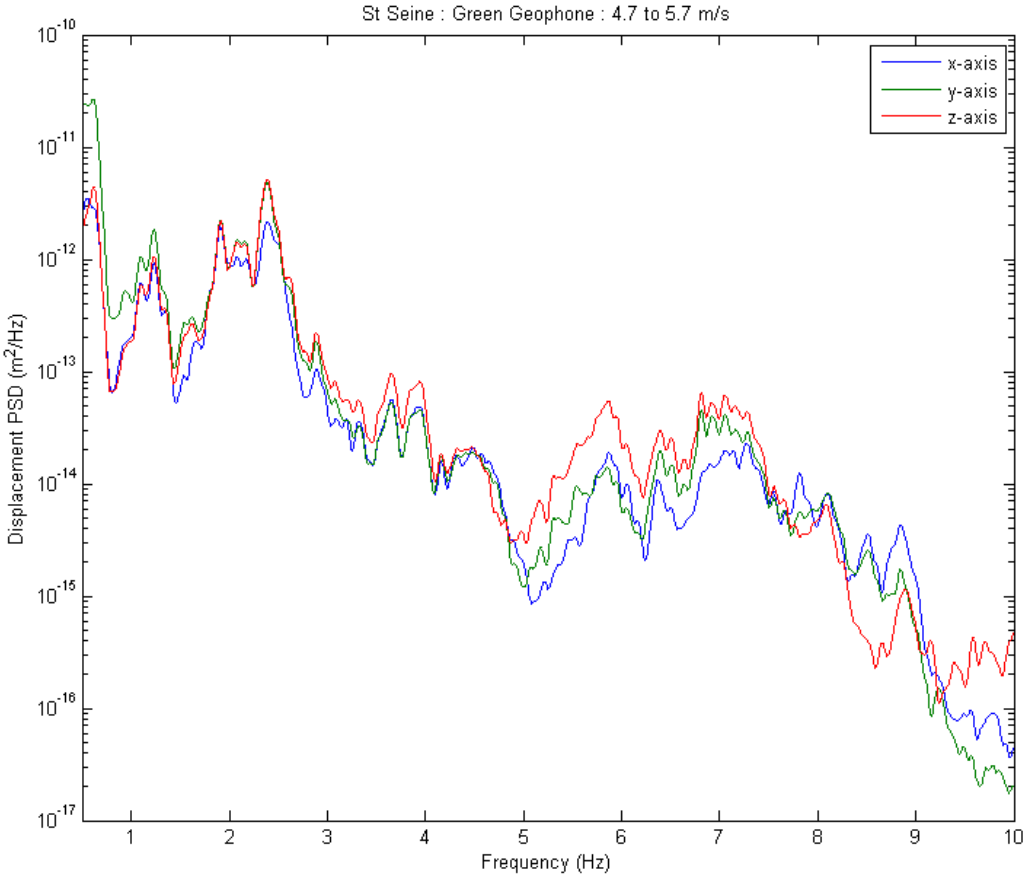

Figure 28 - Comparison displacement PSD for all three axes from the foundation of a Vestas V90, St Seine-l'Abbaye wind farm.

3.6 Azimuth effect

3.6.1 DUN LAW

To determine whether the seismic amplitude varies with azimuth (angular position) relative to the wind direction and the related wind turbine rotor plane, data from Dun Law was binned by wind speed and direction. The sensor at Kelphope 2 was located 52° from true north relative to Dun Law wind farm, which was close to right angles from the prevailing wind direction (Figure 29).

The size of the wind speed bins were 1 ms^{-1} and the size of the wind direction bins are 20°. The data in each bin is relatively sparse, particularly in those away from the prevailing wind direction. To increase the size of the datasets rotation symmetry was assumed so that the up-wind and down-wind bins were combined into a "in-line" with wind dataset and the two bins perpendicular to the wind direction were combined into a "cross-wind" data set (Figure 29).

The rms amplitude was calculated for the -3dB peak gain of the frequency-distance weighting filter (1.71 to 5.76 Hz band) for all spectra in each bin and results outside of a defined percentile range excluded as outliers. Several percentile ranges were examined and the inner 80% was found to best exclude outliers while preserving the most data. The mean was then taken of the inner 80% resulting in spectra for when the sensor was in-line with the wind and at right angles to the wind (cross-wind). Figure 30 shows the resulting spectra comparing in-line and cross-wind data sets recorded in wind speeds of 8 ms^{-1}. The amplitude measured when the sensor is in-line with the wind direction is greater than when the sensor is in a cross-wind position. The rms amplitude at 8 ms^{-1} in the -3dB peak gain band is 0.794 nm measured in-line with the wind and 0.689 nm when the sensor was in a cross-wind position.

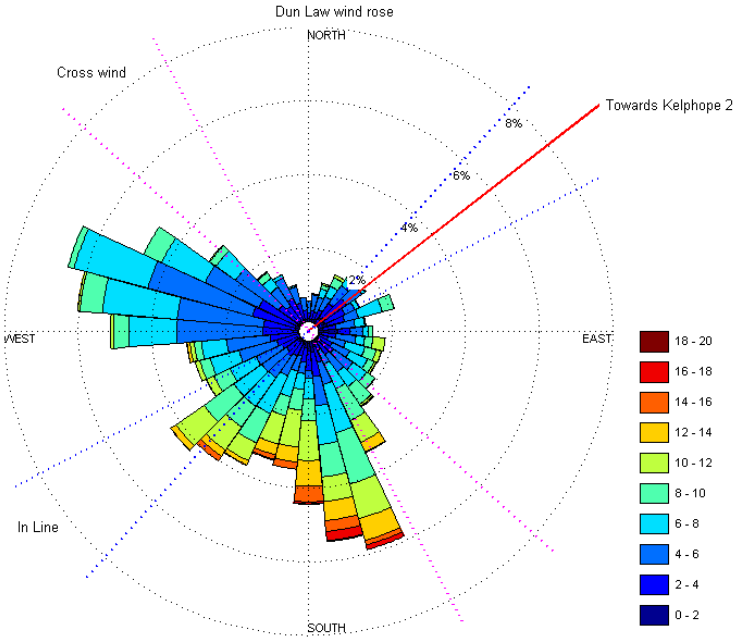

Figure 29 – Wind rose from wind speed and direction data recorded during the 2004 Dun Law survey. The direction to the sensor at Kelphope 2 is shown as are the wind direction sectors and the lines to define "In-line" with the wind and the "cross-wind" directions.

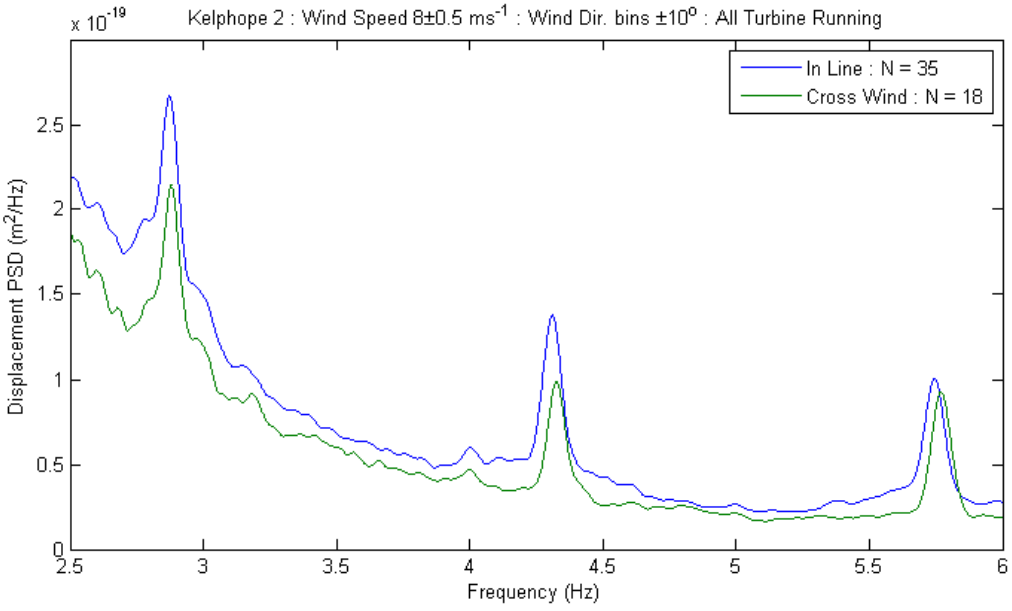

Figure 30 – Spectra formed by taking the mean of data in the inner 80% of the In-line (up-wind or down-wind) and cross-wind data sets measured at Kelphope 2 near the Dun Law wind farm in 2004. The N in the legend represents the number of 10 minute measurements that lie within the inner 80% of the dataset.

3.6.2 CRAIG WIND FARM

To determine whether the seismic amplitude at Craig wind farm varies with azimuth relative to the wind direction and the related wind turbine rotor plane, data was binned by wind speed and direction. This follows the same method as describe for the azimuth effect analysis of the Dun Law data described above (see Section 3.6.1). Sensor AEG5/6351 was placed 12.3° from true north relative to the centre of the Craig wind farm, which is close to being directly down-wind from the prevailing wind direction (Figure 31).

Several percentile ranges were examined and the inner 90% was found to best exclude outliers while preserving the most data. The seismic amplitude measured in-line with the wind direction is greater than that measured in a cross-wind position (Figure 32). The rms amplitude in the -3dB peak gain of the frequency-distance weighting filter (1.71 to 5.76 Hz band) measured in-line with the wind was 0.679 nm, while it was 0.492 nm when measured in a cross-wind positions. The seismic amplitude at Craig wind farm was a factor of 1.38 when measured in-line with the wind direction to that when measured at a position at right-angles to the wind direction.

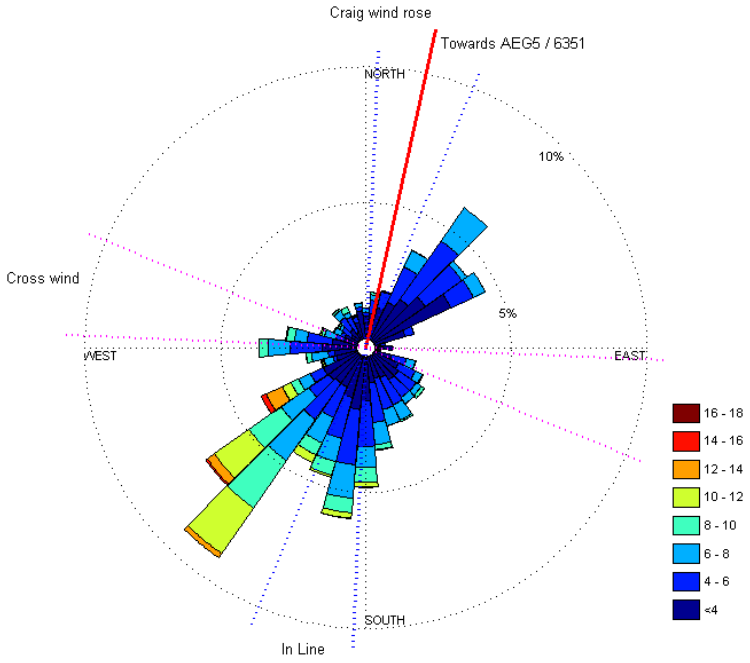

Figure 31 - Wind rose from wind speed and direction data recorded during the 2011 Craig wind farm survey. The direction to the sensor at AEG5/6351 is shown as are the wind direction sectors and the lines to define "In-line" with the wind and the "cross-wind" directions.

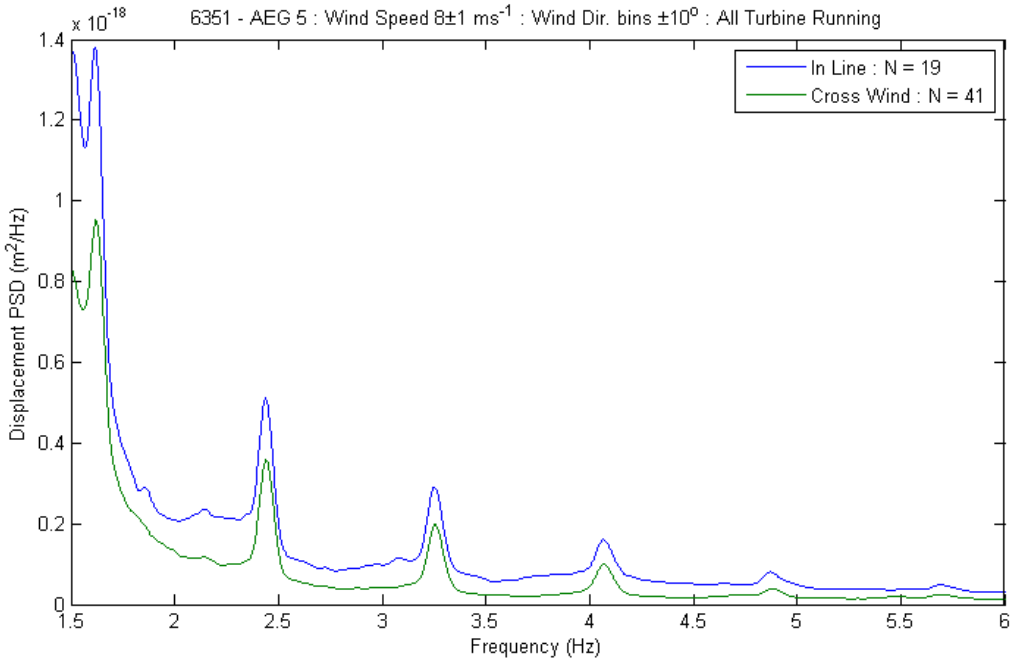

Figure 32 – Spectra formed by taking the mean of data in the inner 90% of the In-line (up-wind or down-wind) and cross-wind data sets measured at AEG5/6351 near the Craig wind farm in 2011. The N in the legend represents the number of 10 minute measurements that lie within the inner 90% of the dataset.

3.6.3 CLYDE

The seismic amplitude at Clyde wind farm was binned by wind speed and direction to examine its variation with azimuth relative to the wind direction and the related wind turbine rotor plane data. This follows the same method as describe for the azimuth effect analysis of the Dun Law and Craig data described above (see Section 3.6.1 and 3.6.2). However, unlike the sensors at Dun Law and Craig which were some distance from the wind farms, the sensors at the Clyde survey were surrounded by the wind farm making it difficult to determine from which direction the highest amplitude seismic vibrations are likely to arrive (Figure 33). The number of turbines within 20° arcs from sensor 4443 are shown in Figure 34 with the greatest numbers lying north and south (Figure 33).

However, the arrival amplitude of seismic vibrations at sensor 4443 will be greatest from the closest turbines which are due east of the sensor. The variation of seismic amplitude with direction will therefore be dependent on the numbers of turbines at each angular position and their distance. To relate the effects of numbers of turbines and their distance each 20° arc was normalised according to equation [1]:

$$N_{norm(r,f)} = \sqrt{\sum_{i=1}^{N}\left(\sqrt{\frac{r_{ref}}{r_i}}\exp\left(-\frac{\pi f(r_i - r_{ref})}{Qc}\right)\right)^2} \quad [1]$$

where N is the number of turbines in each 20° arc at distances r_i from the sensor. The reference distance r_{ref} is 1000 m, f is the frequency in Hz, Q is a factor relating non-geometric attenuation and is equal to 50 for the Southern Uplands and c is the speed of Rayleigh waves taken as 2000 ms^{-1} for the Southern Uplands. Figure 35

shows that when the numbers of turbines and their distance are normalised in this way that the greatest amplitude is expected from the turbines at 110° from sensor 4443, while lower yet still significant amplitudes can be expected from the more numerous though further away turbines due south. To analyse the relationship between azimuth and seismic amplitude sensor 4443 was taken as being 290° from true north relative to the expected maximum contribution direction of Clyde wind farm (i.e. 110° + 180°).

The wind direction had a bimodal distribution during the vibration survey with prevailing winds: 1) from the west where sensor 4443 was directly up-wind, and 2) from due south where the sensor was in a cross-wind position (Figure 36). Several percentile ranges were examined and the inner 90% was found to best exclude outliers while preserving the most data. The seismic amplitude measured in-line and cross-wind positions were similar with slight increases noted for the cross-wind position (Figure 37). The rms amplitude in the -3dB peak gain of the frequency-distance weighting filter (1.71 to 5.76 Hz band) measured in-line with the wind was 1.62 nm, while it was 1.77 nm when measured in a cross-wind positions.

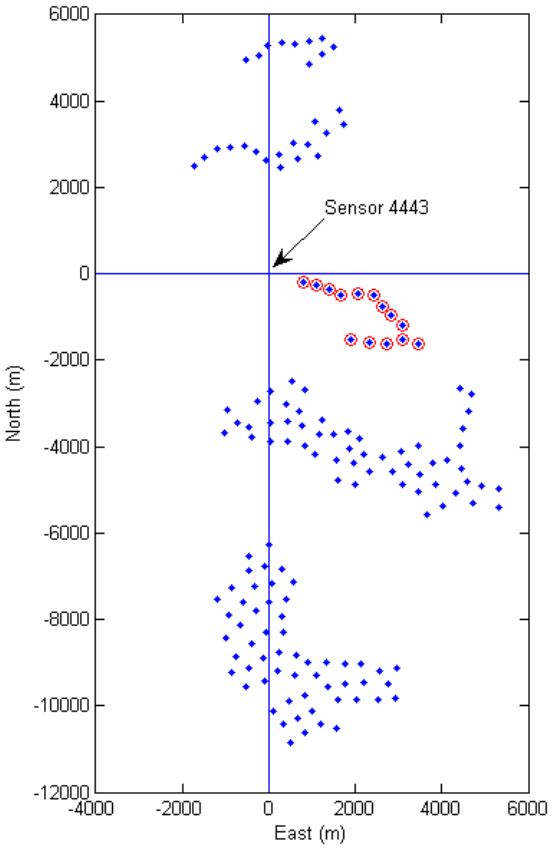

Figure 33 – Wind turbine positions (blue dots) relative to sensor 4443 at Clyde wind farm. While there are significantly more turbines north and south of the sensor, the turbines to the east (circled in red) have a greater influence on the seismic amplitude measured at 4443 due to their proximity.

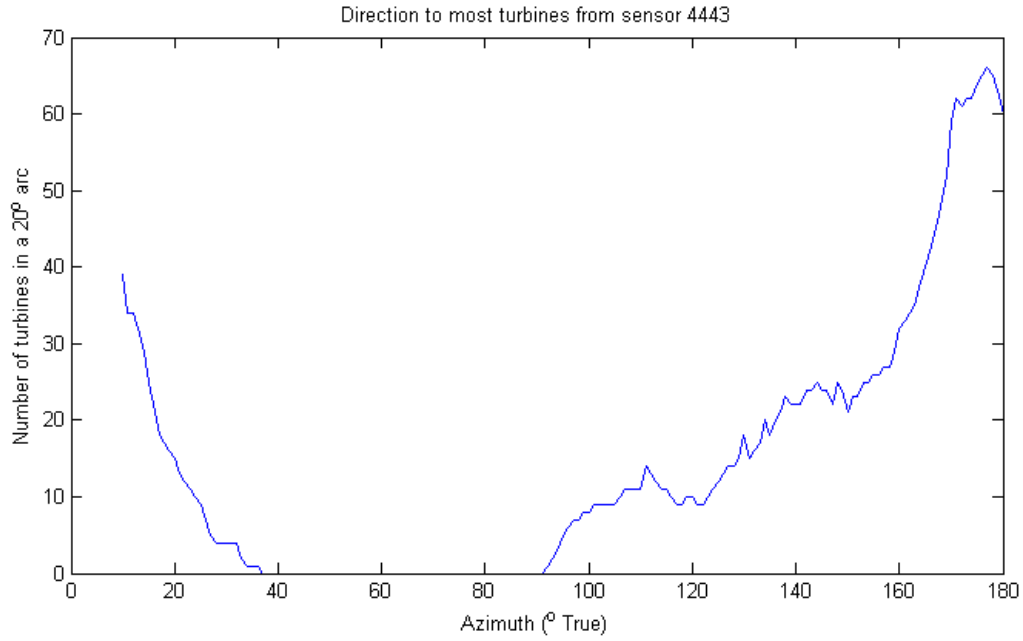

Figure 34 – The number of turbines within 20° arcs measured from sensor 4443. The greatest numbers are north and south of the sensor (in a line running 170° and 350° assuming rotational symmetry). No turbines lie between 40° and 90°, nor 220° and 270°.

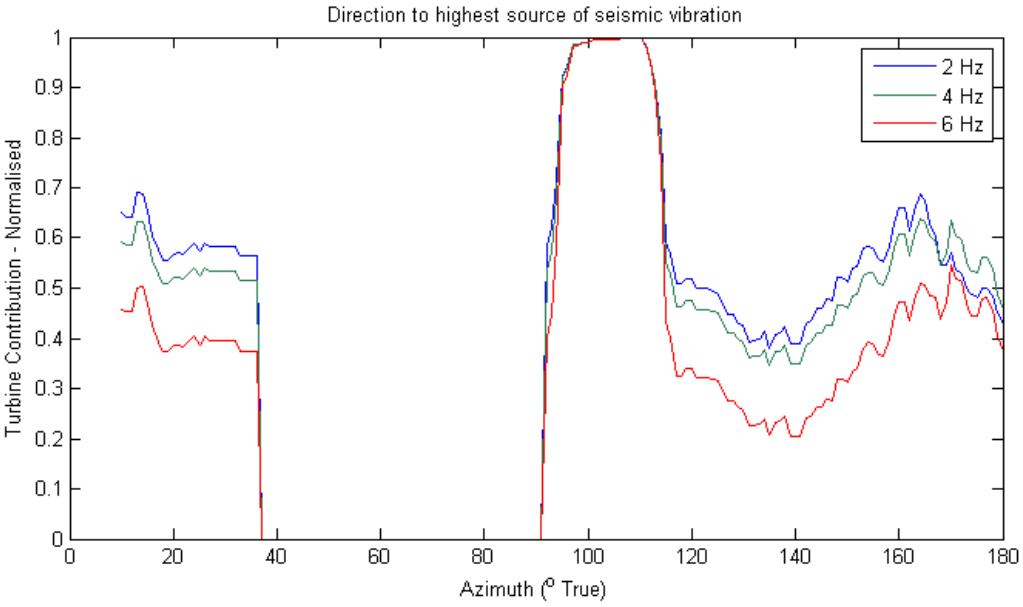

Figure 35 – The number of turbines within 20° arcs measured from sensor 4443 with their proximity considered based on cylindrical spreading and non-geometric attenuation. The non-geometric attenuation is considered for 3 different frequencies. While there are more turbines 170° from the sensor, the proximity of the turbines to the east mean that the greatest amplitude is expected to arrive from 110°. The expected contribution from turbines with angular position have been normalised against the maximum contribution for each frequency (i.e. the maximum direction has a contribution of 1).

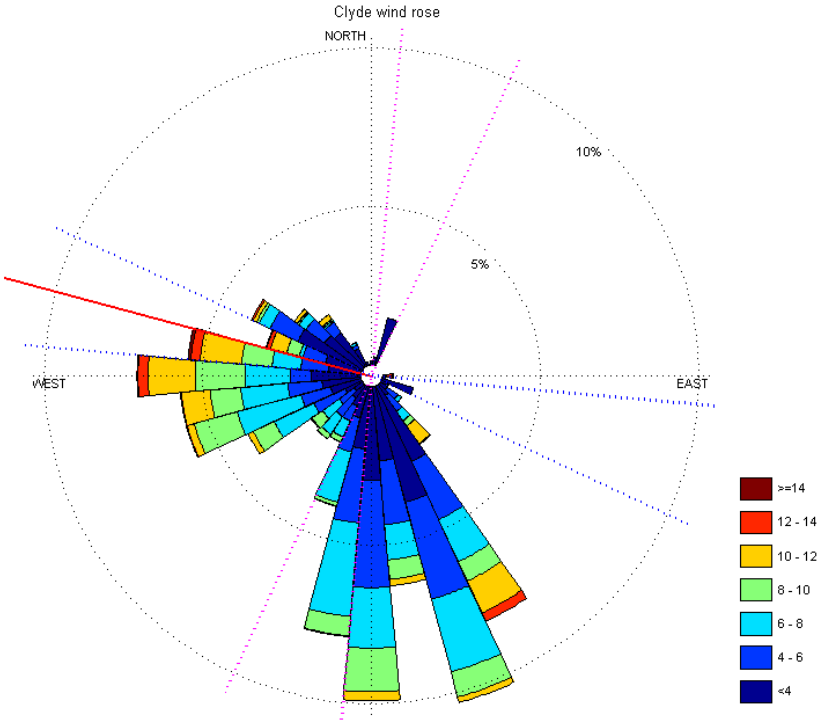

Figure 36 - Wind rose from wind speed and direction data recorded at Clyde wind farm survey. The direction to the sensor at 4443 is shown as are the wind direction sectors and the lines that define "In-line" with the wind and the "cross-wind" directions.

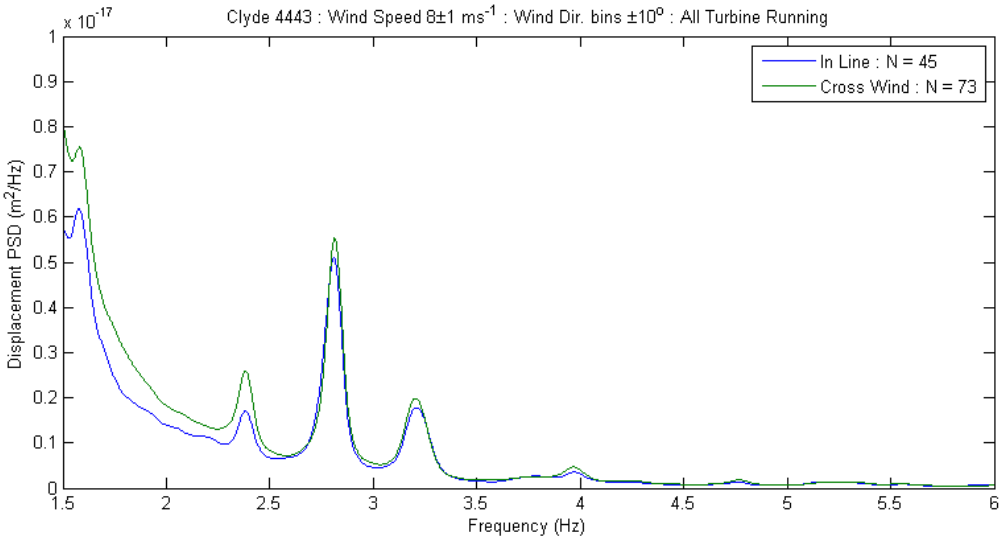

Figure 37 - Spectra formed by taking the mean of data in the inner 90% of the In-line (up-wind or down-wind) and cross-wind data sets measured at sensor 4443 near the Clyde wind farm in 2012. The N in the legend represents the number of 10 minute measurements that lie within the inner 90% of the dataset.

3.7 Discussion

3.7.1 COMPARISON OF FAR-FIELD SPECTRA FROM DIFFERENT WIND TURBINES

The research presented here is to determine whether the seismic vibration produced by Nordex N80 wind turbines and used to estimate the prospect for head room in the budget (see Doc: Doc ref. *FMB_102_TRPO_V6*) is representative of other wind turbines in the Eskdalemuir consultation zone. Seismic wind turbine related vibration measured at Kelphope 2 near Dun Law show similar character to those measured at Craig wind farm with spectral peaks that occur at integer multiples of the blade pass frequency and move to higher frequency at higher wind speeds, related to rotor speed (Figure 14 and Figure 16 and Table 14). The far-field vibration measured at Dun Law and Craig both appear to be with spectral peaks with high power occurring orthogonal to the ground surface (Figure 15 and Figure 18).

Measurements from the Clyde wind farm appear to have different spectral features to those measured at Craig. The spectra include peaks that do not occur at frequencies that are integer multiples of blade pass, such as 2.8 Hz (Figure 24). The 2.8 Hz peak and the 3.2 Hz peak are prominent at 4 ms^{-1} which is a wind speed where the S2.3 turbine is not operational indicating that the peaks are due to structural resonances in the turbine. It is demonstrated with the rpm data that the peaks related to blade pass increase in frequency with wind speed due to the related increase in rotor rate and blade pass. This increase in frequency is not observed at Clyde wind farm, rather the frequency of spectral peaks is insensitive to wind speed. It is interpreted that the far-field spectra is dominated by structural resonances of the S2.3 turbine and there is a likelihood of frequency matching between blade pass multiples and these resonances (i.e. the blade pass multiples lie on turbine resonances, see Table 14).

Given that the far-field seismic vibrations produced by Nordex N80 turbines are dominated by blade pass multiples, whereas the Clyde spectra are dominated by resonance, the N80 is not representative of all turbines in the Eskdalemuir consultation zone.

Dun Law		Craig		Clyde	
Frequency (Hz)	Interpretation	Frequency (Hz)	Interpretation	Frequency (Hz)	Interpretation
		1.65	Blade Pass	1.60	Blade Pass
2.91	Blade Pass	2.16	Resonance	2.39	Blade Pass
4.34	Blade Pass	2.48	Blade Pass	2.79	Resonance
5.79	Blade Pass and Resonance	3.31	Blade Pass	3.21	Blade Pass and Resonance
7.23	Blade Pass	4.14	Blade Pass	3.98	Blade Pass
		4.97	Blade Pass	4.78	Blade Pass
		5.78	Blade Pass	5.20	Resonance
				5.57	Blade Pass

Table 14 – Interpretation of source of vibration in spectra from Dun Law, Craig and Clyde measured at 12 ms^{-1} wind speed.

3.7.2 CHARACTERISATION OF FAR-FIELD SEISMIC VIBRATIONS

Seismic vibrations measured in the far-field that occur at multiples of the blade pass frequency tend to be strongly polarised orthogonally from the surface of the ground in the cases of all blade pass multiples at Dun Law (Figure 15) and Craig (Figure 18); and the 2.4 Hz peak at Clyde (Figure 25). Strong vertical polarisation indicates that the dominant seismic vibrations related to blade pass are propagating as Rayleigh waves.

Some peaks related to structural resonances, such as those at 4.7 Hz and 5.3 Hz by the N80 at Craig (Figure 19) and 5.8 at Dun Law (Figure 15), appear to have seismic vibrations polarised in the horizontal β component (i.e. with little or no vertical component). This observation indicates that modal shapes associated with some structural resonances produce Love waves. An example of such a modal shape would be a torsion mode were the foundation twists back and forth around a vertical axis.

It should be noted that sensor 4443 at Clyde is surrounded by an arc of wind turbines (Figure 5) so seismic waves arrive from all directions making the interpretation of the relationships between the horizontal axes difficult.

3.7.3 RELATIONSHIP BETWEEN ON-TOWER AND FAR-FIELD SEISMIC VIBRATIONS

The relationship between vibrations measured on the base of wind turbines and in the far-field appears very complex. Simple inspection of on-tower and far-field spectra at Craig (Figure 21 and Figure 18) and Clyde (Figure 23) shows that spectral peaks occur at different frequencies and the relationships between their amplitudes are non-linear. In the case of Clyde wind farm it should be noted that while the sensors were deployed linearly from tower T39 there will be contributions from the surrounding 151 turbines. The rate of reduction in seismic vibration observed with increasing distance in Figure 23 does indicate that the signal recorded at the hardstand of tower T39 is dominated by T39.

The relationship between on-tower and far-field seismic vibration was investigated by Strathclyde University with the hope that such a relationship would allow the removal of background noise from far-field sensors and may provide a way of quickly estimating far-field amplitude by simply measuring the foundation vibration of wind turbines. Figure 38 shows a clear difference in the signals produced from seismometers place in the near and far-field at Craig wind farm. Using an adaptive filter on some of the 10 minute datasets does present a potential relationship that could be used to eliminate the background contribution to seismic vibration recorded. However when applied to full datasets the filter produced unstable results. As presented in the Strathclyde University report, Appendix C, measurements conducted at the base of the turbine may be contaminated by some noise source. Should a noise source of similar characteristics be apparent in the far-field then the filter will attribute the contribution of such a noise source to the wind turbine. It therefore removes confidence in the filtered level of seismic vibration that would represent the contribution due to wind turbines. The full details of the adaptive filter investigated can be seen in the report by Andrew Millar, Strathclyde University in Appendix C.

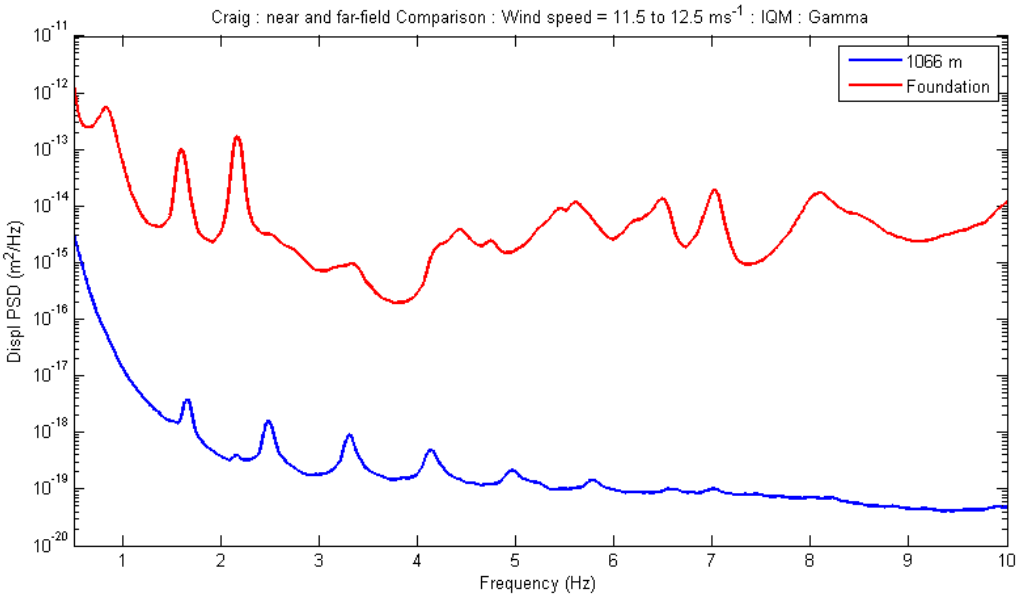

Figure 38 - Near-and far-field comparison of interquartile mean displacement PSD from the vertical axis recorded at the foundation of T3 and AEG-2b/6099 at Craig wind farm at a wind speed of 11.5 to 12.5 m/s.

3.7.4 AZIMUTH EFFECT INTERPRETATION

A directional dependence of seismic amplitude with wind direction was noted at both Craig and Dun Law wind farms. The seismic amplitude was 1.38 times greater when measured up- and down-wind from the wind farm in the 1.71 to 5.76 Hz band. This factor was slightly lower at Dun Law, 1.15, which may be due to the lower rotational speed of the Vestas V47 resulting in fewer blade-pass multiples falling in the 1.71 to 5.76 Hz band so that the background noise has a greater influence on the calculation.

At Clyde wind farm the azimuth effect measured at sensor 4443 was less pronounced with slight increases noted from the cross-wind position. This is likely due to the sensor being surrounded by wind turbines on three sides so that it is non-trivial to determine the down-wind and cross-wind positions. Given these difficulties the authors believe data from sensor 4443 is not suitable for investigating azimuth effect on seismic amplitude.

4 BROADBAND OPERATIONAL NOISE

4.1 Introduction

During phase 0 of this research work an increase in the noise between blade pass multiples was noted at Craig wind farm when data collected while all four turbines were running are compared to periods when no turbines were operational (see. FMB_102_TRP0_V6). The observed increase was considered to be due to the narrow bands used to model background noise coinciding with structural resonances of the turbine; natural statistical variation in the background noise, and/or; variations in ground wave propagation as a function of direction. Following a conservative approach a broadband model will be included in the algorithm to represent possible seismic vibration related to the operation of wind turbines other than those related to structural resonances and blade pass.

4.2 Methodology

4.2.1 CRAIG WIND FARM

Broadband noise models represented by inverse square curves with respect to frequency were fitted to amplitudes between peaks related to blade-pass multiples and structural resonances measured at AEG-5/6351 at Craig wind farm. A model was constructed by subtracting the power when no turbines were operating at Craig wind farm from that measured when all turbines were operational at the same relative wind speeds. The model assumes the ground noise is smooth and that the operational broadband noise decreases monotonically with frequency. The sets of data collected while the turbines were inactive are small at wind speeds higher than 8 ms^{-1} (tens of spectra of 10 minute duration) compared to those collected when all turbine were running (hundreds of spectra). It is therefore assumed that the small dataset while turbines were not running is representative of the local background noise.

The broadband power when all turbines were operational was taken as the minimum amplitude of interquartile mean spectra at 1 ms^{-1} wind speed bins in the narrow bands between spectral peaks:

- 1.9 to 2.1 Hz
- 2.7 to 2.9 Hz
- 3.6 to 3.8 Hz
- 4.4 to 4.6 Hz
- 5.3 to 5.5 Hz
- 7.3 to 7.8 Hz

The contribution of all four turbines to broadband noise was determined by subtracting the mean amplitude when no turbines were running at relevant frequencies and wind speed bins. The *operational broadband noise* of a single turbine at 1 km was then calculated:

$$\boldsymbol{d_{OBN(r,f)}} = \frac{\Delta_{\mathbf{PSD}}}{\sum_{i=1}^{N}\left(\sqrt{\frac{r_{ref}}{r_i}}\exp\left(-\frac{\pi f\left(r_i - r_{ref}\right)}{Qc}\right)\right)^2} \quad [2]$$

where Δ_{psd} is the difference in power between four turbines operating and no turbines operating, N is the number of turbines at distances r_i from the sensor. The reference distance r_{ref} is 1000 m, f is the frequency in Hz, Q is a factor relating non-geometric attenuation and is equal to 50 for the Southern Uplands and c is the speed of Rayleigh waves taken as 2000 ms^{-1} for the Southern Uplands, (MacBeth 1986). Figure 39 and Figure 40 show examples of how the operational broadband noise was calculated for each wind speed bin.

An inverse square curve was fitted through the operational broadband noise for each wind speed bin from 7 ms^{-1} and 10 ms^{-1} of the form:

$$\boldsymbol{OBN}_{(f)} = \frac{\boldsymbol{C_{vw}}}{\boldsymbol{f^2}} \quad [3]$$

where C_{vw} is a constant for the relevant wind speed bin and f is frequency. Following the conservation of energy hypothesis (Section 7), the value of the constant C_{vw} was assumed to increase with the cube of wind speed. The variation of C_{vw} was fitted with least squares to the cube of wind speed resulting in the operational broadband noise model:

$$\boldsymbol{OBN}_{(f,v_w)} = \boldsymbol{C_{OBN}} \frac{\boldsymbol{v_w}^3}{\boldsymbol{f^2}} \quad [4]$$

where C_{OBN} = 1.12e-22 is the best least squares fit. Figure 41 shows how the modelled operational broadband noises for a Nordex N80 varies with wind speed and frequency.

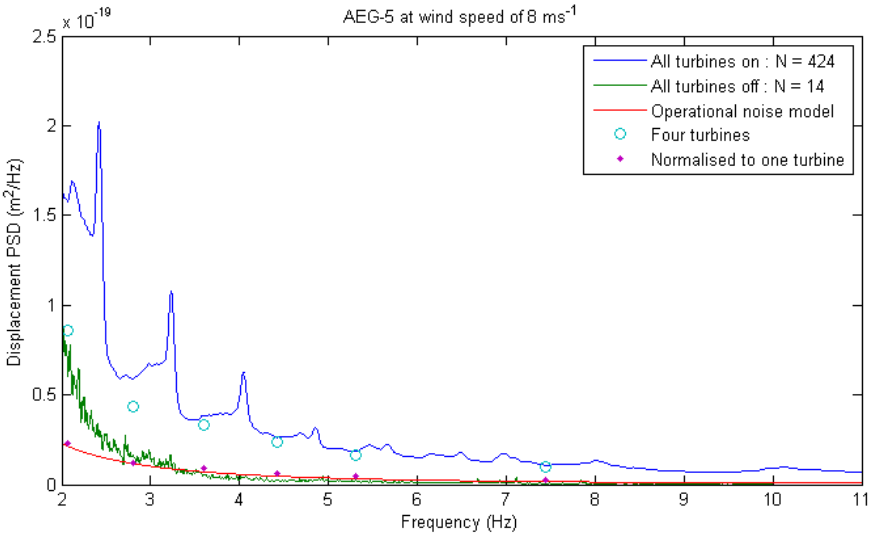

Figure 39 - Interquartile mean of all four turbines at Craig wind farm running compared to when no turbines are running at 8 ms^{-1}. The blue circles show the difference between the minimum amplitude in the narrow bands while all four turbines are running and the background noise when no turbines are running. The magenta dots show the amplitude when the blue circles are normalised to a single turbine at 1 km.

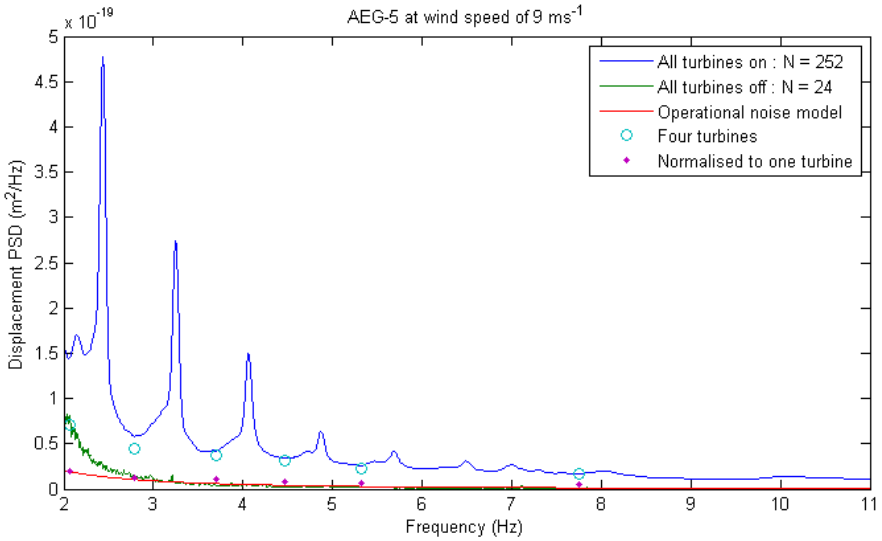

Figure 40 - Interquartile mean of all four turbines at Craig wind farm running compared to when no turbines are running at 9 ms^{-1}. The blue circles show the difference between the minimum amplitude in the narrow bands while all four turbines are running and the background noise when no turbines are running. The magenta dots show the amplitude when the blue circles are normalised to a single turbine at 1 km.

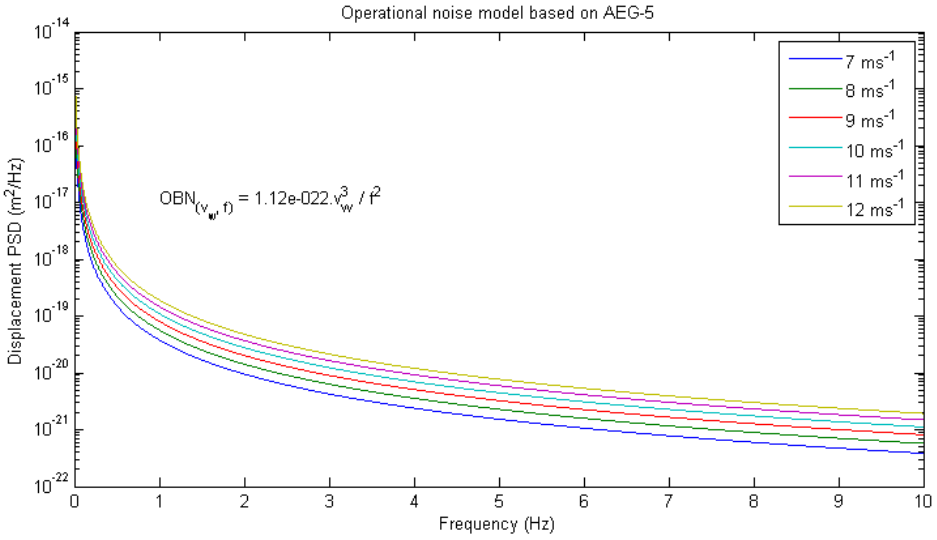

Figure 41 – Operational broadband noise model based on AEG-5/6351 at Craig wind farm for different wind speeds.

4.2.2 CLYDE WIND FARM

A similar procedure as that above was followed to determine the operational broadband noise at Clyde wind farm. No complete shutdown of Clyde was recorded so the process gives the upper limit of operational broadband noise (i.e. if all noise was related to turbine operation and none to ambient background noise).

The broadband power was calculated for the interquartile mean normalised to a single turbine measured at 1 km. The minimum in the following narrow bands were used:

- 1.9 to 2.1 Hz
- 2.45 to 2.56 Hz
- 3.5 to 3.7 Hz
- 4.4 to 4.6 Hz
- 5.6 to 5.9 Hz
- 8.2 to 8.4 Hz

Figure 42 and Figure 43 show how the upper limit to operational broadband noise of Siemens 2.3 turbines was calculated. The C_{OBN} constant for the Siemens 2.3 turbine was calculated to be 8.662e-23 and the Nordex N80 (1.12e-22), which when divided gives a ratio of 1.29. Figure 44 shows how the modelled Siemens 2.3 operational noise varies with wind speed and frequency.

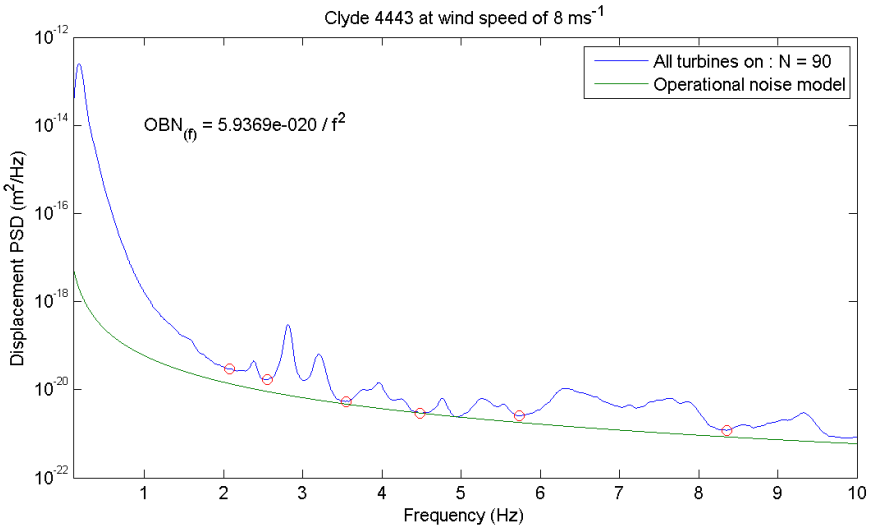

Figure 42 – Upper limit of operational broadband noise based on measurements at sensor 4443 in 8 ms^{-1}

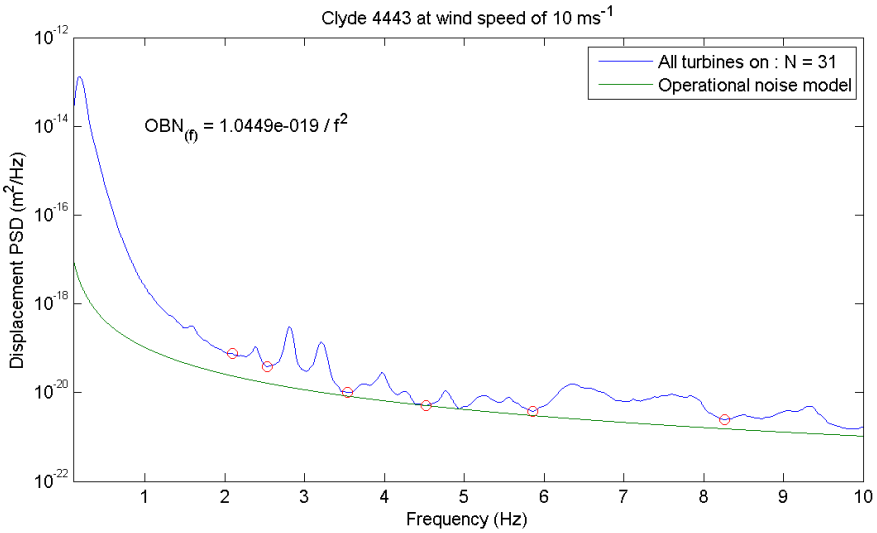

Figure 43 – Upper limit of operational broadband noise based on measurements at sensor 4443 in 10 ms^{-1}

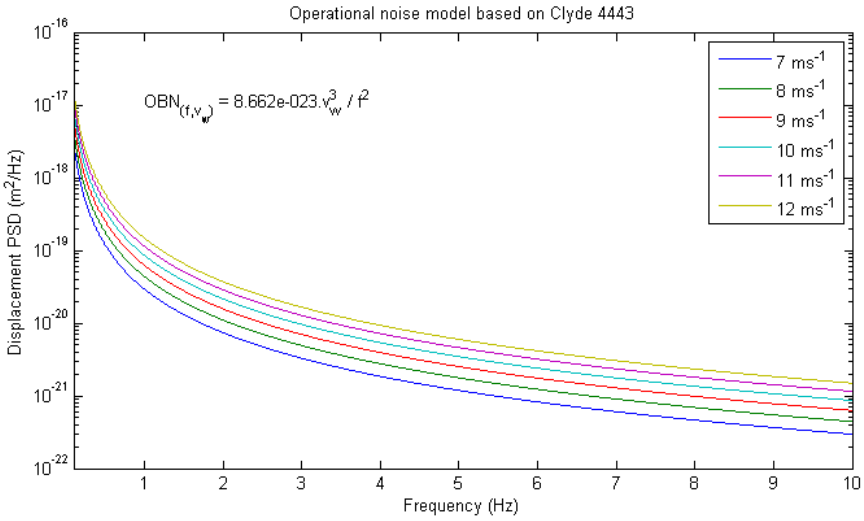

Figure 44 – Operational broadband noise model based on 4443 at Clyde wind farm for different wind speeds.

4.3 Conclusion

- C_{OBN} that relates the operational broadband noise produced by Nordex N80 wind turbines at Craig wind farm will be used in the physics-based algorithm (Section 8) as it predicts higher broadband noise than the Siemens S2.3.
- This is consistent with the conservative approach adopted to produce the algorithm.
- In the physics-based algorithm the C_{OBN} constant will be normalised for rotor area by it being divided by the swept area of a Nordex N80 to give C_{OBN} = 2.2282e-26 [m^2/Hz].[m^{-5}s].

5 FINITE ELEMENT ANALYSIS OF SEISMIC VIBRATION PRODUCED BY WIND TURBINES

5.1 Introduction

A series of finite element analysis (FEA) models have been developed to help better understand the forces of wind turbines that produce low frequency (<10 Hz) seismic vibration. The models are focused on the variation of forces on the turbine related to blade rotation, their interaction with the dynamic structures in wind turbines (i.e. blades and towers) and how these forces are coupled to the underlying rock via the foundations. Models were developed that represent a Nordex N80 2.5 MW turbine. Initially, *near-field* models were produced where the wind turbines were mounted on a cylinder of bedrock with a radius of 50m. Results from the near-field models with a variety of force regimes were compared to on-foundation vibration measurements (See Section 3.5.2) and the regime that best approximated field observations was selected. *Far-field* models were then created where the wind turbines were mounted on a cylinder of bedrock with a radius of 1.25 km and the model was excited using the force regime selected from the near-field models.

The sensitivity of the seismic vibrations on the size of turbine components (tower height, blade length, nacelle mass, blade chord length) and parameters (wind speed, surface roughness length) were examined with a variance model. The variance model was created by modifying individual parameters of the N80 far-field model and comparing the resulting modelled seismic vibration. Results from the variance model will be used to inform which parameters should be include in an algorithm that predicts the amplitude of far-field seismic vibration to safeguard the detection capabilities of the Eskdalemuir seismic array.

5.2 Methodology

Models of Nordex N80 and a generic wind turbine used as a basis for variance modelling were developed in the commercially available finite element package COMSOL Multiphysics. All models presented here were performed in the time-domain with materials modelled as linear-elastic solids.

5.2.1 GEOMETRY

The geometry of key components of the N80 are listed in Table 15. The Nordex N80 geometry was based on data provided to Xi (formerly Reactec) to develop the SQT mitigation device installed at Craig wind farm including the geometries of the tower, nacelle and blades. The nacelles and blades were modelled using three dimensional solid objects with densities appropriate to give the masses listed in Table 15. The towers were modelled using three-dimension shells. In the near-field models the turbines were mounted on cylinders that represent the underlying ground with a radius of 50 m and height of 20 m (Figure 45). In the far-field models the bedrock was modelled as a cylinder of radius 1250 m and height 1000 m that was truncated in the up-wind and one cross-wind direction to form a vesica piscis. This truncation of the bedrock was used to reduce the mesh size required to solve the models and make them more numerically economic. The bedrock of the far-field models have upper layers that are 500 m thick to allow some internal geological architecture (see Material properties below). The models include foundations that are 15 m x 15 m that are commonly used in the Southern Uplands.

	Units	N80
Hub height	m	60
Rotor Diameter	m	80
Blade mass	kg	8620
Hub mass	kg	22884
Nacelle Mass	kg	90000
Nacelle Dimensions	m x m x m	6.348 x 3.4 x 4.312
Rotor speed	rpm	16

Table 15 – Key geometric and mass components of the N80 models

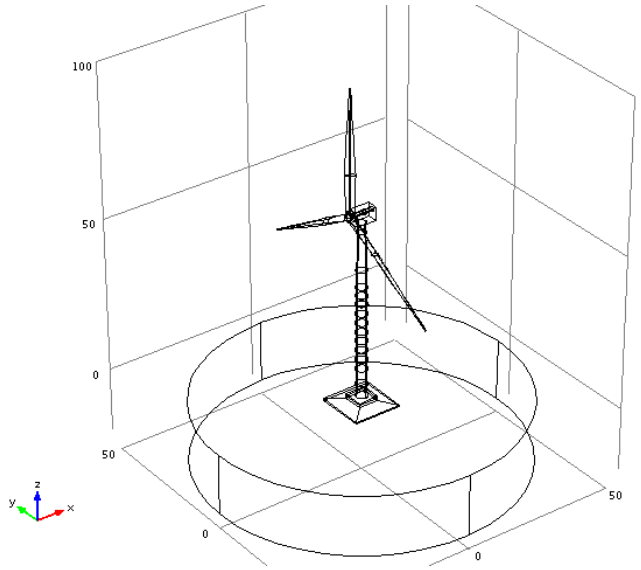

Figure 45 – Geometry used to model the dynamic behaviour of the N80 wind turbine in the near-field

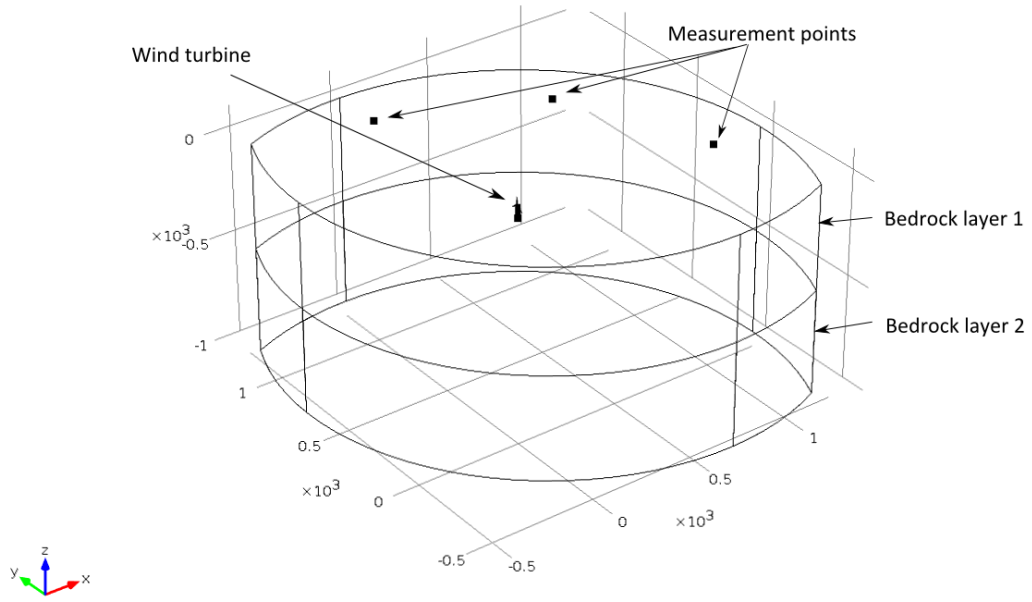

Figure 46 – Bedrock geometry used in far-field models

5.2.2 MATERIAL PROPERTIES

The material properties used in the models are listed in Table 16. The tower, hub and nacelle were modelled as structural steel and the foundations as concrete. The bedrock was modelled such that the elastic properties result in a 500 m upper layer (layer 1) with a P-wave speed of 3000 ms^{-1} and a lower half space (layer 2) with a P-wave speed of 4600 ms^{-1} which are appropriate for the Eskdalemuir region (Bowers, pers. com. 11/12/2013).

To reduce the complexity of the models the blades of the N80 turbine were simplified to solid objects. Parametric eigenfrequency models of individual blades were constructed and both the Young's modulus and chord-width of the blades varied. Eigenfrequency results were compared to blade dynamics information provided to Xi of N80 blades and the most appropriate combination of Young's modulus and chord-width selected (Table 17).

	Young's modulus Pa	Poisson Ratio	Density kg m^{-3}	Damping ratio
Tower	2.00E+11	0.33	7850	0.0025
N80 Nacelle	2.00E+11	0.33	1099*	
N80 Hub	2.00E+11	0.33	1217*	
Foundation	2.50E+10	0.33	2300	
N80 Blades	9.50E+08	0.33	112*	0.008
Bedrock layer 1	2.19E+10	0.2	2700	0.01
Bedrock layer 2	4.76E+10	0.25	2700	0.01

Table 16 – Material and mass properties used in wind turbine models. * Density modified to give correct mass for component.

Modal shape	N80	
	Provided	Xi - Model
1st Flap	1.09	1.01
2nd Flap	2.98	2.63
1st Edge	1.83	1.82
2nd Edge	4.3	5.17

Table 17 – Eigenfrequencies of blades in Hz measured and modelled for an N80 wind turbine. A parametric model where the chord-width and Young's modulus of blades were varied was used to find the best approximation of blade dynamics with final comparisons shown here.

5.2.3 MESHING AND TIME STEP OPTIMISATION

The maximum mesh size and time step were optimised such that the CFL number did not exceed 0.2 (according to the Courant-Friedrichs-Lewy condition) and that there were at least 5 elements per wave length. Given that the maximum frequency of interest is 8 Hz, the maximum mesh size for a wave speed of 3000 ms^{-1} is 75 m. Taking this as the maximum mesh size then a time step of 0.005 s satisfies the CFL condition.

5.2.4 BOUNDARY CONDITIONS AND LOADS

The outer- and lower-boundaries of the bedrock are held in place with a stiffness matrix that have spring constants appropriate to the Young's modulus of the connecting bedrock. The bedrock contains a thin domain neighbouring the outer- and lower-boundary with a low Q-factor to prevent reflection on waves. All boundaries other than the outer- and lower-boundaries are free.

The models are excited with two forces that change with respect to time and represent:

1. The shadow and wake of the blade passing in front of the tower
2. The effect of the vertical wind profile that results in a torque flutter on the drive train as blades being exposed to higher wind speeds are associated lift at higher elevations above ground level than at lower elevations.

The wind imparts a dynamic pressure on the tower that is taken to be:

$$\boldsymbol{P_{tower} = \frac{1}{2}\rho_{air} v_{w(z)}^{\,2}} \qquad [5]$$

where ρ_{air} is the density of air (1.5 $kg.m^{-3}$) and $v_{w(z)}$ is the wind speed as a function of height above the ground according to the log-law:

$$\boldsymbol{v_{w(z)} = v_{hub} \frac{\ln(z/z_l)}{\ln(z_{hub}/z_l)}} \qquad [6]$$

Where z is the height above ground level, z_{hub} is the hub height, v_{hub} is the wind speed at the hub height, 12 ms^{-1}, and z_l is the ground roughness length taken as 0.1 m which is standard for land with crops with occasional large objects such as the terrain at Craig wind farm.

The fluctuation in dynamic pressure on the tower is represented by monitoring the positions of the rotating blades; when a blade passes in front of the tower of the turbine the wind speed is assumed to drop to zero

resulting in a localised and temporal drop in dynamic pressure, Figure 47, while the variation of pressure related to lift and drag on the blades with elevation above ground level is shown in Figure 48.

The wind profile represented in equation [6] is also used to calculate the torque flutter on the rotor. The variation of lift is taken to act in the direction of blade motion and applied to the surface area of the blade according to:

$$\boldsymbol{P_{lift} = \frac{1}{2} c_l \rho_{air} v_{w_{(z)}}{}^2} \quad [7]$$

where c_l is the lift coefficient and is taken as 0.96 that is appropriate to producing 2.05 MW (which is the power that a Nordex N80 produces in wind speeds of 12 ms^{-1}). A drag force also acts in the wind direction with a pressure applied to the blades equal to:

$$\boldsymbol{P_{drag} = \frac{1}{2} c_d \rho_{air} v_{w_{(z)}}{}^2} \quad [8]$$

where c_d is the drag coefficient equal to 0.0069.

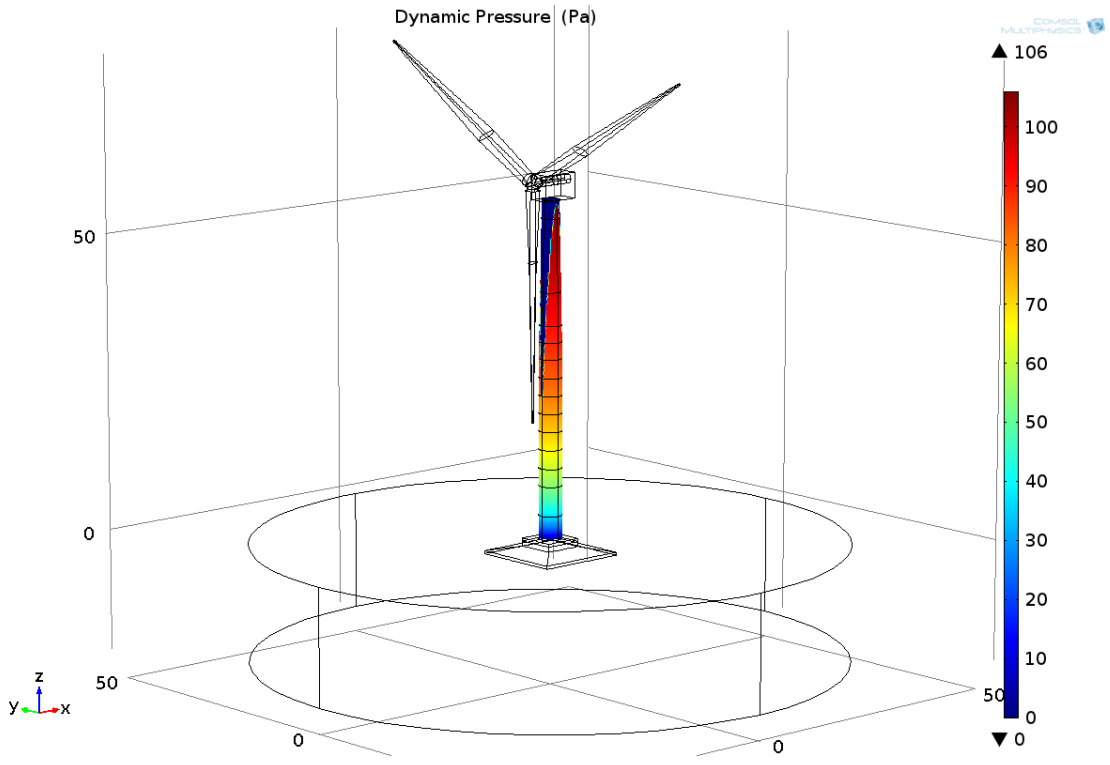

Figure 47 – Dynamic pressure on the tower with the pressure shadow cast by the blade as it passes in front of the tower

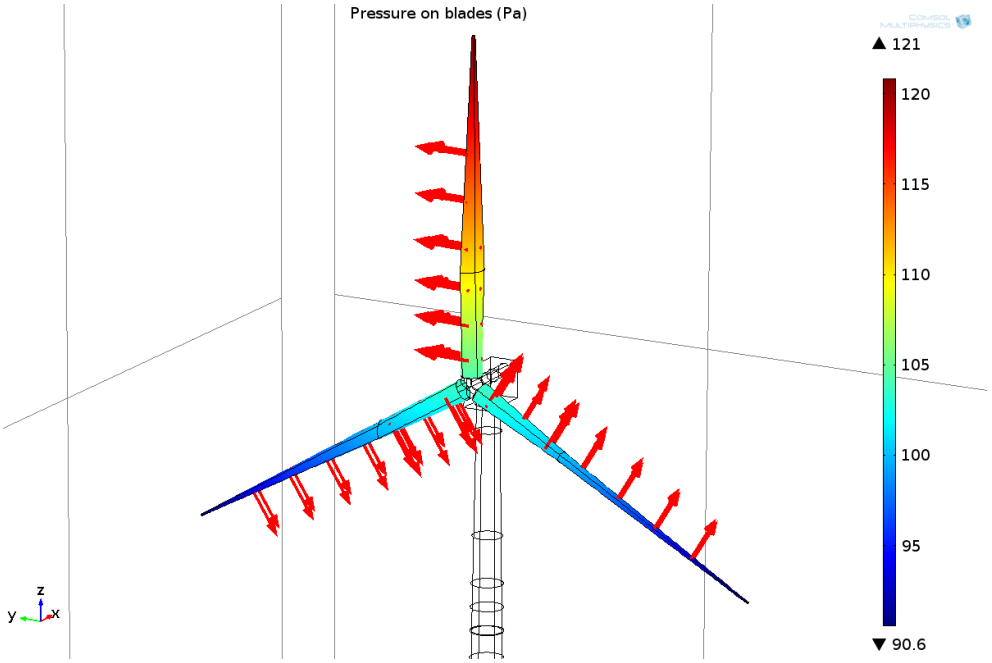

Figure 48 – Variation of pressure related to lift and drag on the blades with elevation above ground level with vectors showing the direction that the resultant force acts.

5.2.5 VARIANCE MODEL

A series of variance models were produced to test the sensitivity of far-field seismic vibrations to certain parameters. The Nordex N80 turbine model described above was used and one parameter changed at a time. The parameters examined are listed in Table 18. The tower thickness in the N80 model varies with height above ground level. To model the change of tower stiffness the tower thicknesses were simply multiplied by a factor such that the relative thicknesses of tower sections remain the same.

Parameter	Units	Values modelled			
Rotor Diameter	m	40	60	80*	100
Hub Height	m	50	60*	80	100
Nacelle Mass	ton	70	90*	110	130
Rotor Rate	rpm	10	16*	20	25
Tower thickness	%	50	100*	150	200
Wind Speed	ms-1	6	9	12*	15
Surface roughness	m	0.0024	0.03	0.1*	0.4

Table 18 – Parameters that were changed in the variance models and the four values examined for each parameter. The tower thicknesses were varied by multiplying the N80 model by a factor with the percentage relative to the base N80 model shown. * indicates the values used in the N80 model.

5.3 Results

5.3.1 NEAR-FIELD CALIBRATION

The acceleration of the foundation at the centre of the tower of the Nordex N80 near-field model was compared to vibration measured in 12 ms^{-1} wind speeds at T4 of Craig wind farm to calibrate the model. The model was sensitive to changes in the width of the blade pass wake. The width of the wake with respect to chord length was varied over a succession of models and a wake that was twice the width of the blade was found to best fit the measured data at T4, Figure 49.

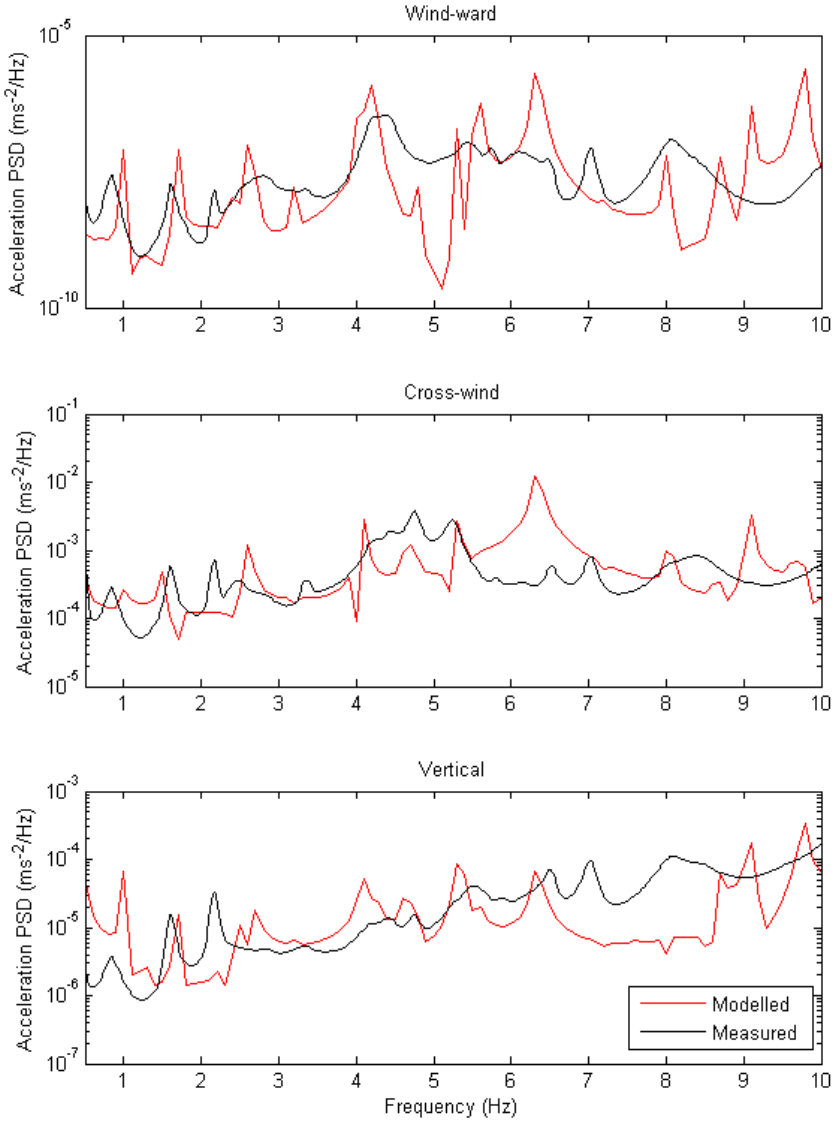

Figure 49 – Comparison of acceleration of a model where the blade pass wake was twice the width of the blade compared to measured on-tower results from T4 at Craig wind farm.

5.3.2 FAR-FIELD AMPLITUDE

The force regime calibrated using near-field models was used in far-field models and the N80 models were run for 40 s of modelling time requiring 8000 time steps each of 0.005 s. The displacement 1 km from the base of the turbine was exported to matlab and the power spectral density determined. The model results correlate well with those measured at AEG-5/6351 (Figure 50).

The model included no forces due to the stochastic variation in wind speed and or those other mechanisms that might produce broadband noise resulting in the modelled amplitude between the blade-pass multiple (at 2.5, 3.3, 4.1, 5 Hz, etc) being far lower than those measured in the field. When the operational broadband noise model (see section 4) is added to the model the result compare very well to the field observations (Figure 51). This comparison also highlights some differences between the model and the field measurements:

- The model does not have a peak related to the second blade pass multiple at 1.6 Hz
- The model does not have a peak at 2.1 Hz related to a rotor resonance
- The model predicts more power in the peaks related to structural resonance than those observed at 4.7 Hz and 5.6 Hz at Craig wind farm.

It should be noted that the data set converted to the frequency domain using Welch's method was only 40 seconds long in the case of the model compared to 10 minutes for the measured observations, which may result in discrepencies in comparing modelled and measured spectra. While low frequency blade pass multiples were not observed in the modelled displacement PSD in the vertical direction, they can be observed in spectra of displacement in the horizontal axes (Figure 53 and Figure 54).

Different wind speeds were modelled (6, 9 and 12 ms^{-1}) and the rotor speed was also varied to those consistent with the operation of the N80 wind turbine. The amplitude of peaks increased with wind speed and peaks related to blade pass freqency moved to high frequency consistent with field observations (Figure 52 and Figure 16). At 4.2 Hz the relationship is complicated by frequency matching between blade pass multiples and the resonance related to the second bending mode resulting in higher power in the 6 ms^{-1} spectrum (Figure 52).

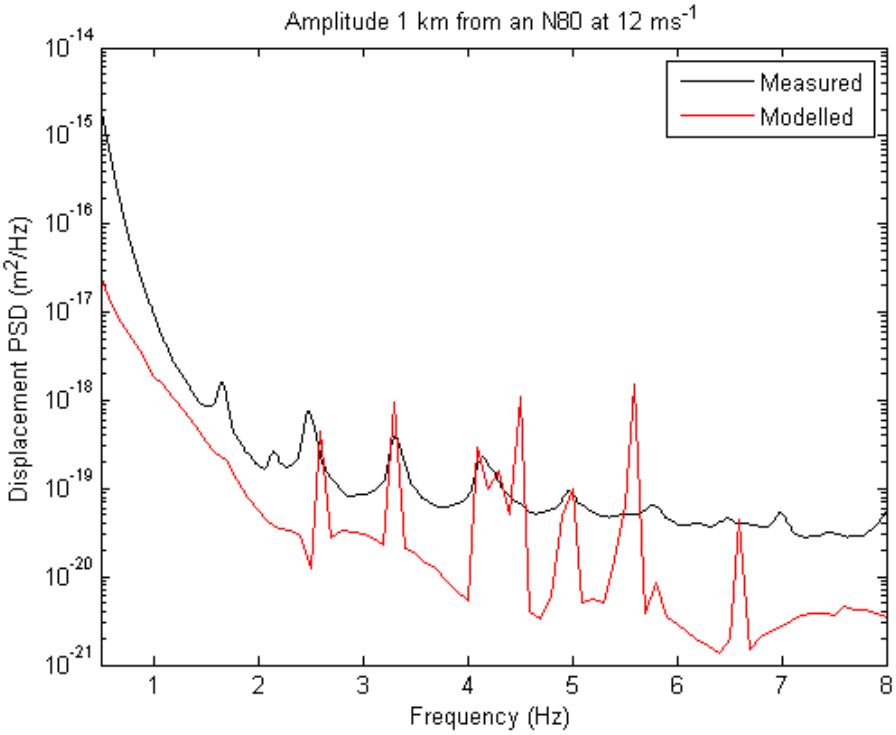

Figure 50 – Comparison of vertical displacement N80 far-field from the model with those measured at AEG-5/6351 at Craig wind farm at wind speeds of 12 ms^{-1}

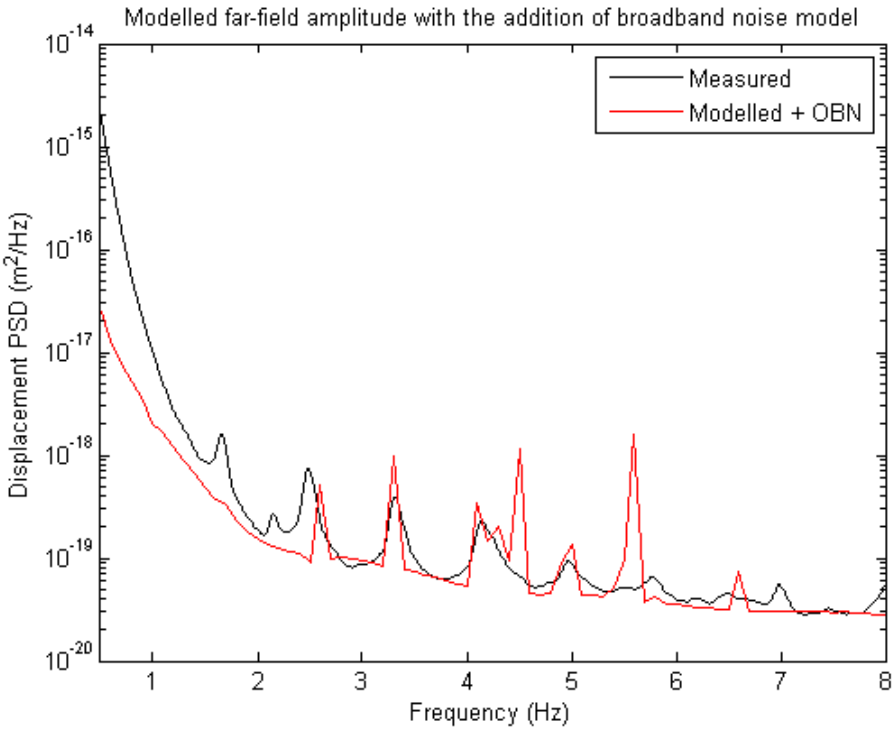

Figure 51 – A comparison of measured vertical displacement PSD at AEG-5/6351 with the modelled results with the operational broadband noise model added to the finite element model.

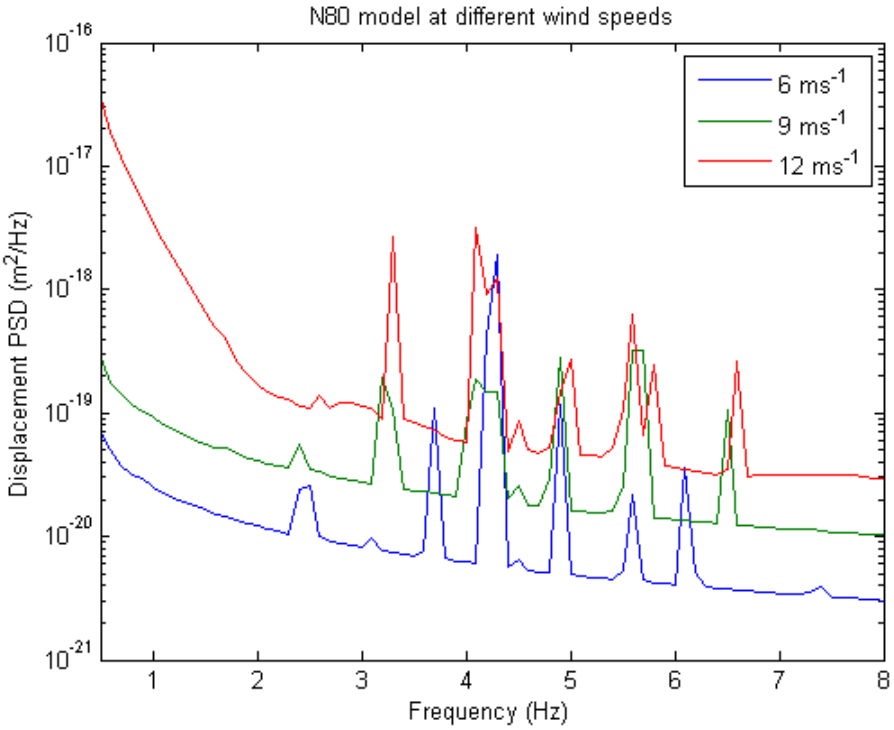

Figure 52 – Comparison of the N80 model vertical motion at different wind speeds 1 km from a N80 including the operational broadband noise model.

5.3.3 CHARACTERISATION OF GROUND WAVES

The surface waves modelled directly down-wind of the wind turbine tend to have peaks with the greatest power normal to the surface (γ-axis) with significant power also found in the axis parallel to the direction of travel (α-axis) (Figure 53). High power in the vertical-component and parallel to the direction of travel are consistent with Rayleigh waves. The surface waves cross-wind have different characteristics than those directly down-wind; 1 km cross-wind peaks with significant power in the direction transverse to the wave propagation direction (β-axis) were modelled (Figure 54). Peaks with high power in the β-axis were modelled at 3.2 Hz, 4.1 Hz and 5.7 Hz and are indicative of Love waves being generated at these specific frequencies and propagating away from the wind turbine perpendicular to the wind direction.

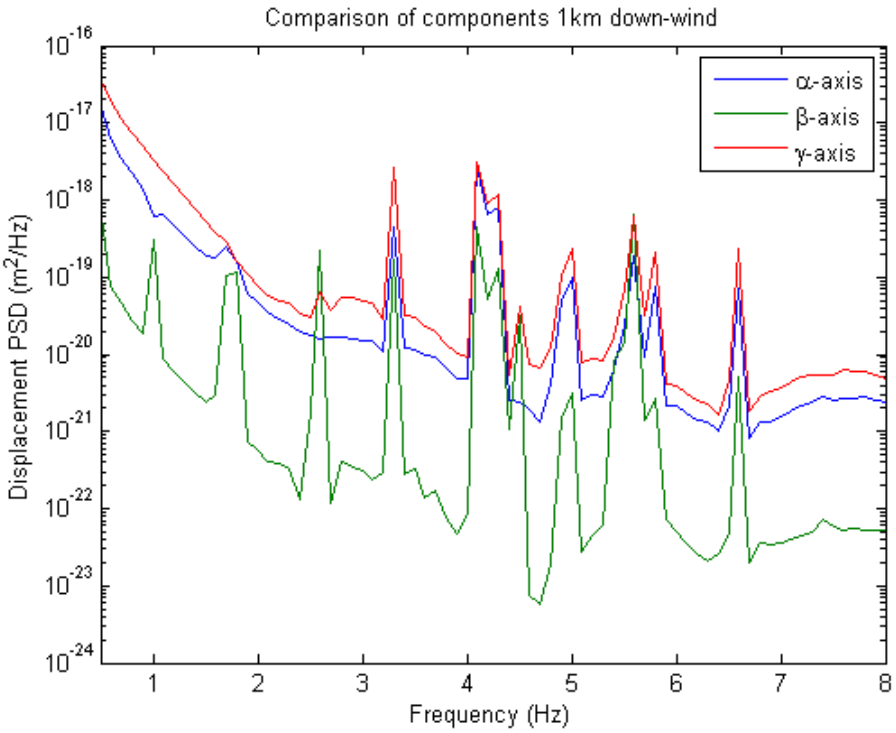

Figure 53 – Comparison of wave components modelled 1km down-wind from a N80 wind turbine. The α-axis is parallel to the direction of travel, the β-axis is transverse to the direction of travel in the plane of the ground surface and the γ-axis is a normal to the surface (i.e. vertically up-ward).

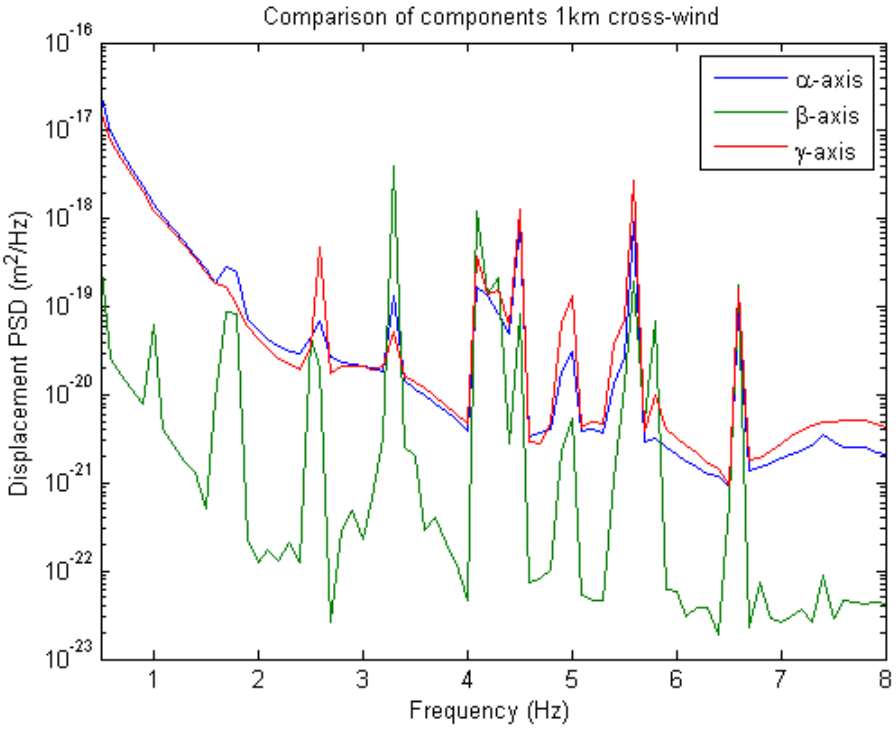

Figure 54 – Comparison of wave components modelled 1km cross-wind from a N80 wind turbine (i.e. in the rotor-plane). The α-axis is parallel to the direction of travel, the β-axis is transverse to the direction of travel in the plane of the ground surface and the γ-axis is a normal to the surface (i.e. vertically up-ward).

5.3.3.1 Azimuth effect

An azimuth effect was detected in the far-field models with high amplitude predicted down-wind from the turbine than from positions across the wind from the turbine for the three wind speeds modelled (Figure 55). At 12 ms^{-1} the amplitude in the 1.5 to 4.5 band 15° from directly down-wind is 1.17 nm compared to 90° from the wind (cross-wind direction) where it is 0.474 nm. The model therefore found that the seismic amplitude down-wind is a factor of 2.5 higher than the cross-wind direction.

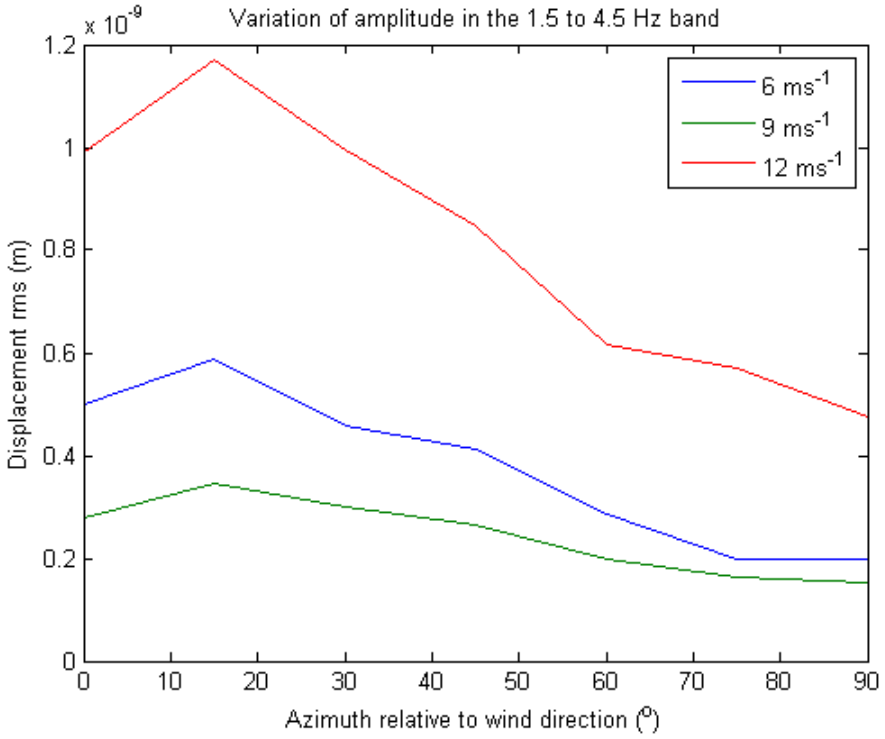

Figure 55 – Seismic amplitude modelled 1 km for the N80 turbine in different angular positions relative to the wind direction (0°) in vertical or γ component

5.3.4 VARIANCE MODELS

Variance models were used to examine the sensitivity of far-field seismic amplitude to the parameters listed in Table 18. The computational expense of the models were reduced by reducing the radius of the bed rock to 600 m leading to a significant reduction in mesh size, and by reducing the model time from 40 s to 12 s. A single parameter was changed during each model run. The change of a single parameter would not be possible in the real world as it would lead to changes in the dynamics which could lead to the turbine failing. For instance, changing the rotational speed without changing the nacelle mass and tower stiffness would in the real world lead to frequency matching between the blade pass and the first bending mode and the probability of catastrophic failure. These models therefore are only indicative and are best used to determine which parameters do not affect the seismic amplitude and are therefore not required in an algorithm to predict seismic amplitude. The amplitudes in the 1.5 to 4.5 Hz band down-wind from the turbine for different parameters are listed in Table 19 for the change of single parameters. Graphs showing the variation of amplitude for each parameter are shown in Appendix D.1 and the spectra are shown in Appendix D.2.

The modelled seismic amplitude was insensitive to surface roughness length (Figure 56) and slightly sensitive to nacelle mass (Figure 57) and tower stiffness (Figure 58). The variation in nacelle mass and tower stiffness did not affect the amplitude or frequency of peaks related to blade-pass multiples. The nacelle mass did however affect the amplitude of the peak related to the second bending model with an increase in power modelled with increasing nacelle mass (Figure 57). The tower stiffness affected the power and frequency of the peak related to the second bending mode; the variation in power will be related to frequency matching with the fifth multiple of blade pass (Figure 58).

Rotor diameter (m)	Amplitude (nm)	Tower thickness (%)	Amplitude (nm)
40	0.732	50	0.525
60	0.802	100	0.668
80	0.668	150	0.361
100	0.363	200	0.271
Hub Height (m)		Wind speed (ms^{-1})	
50	0.160	6	0.167
60	0.668	9	0.375
80	0.693	12	0.668
100	0.295	15	1.042
Nacelle Mass (ton)		Rotor rate (rpm)	
70	0.577	10	0.988
90	0.668	16	0.668
110	0.787	20	1.176
130	1.274	25	0.632
Surface roughness (m)			
0.0024	0.322		
0.03	0.315		
0.4	0.302		

Table 19 – Amplitude in the 1.5 to 4.5 Hz band 450 m down-wind from the turbine when different parameters are changed from those in the Nordex N80 model for vertical or γ component.

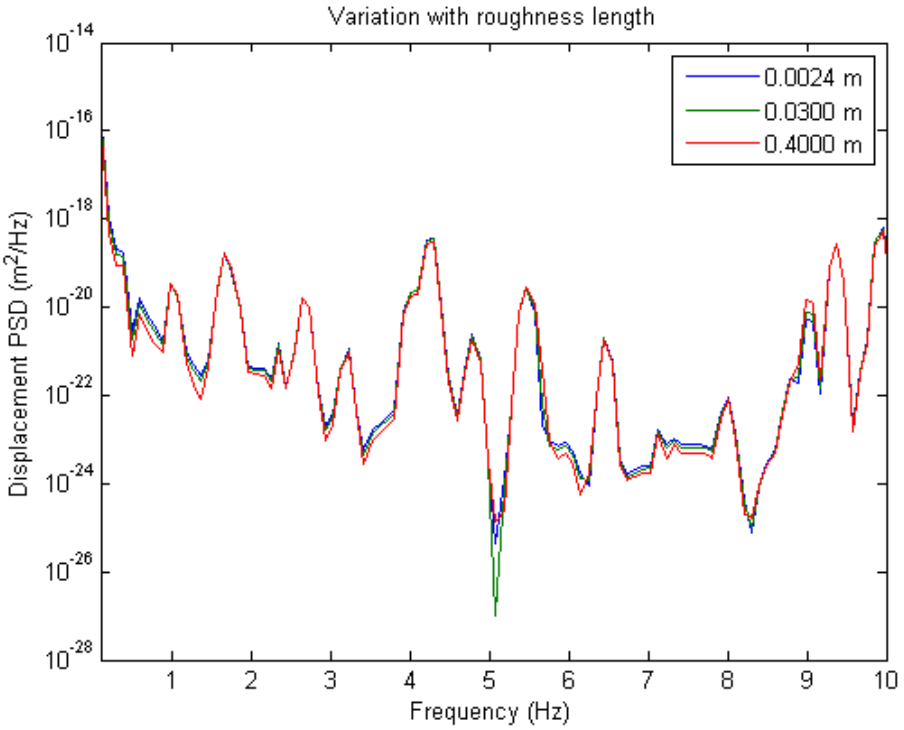

Figure 56 - Variation of seismic amplitude modelled 480 m down-wind from a N80 wind turbine surrounded by terrain with different surface roughness lengths. The amplitude is insensitive to roughness length.

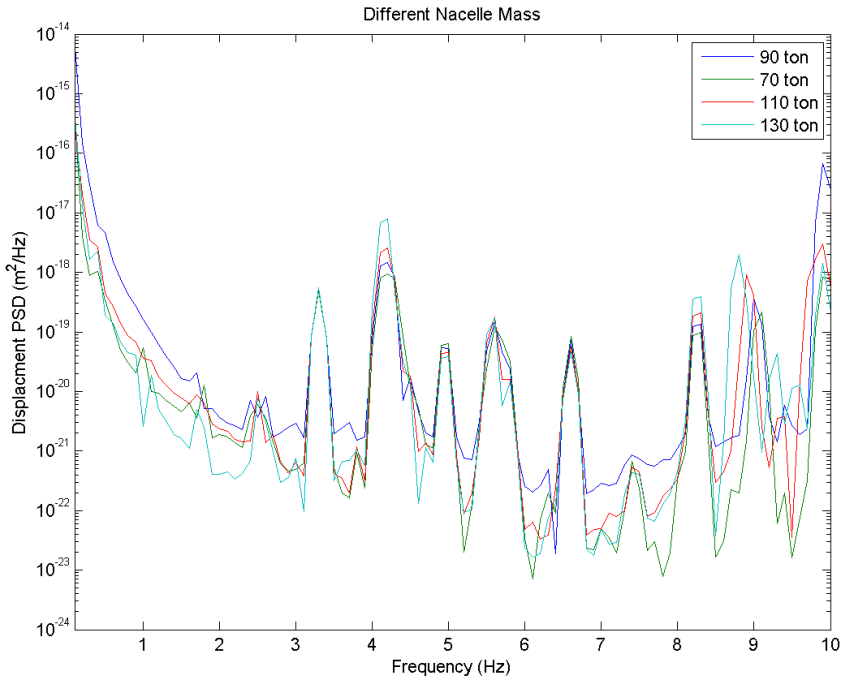

Figure 57 – Variation of seismic amplitude modelled 480 m down-wind from a turbine with different nacelle masses. The amplitude of peaks are insensitive to change in nacelle mass except for those related to structural resonances such as the second bending mode at 4.2 Hz.

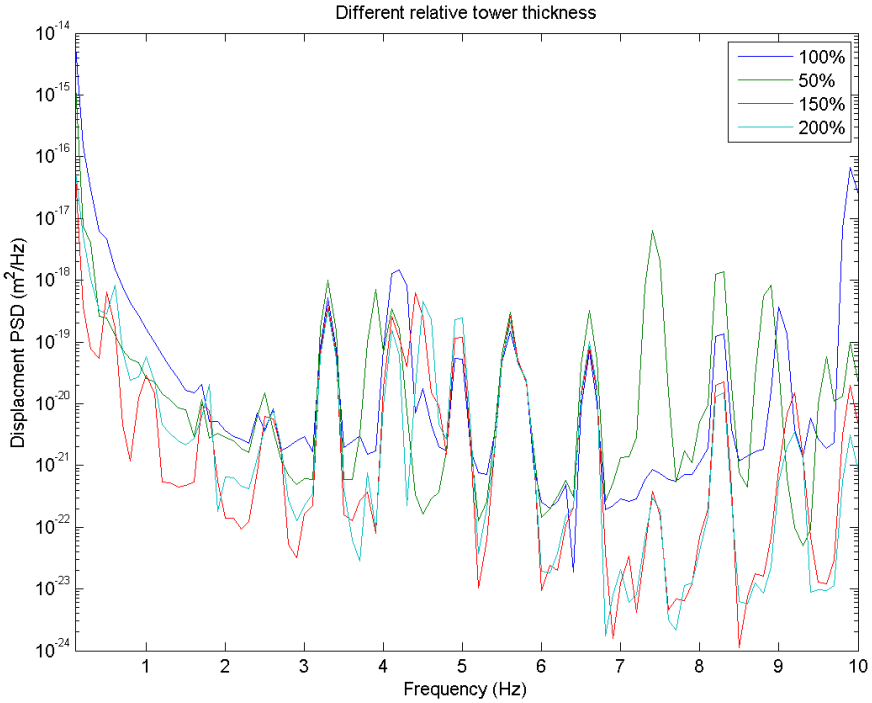

Figure 58 – Variation of seismic amplitude modelled 480 m down-wind from a turbine with different tower stiffness where the stiffness is related by varying the tower thickness relative to an N80 (100% represents an unmodified N80). The amplitude of peaks are insensitive to change in tower stiffness except for those related to structural resonances such as the second bending mode that varies between 3.9 and 5 Hz depending on the tower stiffness.

5.4 Discussion

The near- and far-field models generally correlate well with the measurements of Nordex N80 wind turbines at Craig wind farm. The models show similar amplitudes to those observed in the field and the dominance of Rayleigh waves, particularly down-wind from the turbine. The models show similar relationship between wind speed, seismic amplitude and the positions of blade-pass multiples as those observed at Craig wind farm. Furthermore, the models show a similar azimuth effect to that observed at Craig wind farm. The correlation of the models with field observations suggests that the generation of seismic waves at less than 8 Hz by wind turbines can be explained by the shadow and wake of blade-pass varying the dynamic force on the wind turbine tower combined with torque flutter on the rotor due to the blade moving through a vertical wind profile.

The modelled amplitudes of seismic vibrations related to structural resonances are significantly higher than those measured at Craig wind farm. However, the measurement at Clyde wind farm were dominated by vibrations related to structural resonances, so this behaviour captured by the model has been noted in the field. It should be noted that a physics process at the interface between the foundation and the bedrock (or close to it) has not been included in the model; such as a visco-elastic process (the model only considers elastic behaviour). Such a process would explain the difficulty of relating on-tower measurements to the far-field.

The variance models show that the seismic vibration is insensitive to surface roughness length. The blade-pass multiple peaks are also insensitive to the tower stiffness and nacelle mass, though these two parameters do

affect the power in peaks related to structural resonances. An algorithm therefore need not include roughness length and predictions of blade-pass multiples need not include tower stiffness nor nacelle mass.

6 UTILISATION FACTOR

The 2005 Budget incorporates a utilization factor to reflect the varying wind conditions across the consultation zone as not all wind farms will be operating at their maximum rated power at the same time. A utilization factor of 60% was chosen (Styles, et al. 2005), this was based on a percentage utilisation which is only exceeded 20% of the time. The factor was chosen after input from the BWEA who stated that a group of wind farms, rarely, if ever operate at maximum rated power and that for much of the time they operate at considerably less than rated power. Power output data from five wind farms (Figure 59) was collected for the period 1st July to 30th September 2004 (Styles, et al. 2005).

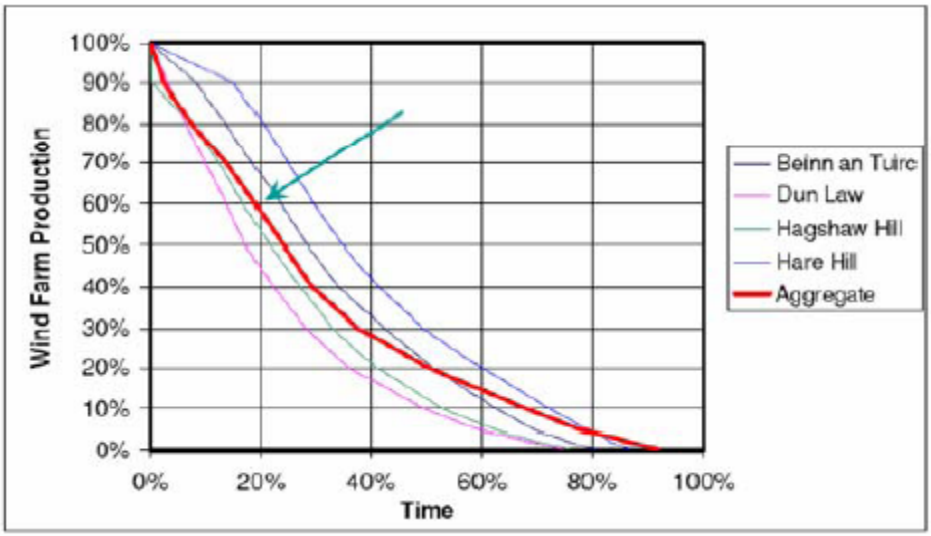

Figure 59 Production Data from wind farms 1st July to 30th September 2004 (Styles, et al. 2005)

6.1 Revised utilisation factor

In order to reasses the utilisation factor the most recent empirical data was gathered and analysed. As wind masts have a higher level of accuracy than nacelle anemometers data from masts was chosen to be the most accurate source of wind speed data. Wind speed data was kindly provided by developers from the FMB. Information from 34 anemometry masts was supplied from seven developers. Prevailing Wind Farm Analysis Ltd were contracted to undertake an assessment of cumulative probabilistic wind conditions across the Eskdalemuir consultation zone. The full report submitted by Prevailing can be seen in Appendix E.

From the potential 34 masts, 14 wind masts were chosen to provide a representative concurrent sample for the EKA consultation zone. The wind measurements were processed, checked and calibrated to ensure a high quality final data set at each mast. Assuming a power curve for a representative turbine in the region (Siemens SWT-2.3-93 turbine), concurrent wind data from the masts for the 2 year period from 1 January 2008 to 31 December 2009 were used to predict a time series of expected power production of an assumed wind

farm at each mast location. The probability of the total power output of these wind farms, exceeding different proportions of their total rated capacity, was then calculated.

Taking the same assumption as for the 2005 study if the percentage utilisation is only exceeded 20% of the time, then the utilisation factor is **82 % (**Figure 60**)**. However, as the conservation of energy approach (Section 7) has been adopted, the rms SGV is proportional to the square-root of 0.82 (i.e., 0.9). The reasoning is that rated-power is approximately proportional to the square of the rotor diameter (swept area), which in turn is proportional to the available kinetic energy from the wind.

There are many contributions to the utilisation factor not currently considered, for example, the length scale of correlation of wind speeds. This may be significant given that turbines closer to the Array have more impact than those further away.

Further work could establish the correlation of wind speed at the array with that at increasing distance from the array. The methodology adopted by Prevailing in their analysis could be extended to achieve this. A revised utilisation factor could also consider the mean-time between failure of wind turbines, the developable areas in the consultation zone (see Section 9), the success-rate of proposed developments (e.g., failure due to cumulative visual impact), and the threshold.

Given that the utilisation factor calculated by Prevailing is close to unity, and the possible further work outlined above, it is recommended that the cumulative SGV algorithm uses a utilisation factor of unity.

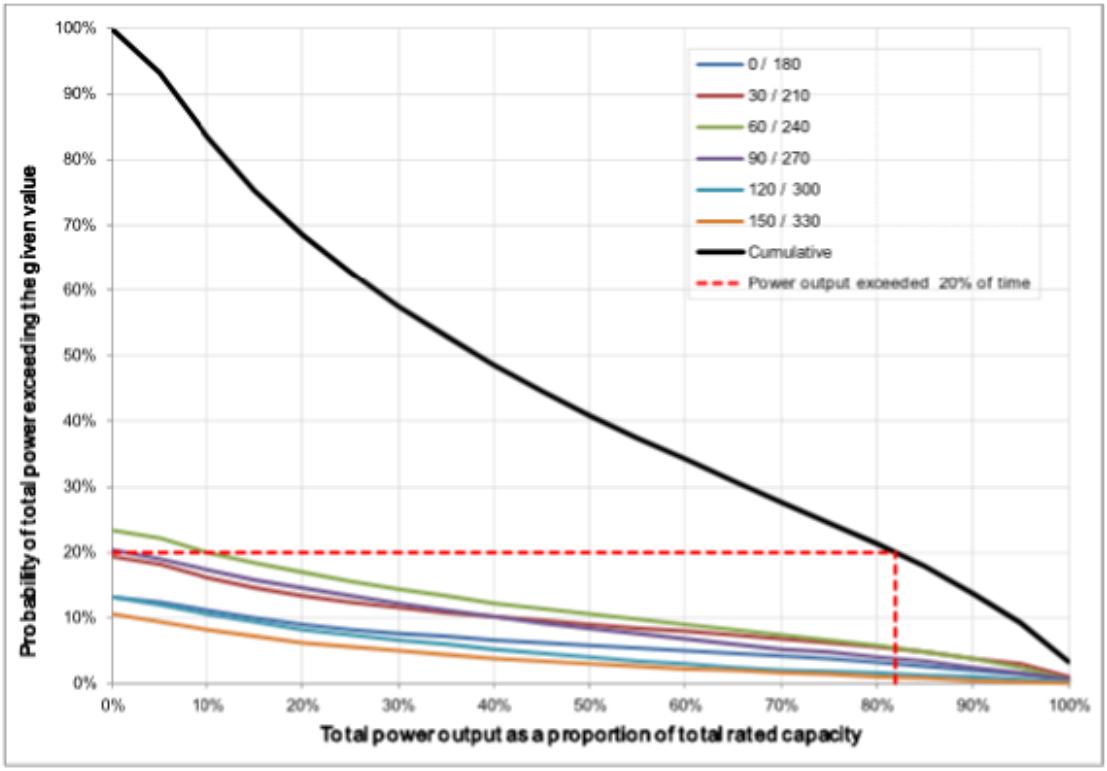

Figure 60 - Cumulative probability of power output across all 14 wind farms, including directional variation, Appendix E.

7 CONSERVATION OF ENERGY APPROACH

7.1 Introduction

A conservation of energy approach will be used as the basis of a physics-based algorithm to predict the amplitude of seismic vibrations generated by wind turbines. The basis of this approach is that the wind passing through the rotor of a wind turbine has a finite amount of energy that can be calculated based on its kinetic energy (i.e. mass air and its velocity). Some portion of kinetic energy is turned into vibration which passes through the foundation and propagates away as seismic energy. If the proportion of energy converted from kinetic energy into seismic vibration is close to constant then a source-term can be calculated based on the kinetic energy passing though the rotor at any unit time. This section tests such a hypothesis and determines whether a conservation of energy approach is appropriate to develop the physics-based algorithm.

7.2 Hypothesis

- A finite amount of kinetic energy moves through the rotor of a wind turbine.
- Some portions of this energy will be converted to electrical energy, noise, seismic vibration or lost by viscous effects. Some portion of the kinetic energy will remain in the wind as air flows away from the wind turbine (Betz' law).
- If the proportions of energy conversion and lost are consistent then the energy in the seismic vibration should be proportional to kinetic energy of the wind moving through the rotor.

7.3 Test

- The kinetic energy in the wind moving through the rotor per unit time is given by the power:
  - $P = \frac{1}{2}\rho A {v_w}^3$

    where ρ is the density of air, A is the swept area of the rotor , and v_w is the wind speed.
- Taking the density of air to be constant, then energy of the seismic vibration should be proportional to the area of the rotor and the cube of the wind speed.
- The energy of the seismic vibration is proportional to the square of its ground velocity
- The Craig, Clyde and Dun Law data sets contain data for different swept areas and different wind speed.
- To test the hypothesis the interquartile mean data from Craig, Clyde and Dun Law wind farms were normalised using different exponents of swept area and wind speed.

7.4 Method

Velocity PSD were normalised to a single turbine measured at 1 km by considering the number of turbines running and the attenuation with distance from each of those turbines to the sensor location by cylindrical spreading and non-geometric attenuation. It is assumed that the arrival of seismic vibrations from each turbine at the sensor are not in-phase and a normalisation factor for the number of turbines and varying distances $N_{norm(r,f)}$ is given by the sum of squares:

$$\boldsymbol{N_{norm(r,f)} = \sqrt{\sum_{i=1}^{N}\left(\sqrt{\frac{r_{ref}}{r_i}}\exp\left(-\frac{\pi f(r_i - r_{ref})}{Qc}\right)\right)^2}} \quad [9]$$

where N is the number of turbines at distances r_i from the sensor. The reference distance r_{ref} is 1000 m, f is the frequency in Hz, Q is a factor relating non-geometric attenuation and is equal to 50 for the Southern Uplands and c is the speed of Rayleigh waves taken as 2000 ms^{-1} for the Southern Uplands, (MacBeth 1986).

Velocity PSD, v_{PSD}, of each spectra measured at 7 ms^{-1} or above at each wind farm were then normalised to v_{norm} by swept area, A, and wind speeds, v_w, with different exponents:

$$\boldsymbol{v_{norm}} = \frac{\boldsymbol{v_{PSD}}}{\boldsymbol{N_{norm} \times A^n \times v_w{}^m}} \quad [10]$$

Where, n and m are exponents that were varied between -2 and 4, and -2 and 6 respectively.

The rms velocity for each normalised spectra was then calculated in the:

- 1.5 to 4.5 Hz band
- 1.71 to 5.76 Hz band
- 2nd, 3rd and 4th blade pass multiples ± 0.25 Hz

and the result squared (as energy is proportional to the square of velocity) and the variance of all data for each combination of n and m compared. The combination of the exponents that have the lowest variance was taken to be the best fit. The swept area A for each turbine is shown in Table 20.

Wind farm	Turbine	Rotor diameter (m)	Swept area (m^2)
Craig	N80	80	5026.5
Dun Law	V47	47	1734.9
Clyde	S23	93	6792

Table 20 – Swept area of rotors at each wind farm used to normalise each spectrum

7.5 Results

The variance rms velocity in the 1.5 to 4.5 Hz band of normalised amplitude using different exponents for wind speed and swept area is shown in Figure 61. Exponents that produce lowest variance in rms velocity in the 1.5 to 4.5 Hz band are n=1 and m =3. Table 21 shows the exponents that result in the lowest variance in all frequency bands examined. Figure 62 shows a comparison of all spectra before being normalised and Figure 63 shows the result of normalisation by wind speed and swept area.

Frequency band	Area exponent - *m*	Wind speed exponent - *n*
1.5 to 4.5 Hz	1	3
1.71 to 5.76 Hz	1	3.25
2nd Blade pass multiple	1.5	2
3rd Blade pass multiple	1	3.5
4th Blade pass multiple	1	3.5

Table 21 – The combination of exponents that produce the minimum variance in the normalised data for different frequency bands

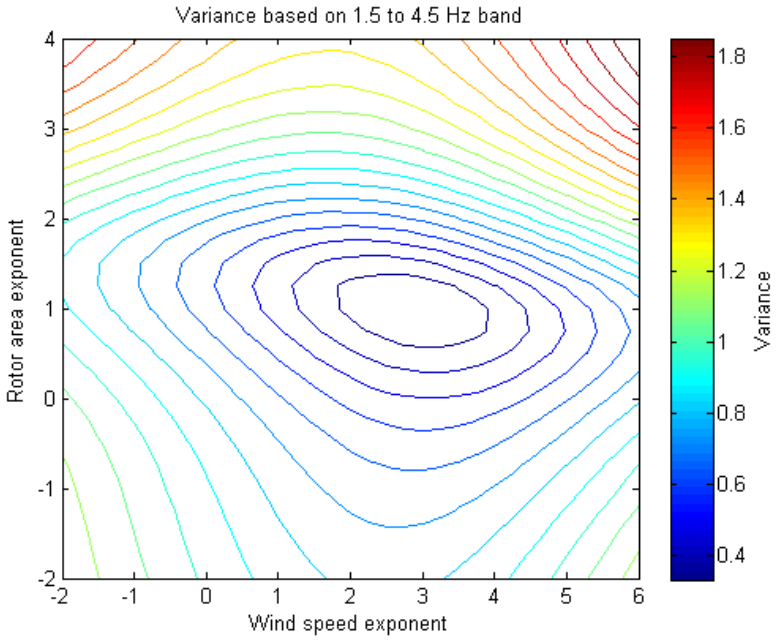

Figure 61 – Variance of rms velocity in the 1.5 to 4.5 Hz band of data from Craig, Dun Law and Clyde wind farms at wind speeds between 7 and 15 ms-1 when normalised using different exponents for wind speed and swept area. The minimum variance is for a rotor area exponent of 1 and a wind speed exponent of 3.

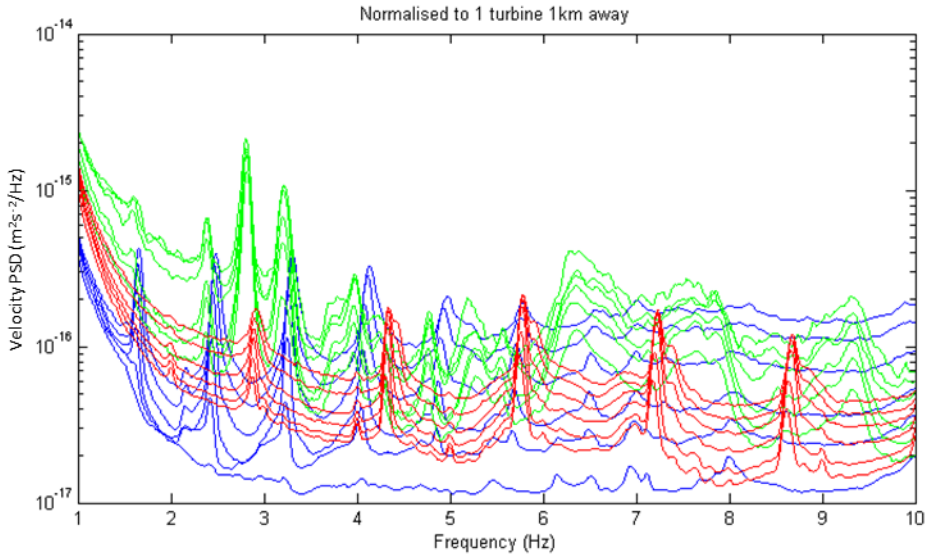

Figure 62 – Comparison of spectra from Craig (blue), Clyde (green) and Dun Law (red) before being normalised by wind speed and swept area

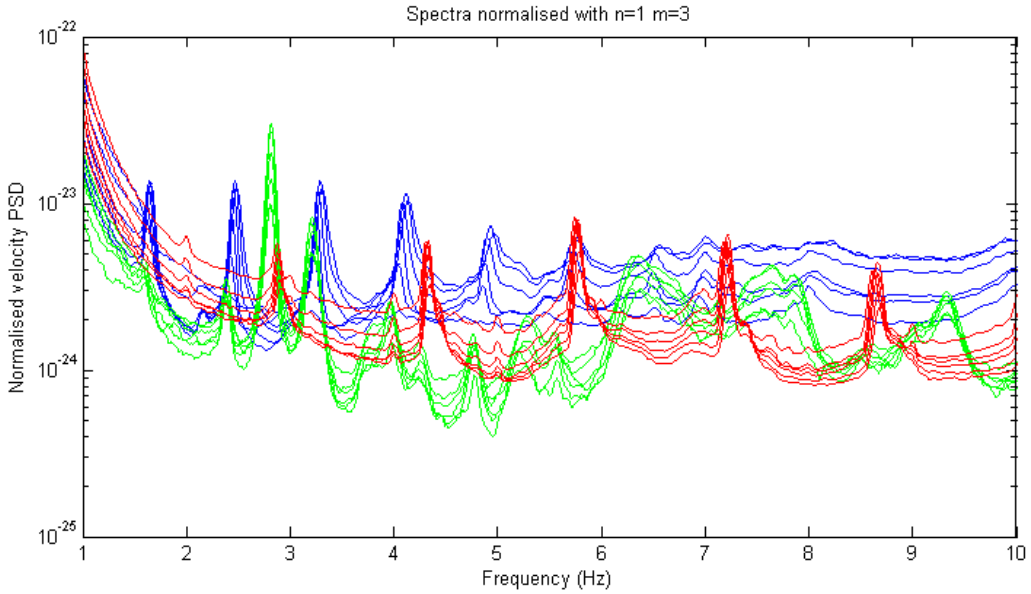

Figure 63 – Comparison of spectra from Craig (blue), Clyde (green) and Dun Law (red) for wind speeds between 7 and 12 ms^{-1} normalised using n=1 and m=3 (units are arbitrary).

7.6 Conclusion

- The exponents that best normalise data for different wind speeds and turbines with different swept areas are ~1 and 3 respectively.
- This result is close to the hypothesis where it was conjectured that the square of the seismic amplitude should vary linearly with the swept area and the cube of wind speed.
- The hypothesis is not disproven.
- The conservation of energy approach is appropriate for developing a physics-based algorithm for predicting seismic vibration from a wind turbine

8 A PHYSICS-BASED ALGORITHM

8.1 Introduction

The kinetic energy contained within the wind travelling through the rotor of a wind turbine for a unit of time increases linearly with the swept area of the rotor and the cube of the wind speed. If some proportion of this kinetic energy is converted to seismic vibration and this proportion is consistent, then the energy of the seismic vibration should also increase linearly with the swept area of the rotor and the cube of the wind speed. The worst-case turbine spectrum can then be normalised by wind speed and swept area of the rotor to conservatively approximate the spectrum produced by any wind turbine for a given wind speed.

An algorithm to estimate the vibration produced by any wind turbine has been developed based on this conservation of energy approach. The algorithm includes a representative worst-case turbine spectrum that has been optimised to fit normalised data from Craig, Clyde and Dun Law wind farms. The amplitude and topology of the representative spectrum is modified based on hub height, swept area and rotational speed to represent any given wind turbine. The algorithm uses a reference wind speed of 12 ms^{-1} at a reference height of 80 m above ground level, which is consistent with the utilization factor calculation. The algorithm uses a frequency-distance weighting curve to calculate the amplitude with respect to its potential harm to EKA.

The algorithm requires the following parameters for each turbine:

- Hub height
- Swept area (based on rotor diameter or tip height)
- Distance of turbine from EKA

All these parameters should be submitted in the normal course of a planning application.

8.2 Methodology

8.2.1 OPTIMISATION OF REFERENCE WORST-CASE TURBINE SPECTRUM

A reference worst-case turbine spectrum has been developed that is a function of the wind speed at the hub height, the swept area of the rotor and the rotational speed (via the blade pass frequency). Parameters that define the spectrum were optimised using data from Craig, Dun Law and Clyde wind farms that were normalised to represent single turbines measured at a distance of 1 km based on:

$$\boldsymbol{d_{norm(r,f)}} = \frac{\mathbf{d_{PSD}}}{\sum_{i=1}^{N}\left(\sqrt{\frac{r_{ref}}{r_i}}\exp\left(-\frac{\pi f\left(r_i - r_{ref}\right)}{Qc}\right)\right)^2} \quad [11]$$

Where, d_{psd} is the displacement PSD, N is the number of turbines at distances r_i from the sensor. The reference distance r_{ref} is 1000 m, f is the frequency in Hz, Q is a factor relating non-geometric attenuation and is equal to 50 for the Southern Uplands and c is the speed of Rayleigh waves taken as 2000 ms^{-1} for the Southern Uplands, (MacBeth 1986).

The reference worst-case spectrum is given by the sum of three functions representing a peak related to a structural resonance, peaks related to blade pass multiples and a curve related to operational broadband noise. The curves are represented by the continuous functions below with explanations and values for the parameters listed in Table 22:

1. The operational broadband noise is based on the difference in power between when all turbines at Craig were running and when no turbines were operational. The broadband noise is modelled as:

$$\boldsymbol{OBN}_{(f,v_w,A)} = \boldsymbol{C}_{\boldsymbol{OBM}} \frac{A{v_w}^3}{f^2} \quad [12]$$

   Where, C_{OBM} best fit to data from AEG-5/6351, f is frequency in Hz, A is the swept rotor area in m^2 and v_w is wind speed in ms^{-1}.

2. A peak representing the second bending mode of the Siemens 2.3 turbine is represented as the normal distribution:

$$\boldsymbol{BM}_{(f,v_w,A,f_{BM})} = \boldsymbol{C}_{\boldsymbol{BM}} A{v_w}^3 \left(\exp\left(-\frac{(f-f_{BM})^2}{2{\sigma_{BM}}^2} \right) \right) \quad [13]$$

   Where, f_{BM} is the resonant frequency of the second bending mode, C_{BM} defines the amplitude of the peak and σ_{BM} defines the width of the peak. The constants C_{BM} and σ_{BM} were optimised against the interquartile mean of all wind speed bins between 7 and 12 ms^{-1}. The optimisation used the lowest value of C_{BM} that enclosed the peak related to the structural resonance at all wind speeds (see Appendix F.1 for figures showing fit). It should be noted that the amplitude of the second bending mode measured at Clyde increases almost linearly with wind speed as opposed to with the cube as in equation [13] (see Appendix F.1). To maintain consistency and following a conservative worst-case scenario the algorithm will use the cube of wind speed for the peak related to structural resonance.

3. Peaks related to blade pass multiples are represented by the sum of a series of normal distributions each relating to integer multiples:

$$\boldsymbol{BP}_{(f,v_w,A,f_{BP})} = \boldsymbol{C}_{\boldsymbol{BP}} A{v_w}^3 \sum_{n=1} \left(\exp\left(-\frac{(f-nf_{BP})^2}{2{\sigma_{BP}}^2} \right) \frac{1}{(nf_{BP})^{\beta}} \right) \quad [14]$$

   Where, n is the integer multiple, f_{BP} is the blade pass frequency and C_{BP} is a constant defining the amplitude of the peak, β defines how the amplitude of peaks varies with frequency and σ_{BM} defines the width of peaks. The values of C_{BP} and β were optimised using the 2nd to 6th blade pass multiples for all wind speeds between 7 and 12 ms^{-1} at Craig, Clyde and Dun Law wind farms. The optimal values were taken as the combination of C_{BP} and β that gave the best least squares fit that still enclosed all blade-pass multiples at all wind speeds. The fit of C_{BP} and β to the data are shown in Appendix F.1.

The functions defined in equations [12] to [14] are summed to give the worst-case turbine spectrum as a function of frequency for any turbine dependent on wind speed, swept area and blade pass frequency:

$$\boldsymbol{WCT}_{(f,v_w,A,f_{BM},f_{BP})} = \boldsymbol{OBN}_{(f,v_w,A)} + \boldsymbol{BM}_{(f,v_w,A,f_{BM})} + \boldsymbol{BP}_{(f,v_w,A,f_{BP})} \quad [15]$$

Symbol	Description	Value
f	Frequency	
A	Swept area of the rotor of any given wind turbine	
v_w	Wind speed at the hub height of any given wind turbine	
C_{OBM}	Operational broadband noise multipliers	2.2282e-26 $[m^2/Hz].[m^{-5}s]$
f_{BM}	Frequency of bending mode	2.808 Hz
C_{BM}	Bending mode amplitude multiplier	1.595e-22/12^3 $[m^2/Hz].[m^{-5}s^3]$
σ_{BM}	Bending mode shape parameter	0.05 Hz
rpm	Rotational speed of rotor	
f_{BP}	Blade pass frequency of a given turbine at a given wind speed	
n	Blade pass multiple (integer)	
C_{BP}	Blade pass amplitude multiplier	4.9661e-22/12^3 $[m^2/Hz].[m^{-5}s^3]$
σ_{BP}	Blade pass shape parameter	0.04 Hz
β	Blade pass amplitude exponent	1.76

Table 22 – Parameters and values used to construct the reference worst-case turbine spectrum

8.3 The physics-based algorithm

The algorithm has been developed so that the parameters used to define the shape of the worst-case turbine spectra are submitted with planning documents as a matter of course. This approach is used to make the physics-based algorithm more easily applicable to regulation of seismic vibration at EKA. Equation [15] is dependent on wind speed and blade pass frequency. The algorithm will define the wind speed based on hub height using a log-law and will define the blade pass frequency based on the rotor diameter. Thus, the shape of the worst-case spectra for any given turbine can be defined by hub height and rotor diameter.

8.3.1 WIND SPEED AT HUB HEIGHT

A log-law is used to determine the wind speed at the hub height of any given turbine based on a reference wind speed of 12 ms^{-1} at a reference height of 80 m. The wind speed at any hub height is given by:

$$v_w = v_{ref} \frac{\ln(z_{hub}/z_l)}{\ln(z_{ref}/z_l)} \quad [16]$$

where z_{ref} is the reference height of 80 m, v_{ref} is the reference wind speed at 12 ms^{-1}, z_{hub} is the hub height for the given turbine and z_l is the standard ground roughness length taken as 0.05m (from the ETSU-R-97 Standard used to access wind turbine acoustics) (Figure 64). Thus v_w can be calculated for any given turbine based on its hub height.

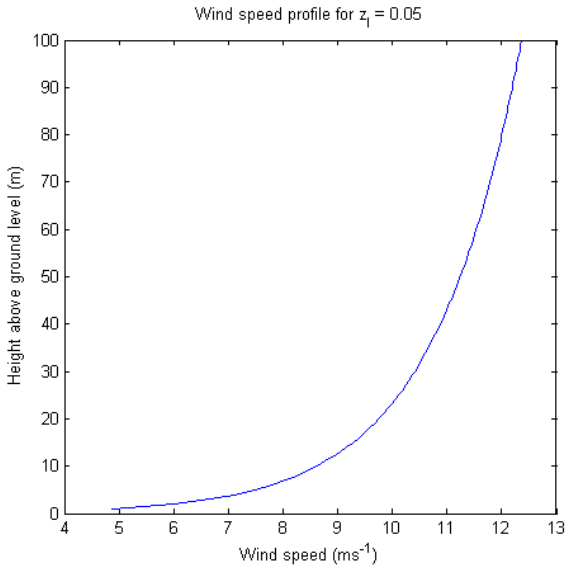

Figure 64 – Wind speed profile based on a log-law with a ground roughness length of 0.05 m

8.3.2 ROTOR SPEED VARIATION WITH BLADE LENGTH

The rotational speed of wind turbines tends to be controlled by the maximum tip speed. As tip speeds increase the acoustic emissions of the turbine also increase, as does the centripetal forces on the blades. These engineering constraints tend to keep tip speeds below 100 ms^{-1}. Furthermore, the efficiency of turbines directly relates to the ratio between tip speed and wind speeds so that tip speeds tend to group between 50 ms^{-1} to 90 ms^{-1}. A survey of 63 on-shore turbines with hub heights between 35 m and 142 m, rotor diameters between 44 m and 116.8 m and rated powers between 0.5 MW and 3.4 MW (see Appendix F.2) show tip speeds tend to be between 70 and 80 ms^{-1} with a median tip speed of 77.5 ms^{-1} (Figure 65). The mean tip speed of the sample set is 78.78 ms^{-1} with a standard deviation of 7.75 ms^{-1}.

The tip speed is independent of the rotor diameter and rotational speed. The rotational speed of any turbine, and by extension its blade pass frequency, will be calculated in the algorithm by assuming the all turbines have the median tip speed of 77.49 ms^{-1}:

$$\boldsymbol{f_{BP} = 3 \times \frac{77.49}{\pi \emptyset_R}} \quad [17]$$

where $\emptyset_R$ is the rotor diameter (m) and the 3 is for a three bladed turbines. The swept area of the rotor is also related to the rotor diameter by:

$$\boldsymbol{A = \pi \left({}^{\emptyset_R}/_{2} \right)^2} \quad [18]$$

equations [16], [17] and [18] can now be inserted into equations [12] to [15] so that the worst-case turbine can be defined by hub height and rotor diameter.

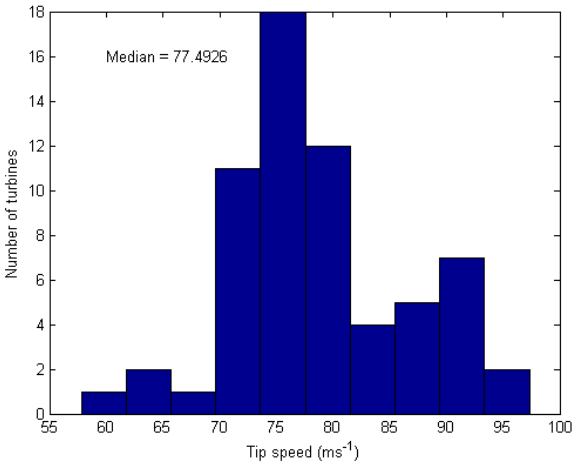

Figure 65 – Histogram showing the distribution of tip speeds from 63 different turbines for wind at a variety of hub heights, rated powers and rotor diameters (see Appendix F.2).

8.3.3 FREQUENCY-DISTANCE WEIGHTING FUNCTION FOR EKA

The algorithm calculates the amplitude with respect to its impact on the detection capabilities of EKA using a frequency-distance function. The amplitude for any turbine at a distance *r* from EKA is then given by:

$$\boldsymbol{Amp}_{(f,z_{hub}\emptyset_R,r)} = \sqrt{\int_{0.5}^{8} \boldsymbol{WCT}_{(f,z_{hub}\emptyset_R,r)} \boldsymbol{w}_{(r,f)} \boldsymbol{df}} \qquad [19]$$

where $w_{(r,f)}$ is the frequency-distance weighting function (Bowers 2013).

8.3.4 SENSITIVITY OF CALCULATED AMPLITUDE TO SITE-SPECIFIC PARAMETERS

To simplify the physics-based algorithm two parameters that vary with turbines and sites are treated as constants: the roughness length used to determine wind speed, the tip speed used to infer the rotational speed of the rotor and the blade pass frequency. The values of these two parameters were varied and the amplitude calculated using equation [19] for a turbine with a rotor diameter of 80 m and hub height of 100 m at a distance of 20 km from EKA. The sensitivity of amplitude to roughness length is shown in Figure 66 and the sensitivity to tip speed is shown in Figure 67. The calculated amplitude was insensitive to the roughness length with only a 2% variation over the broad range of lengths examined. The amplitude was more sensitive to the tip speed over the broad range of speeds examined, however over the 70 ms^{-1} to 80 ms^{-1} range that most turbines operate the amplitude only varied by 3%. The authors are satisfied that the setting of the roughness length and tip speed as constants does not introduce large errors into the physics-based algorithm.

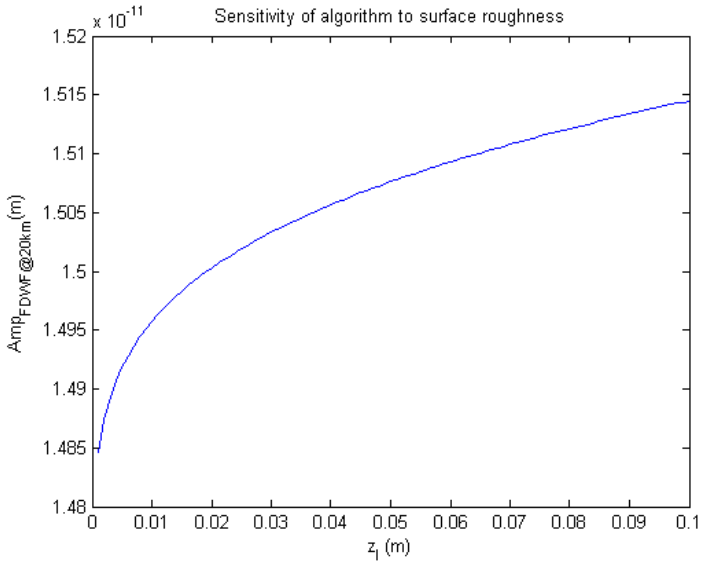

Figure 66 – Sensitivity of physics based algorithm to changes in the value of surface roughness z_l for a turbine with a rotor diameter of 80 m, hub height of 100 m and at a distance of 20 km from EKA.

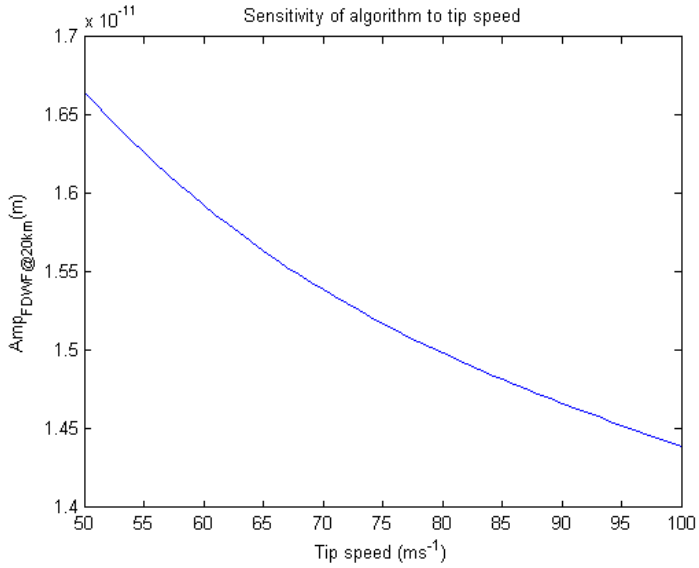

Figure 67 - Sensitivity of physics based algorithm to changes in the value of tip speed for a turbine with a rotor diameter of 80 m, hub height of 100 m and at a distance of 20 km from EKA.

8.4 Application of the physics-based algorithm

The worst-case amplitude with respect to EKA can now be calculated for any wind turbine based on the physics-based algorithm. The wind speed is calculated based on the turbine hub height and the swept area is calculated based on the rotor diameter. Example parameters for three different turbines are listed in Table 23, with the resulting representative worst-case spectra shown in Figure 68. Examples of the application of the frequency-distance weighting function to these representative worst-case spectra are shown for distances from EKA of 10 km, 30 km and 50 km in Figure 69, Figure 70 and Figure 71 respectively; peaks progressively move to lower frequency and amplitude reflecting the frequency-dependent attenuation of seismic vibration

(where high frequency vibrations attenuate more rapidly). Figure 72 shows how the worst-case amplitude for each turbine varies with distance from EKA.

Wind farm	Turbine	Hub Height (m)	Rotor diameter (m)	Swept area (m^2)
Craig	N80	60	80	5026.5
Dun Law	V47	40	47	1734.9
Clyde	S23	78.3	93	6792

Table 23 – Parameters from different wind turbines used to determine representative worst-case spectra for turbines.

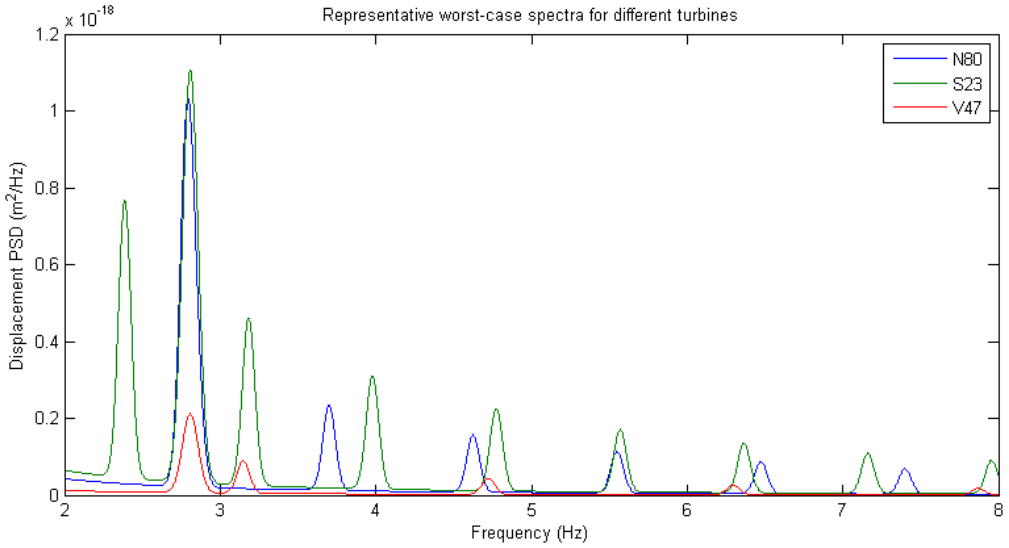

Figure 68 – Representative worst-case spectra for different wind turbines based on rotor diameter and hub height

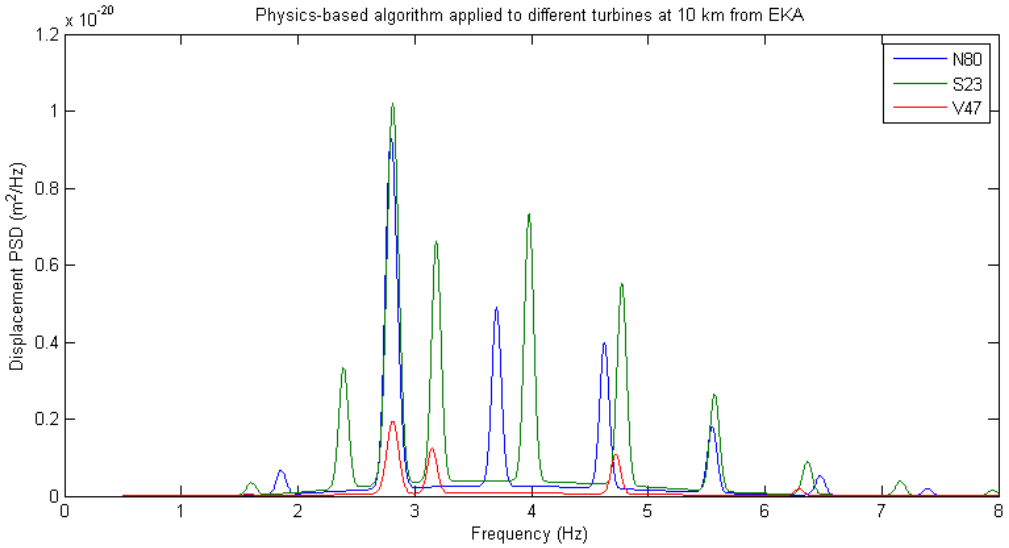

Figure 69 – Frequency-distance weighting function appropriate for 10 km from EKA applied to representative worst-case spectra for different wind turbines based on rotor diameter and hub height

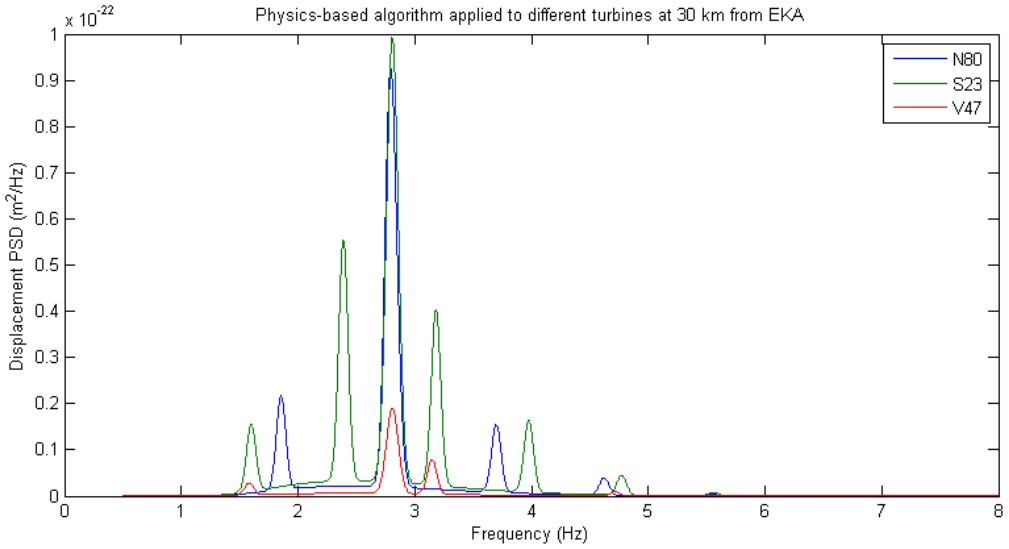

Figure 70 - Frequency-distance weighting function appropriate for 30 km from EKA applied to representative worst-case spectra for different wind turbines based on rotor diameter and hub height

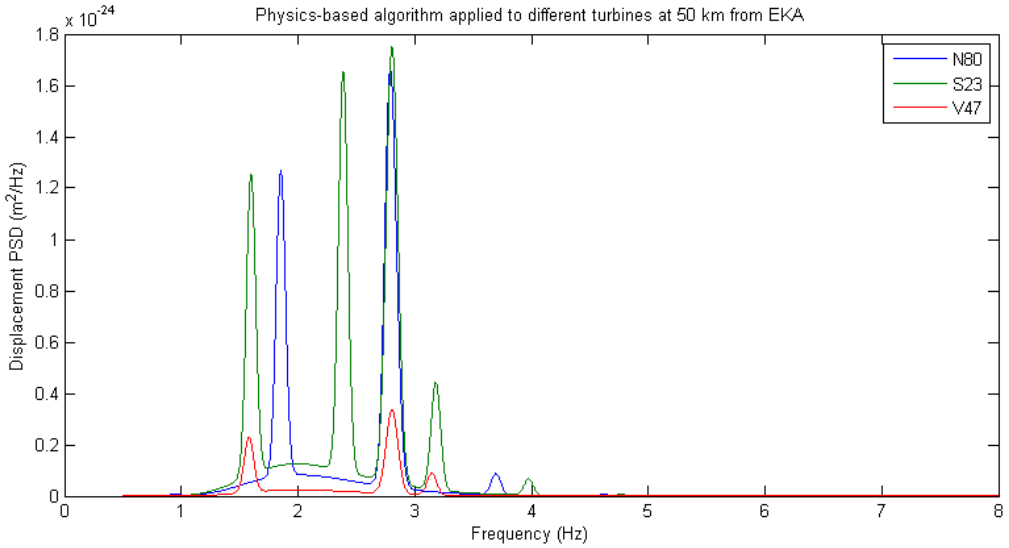

Figure 71 - Frequency-distance weighting function appropriate for 50 km from EKA applied to representative worst-case spectra for different wind turbines based on rotor diameter and hub height

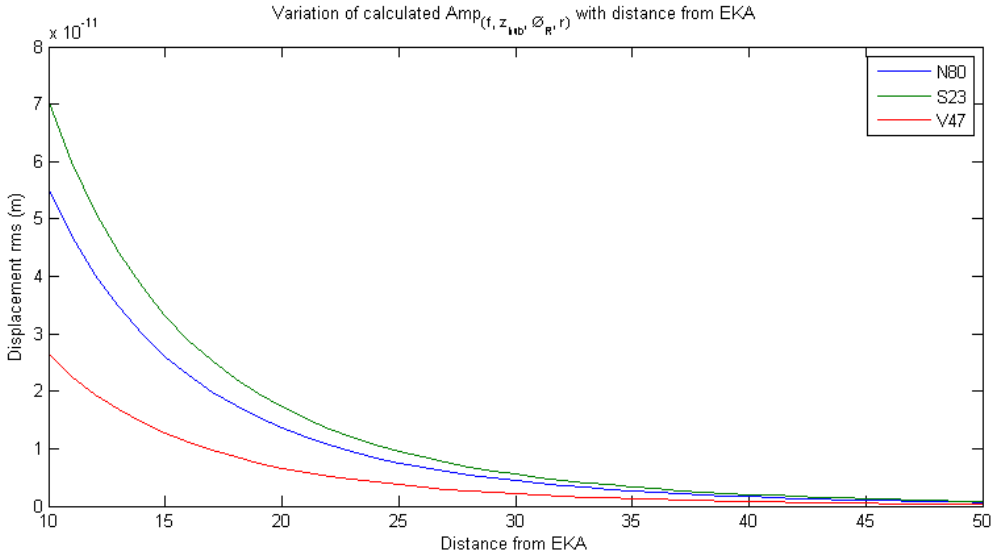

Figure 72 – Variation of calculated amplitude with distance from EKA for representative worst-case spectra for different wind turbines based on rotor diameter and hub height

8.4.1 CALCULATION OF CUMULATIVE SEISMIC VIBRATION AT EKA

The distance of individual turbines from EKA, their hub heights and rotor diameters can now be inserted into equation [19] to determine the cumulative amplitude of all wind turbines. The distances used are those in "Dec 13 master allocated budget.xls" and "Dec 13 master objections.xls" issued to Xi by David Boyd of MoD on 21/1/2014; hub heights and rotor diameters can be found in Appendix F.3. Calculations were made with double precision values and a frequency step of 0.001 Hz. The amplitude calculated using the physics-based algorithm and multiplied by the utilisation factor of unity for each of the wind farms allocated budget are listed in Table 24 and for those currently subject to objection in Table 25. The cumulative amplitude of all turbines currently allocated budget and currently subject to objection with an utilisation factor of unity is **0.1938325 nm.**

Wind farm	Number of Turbines	Average distance to EKA (km)	Average hub height (m)	Average rotor diameter (m)	Amplitude (nm)
Bowbeat	24	42.304	45	62	0.0044189
Carlesgill	5	20.050	70	80	0.0316142
Halkburn - Long Park	19	42.854	60	80	0.0054466
Clyde	152	29.993	78.3	93	0.0733050
Harestanes	71	27.296	70	80	0.0516526
Dalswinton	15	35.872	67	80	0.0096084
Minsca	17	24.816	80	84	0.0359219
Carcant	3	49.191	80	54	0.0007891
Ewe Hill	22	19.016	70	80	0.0753827
Langhope Rig	10	21.359	80	90	0.0446930
Andershaw	14	46.639	80	90	0.0040505
Middle Hill - Glenkerie	11	29.240	85	70	0.0145149
Langshaw Farm	1	43.780	30	19	0.0001834
Earlshaugh	22	21.097	71.82	85.91	0.0643968

Table 24 – Wind farms currently allocated budget with amplitude calculated using the physics-based algorithm and a utilisation factor of 1. The amplitudes are calculated based on each turbines individual distances, hub height and rotor diameter. Average distance to EKA, hub heights and diameters are shown here as they are indicative (see Appendix F.3 for actual hub heights and rotor diameters).

Wind farm	Number of Turbines	Average distance to EKA (km)	Average hub height (m)	Average rotor diameter (m)	Amplitude (nm)
Minnygap	10	25.271	80	90	0.0283227
Carlesgill Ext	1	19.070	70	80	0.0157426
Newfield - Balgray Caslemilk	21	20.815	80	90	0.0705475
Burnhouse - Rowantree	19	49.196	80	90	0.0037787
Townhead 2	1	37.336	30	19	0.0003448
South Mains	3	48.754	60	48	0.0006859
Hall Burn	6	39.806	84	94	0.0052608
Whinneyrig	1	36.110	36.5	19.2	0.0004136
Bluecairn	1	45.736	37	20.9	0.0001788
Rivox	1	23.373	15	8.56	0.0005493
Shaw Park	9	44.918	64	71	0.0027316
Auchencairn	16	34.644	80	82	0.0119625
Clyde Extension	54	29.897	87.22	103.44	0.0494467
Glentaggart	5	47.921	80	104	0.0025729
Solwaybank	15	25.660	80.5	92	0.0341980
Middle Muir	17	45.664	100	104	0.0060604
Blackwood	5	37.326	92	80	0.0051282
Barrel Law	8	19.372	80	90	0.0509726
Land N of Midtown Farm	1	47.861	24.6	19.2	0.0001206
Kirkhill	1	34.635	15	10.4	0.0002023
Cloich Forest	18	42.958	80	104	0.0076884
Muircleugh	6	46.594	65	90	0.0025497
Sleetbeck Plantation	1	36.241	41.2	29	0.0007048
Woodheads Farmhouse	1	47.290	30.6	19.2	0.0001339

Wind farm	Number of Turbines	Average distance to EKA (km)	Average hub height (m)	Average rotor diameter (m)	Amplitude (nm)
Leadhills	14	43.872	90	94	0.0055950
Glenkerie Extension	6	29.673	80	64	0.0090926
Girthgate	24	47.907	80	102.25	0.0055455
Lion Hill	4	29.516	80	93	0.0117345
Crookedstane Farm	4	31.356	80	93	0.0096763
Windy Edge	17	23.545	77.65	82	0.0403663
Parkgatestone Farm	4	35.715	18.79	7.28	0.0002694
Scotstoun Bank	1	41.115	18.5	20.2	0.0002267
Lampits Farm 2	1	49.982	49.5	30	0.0002113
Broomhill Farm	1	49.907	50	48	0.0003446
Solway re-sub (Beckburn)	9	36.871	80	92.5	0.0082930
Harestanes Ext	7	27.283	80	93	0.0198313
Twentyshilling Hill	9	48.029	85	80	0.0025327

Table 25 – Wind farms currently objected to on the basis of seismic vibration with amplitude calculated using the physics-based algorithm and an utilisation factor of 1. The amplitudes are calculated based on each turbines individual distances, hub height and rotor diameter. Average distance to EKA, hub heights and diameters are shown here as they are indicative (see Appendix F.3 for actual hub heights and rotor diameters). The Solway and Hall Burn farms appear twice on the tables issued to Xi due to the farms having been re-submitted to planning; in both cases the higher amplitude of the entry has been included, which are Solway re-sub (Beckburn) and the initial Hall Burn submission.

As the study gathered no empirical data for turbines of hub height less than 40 m, a logical approach to ensure the calculated seismic amplitude is based on current findings is to set a default minimum hub height of 40 m. By adopting this approach and setting all towers less than this default to 40 m produces amplitudes given in Table 26. The cumulative amplitude of all turbines currently allocated budget and currently subject to objection with an utilisation factor of unity and minimum hub height of 40 m is **0.1938333 nm**

Wind farm	Number of Turbines	Average distance to EKA (km)	Average hub height (m)	Average rotor diameter (m)	Amplitude (nm)
ALLOCATED					
Langshaw Farm	1	43.780	40	19	0.0001959

Wind farm	Number of Turbines	Average distance to EKA (km)	Average hub height (m)	Average rotor diameter (m)	Amplitude (nm)
OBJECTED					
Townhead 2	1	37.336	40	19	0.0003683
Whinneyrig	1	36.110	40	19.2	0.0004222
Bluecairn	1	45.736	40	20.9	0.0001820
Rivox	1	23.373	40	8.56	0.0006970
Land N of Midtown Farm	1	47.861	40	19.2	0.0001350
Kirkhill	1	34.635	40	10.4	0.0002567
Woodheads Farmhouse	1	47.290	40	19.2	0.0001424
Parkgatestone Farm	4	35.715	40	7.28	0.0003225
Scotstoun Bank	1	41.115	40	20.2	0.0002725

Table 26 - Updated amplitude calculated for the sites listed in Table 24 and Table 25 affected by the minimum hub height default of 40 m due to the lack of empirical data below this height.

9 ANALYSIS FOR SIZE OF EXCLUSION ZONE

9.1 Introduction

In order to allow a policy decision to be made on the potential extension of the current 10 km exclusion zone an analysis is presented here which reviews the potential for wind farm development within the consultation zone. Calculations are performed to determine the distance at which the budget would be reached based on the potential developable land, turbine density, utilisation factor and the success of planning applications using a representative 2.3MW Turbine. Many regions within the Eskdalemuir consultation zone would not be considered for wind energy development due to having low wind speed conditions, being on very steep ground, too close to housing or sites of natural and/or cultural heritage. Tim French of RES has provided Xi with an estimate of the proportion of land that may have potential for wind energy development as a function of distance from EKA. An estimate of the most efficient use of land in the consultation zone can be made by populating the developable land within the consultation zone with wind turbines at some reasonable spacing and using the physics-based algorithm. The information in this section is designed wholly to inform policy related to the size of the exclusion zone surrounding EKA.

9.2 Approach

The percentage of developable area within annuli centred on EKA provide by RES are shown in Table 27. These have been divided into 1 km sub-annuli, where the percentage of developable area is assumed to be consistent with those shown in Table 27. Each annulus was populated with turbines equivalent to a Siemens

2.3 with a hub height of 80m and a rotor diameter of 93 m. Turbines are commonly spaced between ~4 and 8 rotor diameters apart to maximise a wind farm's electrical generation efficiency. However as a developer cannot always build to the extremities of a site the effective density is often lower than the ~4 diameter layout. The density of Clyde wind farm (the largest turbine site currently within the consultation zone) has a density of turbines at approximately 8 rotor diameter spacing, specifically 1.89 turbines per square kilometre. Taking a spacing of 8 rotor diameters for a turbine with a 93 m diameter results in a spacing of 372 m to the nearest neighbour which equates to a density of 1.8066 turbines per square kilometre. Five potential densities of turbine deployment have been used for calculating the distance at which the threshold is reached; 4D, 6D, 8D, 10D and 1 turbine per square kilometre. The physics-based algorithm was applied to each turbine with the distance taken as the inner radius of each annulus.

Whilst utilisation is not to be applied to the budget algorithm calculations unless further work is to be conducted (Section 6), the incorporation of different potential utilisation factors has been performed here to demonstrate the sensitivity to utilisation factor on the point at which the distance at which the threshold is reached (Table 28).

The calculation in Table 28 assumes that 100% of the land would gain ultimately planning permission and therefore be developed. Due to numerous planning factors, including cumulative visual impact this would not be the case in practise. Applying a planning success % to this land would allow these factors to be incorporated when assessing the region of the exclusion zone. RenewableUk have published documentation on the success rates in their state of the industry report (RenewableUK 2013). The report presents historic approval rates by UK country for both local government and ministerial approval by scheme and also MW. It states that the 'UK average rate of consent has continued to fall from the 84 % of capacity approved in 2008/09, to 68 % of capacity consented in 2011/12 and 62 % in 2012/13'. Table 29 uses planning success rated of 50, 75 and 100 % to illustrate the effect that planning success would likely have on development in the region. The numbers of turbines in each annulus based on this spacing is listed in Table 30.

Distance From Array	Percentage Area Developable
10-12km	13
12-14km	11
14-16km	14
16-18km	16
18-20km	11
20-22km	10
22-24km	11
24-26km	13
26-28km	14
28-30km	10
30-35km	8
35-40km	7
40-50km	10

Table 27 – Percentage of area in annuli around EKA that could be developed for wind energy. This assumes that certain areas cannot support wind turbines due to wind conditions, geography and cultural impact.

9.3 Results and Worked Example

In addition to the previously described scenarios of Table 28 and Table 29, as a worked example the area in each annuli, the developable area and number of turbines based on 1 turbine per square kilometre are shown in Table 30. The cumulative amplitude for each of the turbines in each annulus was calculated with the physics-based algorithm with a utilisation of unity and the running amplitude is the quadrature sum of all turbines from the outside annulus (49-50km) moving inward. The 0.336 nm threshold is reached in the 13-14km annulus (Table 30). The relationship between the running amplitude and distance from EKA is shown in Figure 73. For the set of assumptions used the physics-base algorithm calculates that the threshold would be met when all developable areas are filled up to within 13.178 km of Eskdalemuir.

Success = 100%		Turbine Spacing				
		4D	6D	8D	10D	1 turbine per 1km
Utilisation						
0.82	Zone (km)	20.24	16.66	14.19	11.76	11.21
	# Turbines	4473	2177	1291	867	753
	GW	10.28	5.00	2.96	1.99	1.73
0.9	Zone (km)	21.33	17.30	15.00	12.75	12.04
	# Turbines	4375	2120	1291	857	744
	GW	10.06	4.87	2.96	1.97	1.71
1	Zone (km)	22.52	18.13	15.96	13.95	13.18
	# Turbines	4262	2078	1266	846	734
	GW	9.80	4.77	2.91	1.94	1.68

Table 28 - Table showing distance from the array at which budget is reached (zone), total number of turbines and GW for various turbine spacing and utilisation factors.

Utilisation = 1.0		Turbine Spacing				
		4D	6D	8D	10D	1 turbine per 1km
Success						
50%	Zone (km)	18.71	15.43	12.64	10.69	10.13
	# Turbines	2341	1121	674	449	391
	GW	5.38	2.57	1.55	1.03	0.89
75%	Zone (km)	20.89	17.06	14.71	12.53	11.76
	# Turbines	3360	1596	974	651	572
	GW	7.72	3.67	2.24	1.49	1.31
100%	Zone (km)	22.52	18.13	15.96	13.95	13.18
	# Turbines	4262	2078	1266	846	734
	GW	9.80	4.77	2.91	1.94	1.68

Table 29 - Table showing distance from the array at which budget is reached (zone), total number of turbines and GW for different planning success rates.

Inner Radius (km)	Outer Radius (km)	Area (km^2)	Percentage developable	Developable Area (km^2)	Number of turbines	Amplitude in Annulus (nm)	Running Amplitude (nm)	Running Capacity (MW)
49	50	311.02	10	31.10	32	0.0051728	0.0051728	73.6
48	49	304.73	10	30.47	31	0.0055535	0.0075895	144.9
47	48	298.45	10	29.85	30	0.0059640	0.0096524	213.9
46	47	292.17	10	29.22	30	0.0065162	0.0116460	282.9
45	46	285.88	10	28.59	29	0.0070057	0.0135908	349.6
44	45	279.60	10	27.96	28	0.0075339	0.0155393	414
43	44	273.32	10	27.33	28	0.0082525	0.0175947	478.4
42	43	267.04	10	26.70	27	0.0088846	0.0197107	540.5
41	42	260.75	10	26.08	27	0.0097494	0.0219900	602.6
40	41	254.47	10	25.45	26	0.0105080	0.0243717	662.4
39	40	248.19	7	17.37	18	0.0096120	0.0261987	703.8
38	39	241.90	7	16.93	17	0.0102792	0.0281431	742.9
37	38	235.62	7	16.49	17	0.0113225	0.0303353	782
36	37	229.34	7	16.05	17	0.0124844	0.0328038	821.1
35	36	223.05	7	15.61	16	0.0133684	0.0354232	857.9
34	35	216.77	8	17.34	18	0.0156674	0.0387333	899.3
33	34	210.49	8	16.84	17	0.0168427	0.0422368	938.4
32	33	204.20	8	16.34	17	0.0186528	0.0461722	977.5
31	32	197.92	8	15.83	16	0.0200648	0.0503435	1014.3
30	31	191.64	8	15.33	16	0.0222761	0.0550518	1051.1
29	30	185.35	10	18.54	19	0.0269859	0.0613102	1094.8
28	29	179.07	10	17.91	18	0.0292403	0.0679259	1136.2
27	28	172.79	14	24.19	25	0.0384185	0.0780379	1193.7
26	27	166.50	14	23.31	24	0.0420316	0.0886373	1248.9
25	26	160.22	13	20.83	21	0.0439741	0.0989459	1297.2
24	25	153.94	13	20.01	21	0.0492694	0.1105340	1345.5
23	24	147.65	11	16.24	17	0.0497610	0.1212185	1384.6
22	23	141.37	11	15.55	16	0.0542994	0.1328245	1421.4
21	22	135.09	10	13.51	14	0.0572546	0.1446390	1453.6
20	21	128.81	10	12.88	13	0.0623366	0.1575001	1483.5
19	20	122.52	11	13.48	14	0.0732753	0.1737111	1515.7
18	19	116.24	11	12.79	13	0.0802012	0.1913316	1545.6
17	18	109.96	16	17.59	18	0.1075133	0.2194696	1587
16	17	103.67	16	16.59	17	0.1194243	0.2498581	1626.1
15	16	97.39	14	13.63	14	0.1243207	0.2790783	1658.3
14	15	91.11	14	12.75	13	0.1379745	0.3113224	1688.2
13	14	84.82	11	9.33	10	0.1399937	0.3413501	1711.2
12	13	78.54	11	8.64	9	0.1544115	0.3746502	1731.9
11	12	72.26	13	9.39	10	0.1903102	0.4202151	1754.9

Inner Radius (km)	Outer Radius (km)	Area (km^2)	Percentage developable	Developable Area (km^2)	Number of turbines	Amplitude in Annulus (nm)	Running Amplitude (nm)	Running Capacity (MW)
10	11	65.97	13	8.58	9	0.2124681	0.4708752	1775.6

Table 30 – The developable areas in 1km annuli around to EKA with seismic amplitude calculated using the physics-based algorithm for turbines with utilisation factor of 1, hub heights of 80 m and rotor diameter of 93 m. The running amplitude is based on moving from the outside of the consultation zone inward towards EKA. The red figure shows where the 0.336 nm threshold has been breached.

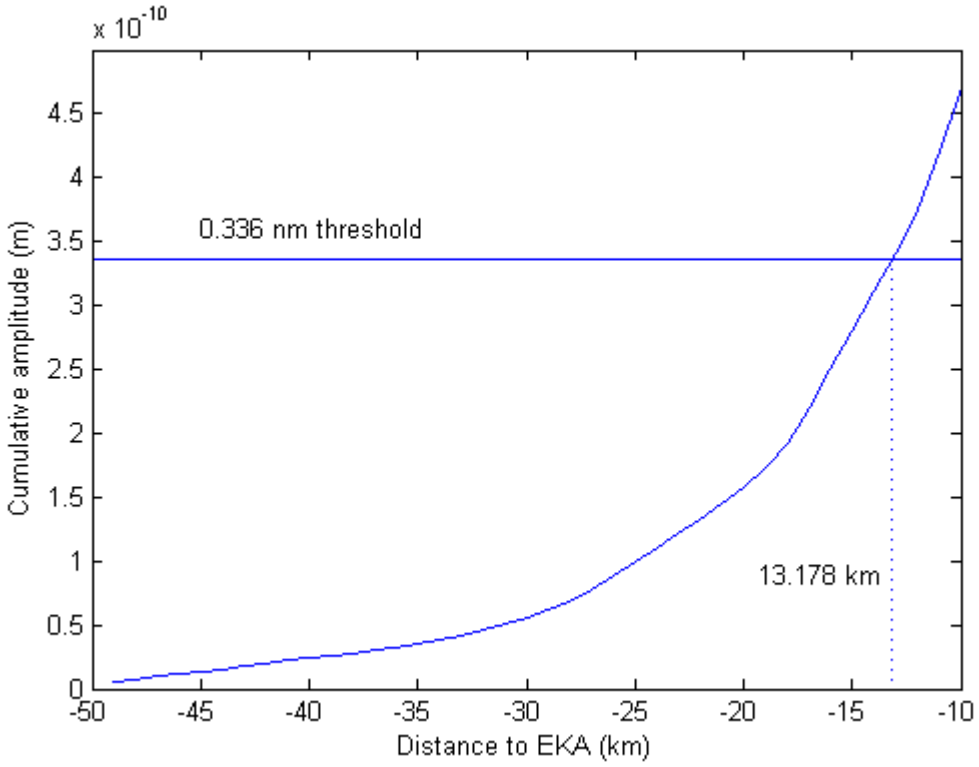

Figure 73 - The cumulative amplitude with distance moving from the edge of the 50 km consultation zone towards EKA. Based on one turbine per kilometre, a utilisation factor of 1, with a hub height of 80m and rotor diameter of 93 m the threshold is met at a distance on 13.178 km.

9.4 Discussion

Due to the nature of the propagation of seismic waves turbines close to the EKA have a much larger impact than those at distance. To determine the distance to which a revised exclusion zone is recommended the potential developable area has been considered and assumptions must be made on both the density of turbines and the likely success rate for planning approval on specific sites. It should also be noted, if turbines were built with equivalent rotor and tower sizes that produced higher than 2.3MW then the overall capacity for the region would be greater. Moving the exclusion zone from 10 km to 15 km would result in the exclusion of 51 potential turbines with the capacity of around 120MW based on the worked example with turbine

spacing of 1 per square kilometre. It is recommended that Table 28 and Table 29 are used as guidance in order to form policy on the exclusion zone.

10 DISCUSSION

10.1 Generation of seismic vibrations by wind turbines

The nature of seismic vibrations produced by wind turbines are complex resulting in an historic difficulty in measuring and characterising them. Elements that contribute to their complex nature include the lack of a linear relationship between on-tower and far-field vibrations; and the variation in the amplitude and character of vibrations with azimuth relative to the wind direction.

At low frequencies (< 8 Hz) the far-field seismic vibrations are produced by periodic changes in the dynamic load of the wind on the tower as the blade passes before it (referred to as *blade-pass*) combined with vibrations related to the excitation of structural resonances in the wind turbine. Far-field amplitudes and wave characteristics modelled using finite element methods correlate well with data from Craig wind farm and show that low frequency far-field seismic vibrations can be explained by the blade-pass force on the tower, torque flutter of the rotor as it rotates through a vertically oriented wind profile and the interaction of these forces with the blade and tower dynamics of the turbine.

Of the wind farms examined, the turbines at Craig and Dun Law produce seismic vibrations dominated by spectral peaks related to blade-pass and their multiples (Figure 16), while turbines at the Clyde wind farm produce seismic vibrations that tend to be dominated by structural resonance (Figure 24). The strong association of far-field seismic vibration with resonant frequency at Clyde may be due to frequency matching between resonances and blade-pass multiples, such that the resonance appears to dominate.

Field observations and modelling both indicate that there is an azimuth effect where the amplitude of seismic vibrations varies with angular position relative to the wind direction. Empirical data from Craig wind farm show that amplitude measured up- and down-wind of the wind farm are 1.4 times higher than those measured in cross-wind positions (90° to the wind) (Figure 32). Modelling found a similar relationship though the up- and down-wind amplitudes were 2.5 times higher (Figure 55). The slight discrepancy between the modelled and measured azimuth factor is likely due to ambient noise being incorporated in the measured rms amplitude, whereas the model includes no ambient noise (it is effectively all *signal*).

The azimuth effect may be further complicated by the nature of the seismic vibrations produced by the wind turbine also varying with angular position. The models predict that wind turbines produce Rayleigh waves that propagate up- and down-wind from the turbine (Figure 53). However, at certain frequencies related to structural resonances, the model predicts that the turbines produce Love waves that propagate away at high angles to the wind direction (cross-wind) (Figure 54). The relationship between resonances and Love waves were also observed in measured data from Craig wind farm (Figure 19).

The purpose of this research work is to produce an algorithm that predicts the seismic amplitude in the far-field produced by wind turbines that protects the detection capabilities of EKA. The algorithm needs to be sufficiently broad that it can be implemented using parameters that are easily accessible. The complex nature of seismic vibration produced by wind turbines has been generalised to a workable algorithm by combining field observation with modelling results. Variance modelling was used to determine that seismic vibrations are relatively insensitive to the surface roughness length of the local terrain, the nacelle mass and the tower stiffness and that these parameters are not required in the algorithm. A conservation of energy approach

showed that a physics-based algorithm could be constructed based on wind speed and the swept area of wind turbine rotors and tests using field survey results support this hypothesis. Assumptions on the tip speed and the vertical profile of wind speed were used to reduce the input requirements of the physics-based algorithm to hub height, rotor diameter and distance from EKA of any given wind turbine. The physics-based algorithm predicts the worst-case far-field amplitude of any given turbine when the wind speed is 12 ms^{-1} at a reference height of 80 m.

10.2 Conservatism in the physics-based algorithm

A conservative approach was used to design the physics-based algorithm to ensure that it protects the detection capabilities of EKA. The algorithm produces a spectrum to represent any wind turbine based on its rotor diameter and hub height. The representative spectrum combines the following worst-cases scenarios:

- The constants in the physics-based algorithm were selected such that they always *over fit all* peaks related to blade-pass and the second bending mode between 7 ms^{-1} and 12 ms^{-1} (Appendix F). This approach is very conservative and results in the power in many peaks being significantly over estimated.
- The power in the peak related to the second bending mode measured at Clyde increases close to linearly with wind speed. However, the physics-based algorithm increases the amplitude with the cube of wind speed significantly over-estimating its power at wind speeds above 9 ms^{-1}, (Appendix F-2).
- The far-field seismic vibrations from turbines examined tend either to be dominated by blade-pass multiples *or* structural resonances. The physics-based algorithm uses both blade-pass multiples *and* structural resonances.
- The constants used for the blade-pass component of the physics-based algorithm were largely dependent on their fit to data from AEG-5/6351 at Craig wind farm. This sensor was down-wind from the wind farm (based on the prevailing wind direction) and will therefore include amplitudes that were biased high by the azimuth effect.

These successive levels of conservatism build in significant safety into the physics-based algorithm such that no additional factor of safety is required.

10.3 Implication of physics-based algorithms

An advantage of the physics-based approach taken to design the algorithm is that with minor modifications it may be possible to extend it to other types of wind turbine systems not covered by this study. The algorithm calculates the rotational speed of any wind turbine in order to position the peaks related to blade-pass multiples. The algorithm predicts that small wind turbine systems with small rotor diameters and high rotational speed have fewer (or no) blade-pass multiples in the 0.5 to 8 Hz passband and will therefore have a negligible effect on EKA. Furthermore, small turbines with low hub heights will be subjected to lower wind speeds and will therefore produce significantly lower amplitude seismic vibrations.

The algorithm is based on three bladed turbines. It would require a minor change to make the algorithm applicable to systems with one, two or more than three blades, so long as the modelled tip speed of those turbines is also modified. The physics-based algorithm could also be modified to represent other turbines (e.g. lattice tower, down-wind turbines) or mitigation system (e.g. tuned mass damper, foundation isolation) by

using field-based measurement to calculate the constants C_{OBM}, C_{BM}, C_{BP} and β appropriate to the turbine design.

10.4 Further work

If this research were to be re-visited at some future point there are several areas that would contribute to the understanding of seismic vibrations from wind turbines and the operation of the physics-based algorithm:

- The structural resonance component of the physics-based algorithm based on the Siemens 2.3 turbine increases close to linearly with wind speed. Following a conservative approach the relationship is taken as an increase with the cube of wind speed. Measurement of other turbines that have significant power in peaks related to resonance could be used to prove that this relationship is closer to linear and thereby reduce the amplitude predicted by the physics-based algorithm.
- The β-term in the algorithm determines the decay in the amplitude of blade-pass multiples with increasing frequency. Currently, there is no physical mechanism for what controls the value of the β-term; a better understanding of how successive blade-pass pulses interact may lead to some further insight into the β-term and seismic waves more generally.
- The wind turbine-foundation-bedrock system has been considered in this research as acting purely elastically. However, there is a non-linear relationship between no-tower and far-field measurements indicating that there may be some near-field mechanism not considered in the models, such as localised visco-elastic behaviour. A better understanding of the dynamic behaviour at the interface between the foundation and the bedrock, and within the near-field may provide information for mitigation systems, foundation design and the reduction of the cost of future field surveys.
- To further develop the methodology of the utilisation factor, work could establish the correlation of wind speed at the array with that at increasing distance from the array. A revised utilisation factor could also consider the mean-time between failure of wind turbines, the developable areas in the consultation zone), the success-rate of proposed developments (e.g., failure due to cumulative visual impact), and the threshold.

11 CONCLUSIONS

- The work presented in this document is valid for a three bladed, up-wind, horizontal axis wind turbine mounted on a tubular steel tower with a gearbox transmission under normal operating conditions and typical foundation conditions.
- Far-field vibrations were analysed produced by Nordex N80 turbines at Craig wind farm, Siemens S2.3 turbines at Clyde wind farm and Vestas V47 wind turbines at Dun Law. Seismic vibrations from wind turbines are produced by a combination of blade pass and structural resonances. The Nordex N80 and Vestas V47 turbines produce seismic vibrations dominated by the blade pass frequency. Conversely, the Siemens S2.3 turbine produced seismic vibrations dominated by structural resonances. Given that the mechanism of seismic vibration generation is different for the Nordex N80 and Siemens S2.3 turbines, it cannot be said that the Nordex N80 is representative of all wind turbines in the Eskdalemuir consultation zone.
- Seismic vibration produced by blade pass in wind turbines propagate with large vertical components of motion and are interpreted as Rayleigh waves. Some peaks related to wind turbine structural

resonances were noted in the far-field that had little or no vertical component and are therefore interpreted to propagate as Love waves.

- An azimuth effect was detected with higher amplitudes measured in directions parallel to the wind direction than in directions orthogonal to the wind direction. At Craig wind farm the amplitude was 1.38 times higher when measured in line with wind direction relative to the cross-wind position. At Dun Law a smaller factor of 1.15 was detected, while no azimuth affect was detected at Clyde due to sensor being placed at the centre of the wind farm.
- No linear relationship was found between on-tower and far-field seismic vibrations. The relationship between on-tower and far-field seismic vibrations appears to be very complex and we recommend against using on-tower measurements to extrapolate to far-field behaviour.
- Finite element modelling demonstrated that the observed seismic vibration can be explained by the periodic drop in dynamic pressure from the wind on the tower as the blade passes combined with torque flutter on the rotor as blades move through the vertical wind profile.
- The finite element models predict an azimuth effect similar to that noted in empirical measurements of Craig and Dun Law wind farm.
- The finite element models showed that the seismic wave generated by a wind turbine have a complex nature with Rayleigh wave propagating up- and down- wind from the turbine and Love waves generated at some discrete frequencies that propagate in the cross-wind direction.
- Variance models showed that the seismic vibrations produced by wind turbines are insensitive to the roughness length of the surrounding terrain. The variance models also showed that the blade-pass related peaks are insensitive to the nacelle mass and tower stiffness.
- A conservation of energy approach was examined based on the hypothesis that seismic amplitude varied linearly with the swept area of the rotor and the cube of wind speed. The conservation of energy approach was tested against data from Clyde, Craig and Dun Law wind farms and the results support the hypothesis.
- A physics-based algorithm was based on the conservation of energy approached. Data from Clyde, Craig and Dun Law wind farms were used to fit a series of constants to curves relating blade-pass multiples, a structural resonance and operational broadband noise. A conservative approach was taken where the constants were fitted such that they always over-estimate seismic power at all wind speed between 7 ms^{-1} and 12 ms^{-1}.
- The physics-based algorithm uses the rotor diameter and hub height to predict the worst-case seismic amplitude of any given turbine. The rotor diameter and hub height are submitted with planning documents as a matter of course.
- The physics-based algorithm includes the frequency-distance weighting function.
- Based on the physics-based algorithm and an utilisation factor of unity the cumulative amplitude of all wind turbines allocated budget and currently subject to objection is **0.1938325 nm**. This is significantly less than the 0.336 nm threshold.
- Applying a default minimum hub height of 40 m to the sites with towers below this level and recalculating the cumulative amplitude for all turbines allocated budget and currently subject to objection results in a cumulative amplitude of **0.1938333 nm**
- A method for understanding the physical implications of an exclusion zone has been developed, and different scenarios investigated.
- Xi Engineering Consultants Ltd recommend that the 2005 model currently used by the MOD to safeguard Eskdalemuir seismic array be replaced by the physics-based algorithm presented in this report.

12 BIBLIOGRAPHY

Baker, V.R. “Channeled Scabland: A Guide to the Geomorphology of the Columbia Basin, Washington.” *Comparative Planetary Geology Field Conference held in the Columbia Basin .* Washington, D.C.: National Aeronautics and Space Administration, 1978. 173-177.

Bowers, Dr David. “Initial study of seismic ground vibration data from mega-watt class wind turbines Interim Report.” 2013.

England, R.J. *Microseismic and infrasound monitoring of low frequency noise and vibration from windfarms.* University of Keele: Unpublished Ph.D Thesis, 2006.

Fiori, I., et al. “A study of the seismic disturbance produced by the wind park near the gravity wave detector GEO-600.” *The 3rd International Meeting on Wind Turbine Noise.* Aalborg, Denmark, 2009.

Guralp Systems. *Creating low noise environments for surface seismometers.* April 2006. http://www.guralp.com/creating-low-noise-environments-for-surface-seismometers/ (accessed August 17, 2012).

—. *The Eskdalemuir Seismic Array.* November 2002. http://www.guralp.com/the-eskdalemuir-seismic-array/ (accessed September 20, 2012).

Legerton, M.L., D.M.J.P. Manley, J.W. Sargent, D.J. Snow, and P. Styles. “Low frequency noise and vibrtion levels at a modern wind farm.” *Proceedings of Internoise 96.* Liverpool, 1996. 459-462.

MacBeth, C. and Burton, P.W. “Propogation of 0.7-2.5Hz Rayleigh Waves in Scotland.” *Geophys. J. Roy. Ast. Soc*, 1986: 84, 101-120.

RenewableUK. “Wind Energy in the UK State of the Industry Report 2013.” 2013.

Saccorotti, G, D Piccinini, L Cauchie, and I Fiori. “Seismic Noise by Wind Farms: A Case Study from the Virgo.” *Bulletin of the Seismological Society of America*, 2011: 568-578.

Schofield, R. *Seismic Measurements at the Stateline Wind Project.* Laser Interferometric Gravitational wave Observatory, 2001.

Snow, D.J., and P. Styles. “Low freqeuncy noise and vibrations measured at a modern wind farm.” ETSU W/13/00392/REP, 1997.

Styles, P, I Stimpson, S Toon, R England, and M Wright. “Microseismic and Infasond Monitoring of Low Frequency Noise and Vibration from Windfarms.” 2005.

Styles, P., R. England, I.G. Stimpson, S. Toon, B. Bowers, and H. Malcolm. “A detailed study of the propagration and modelling of the effects of low frequency seismic vibration and infrasound from wind turbines.” *Proceedings of the 1st International Meeting on Wnd Turbine Noise.* Berlin, Germany, 2005.

Styles, P., R.F. Westward, S.M. Toon, M.-P. Buckingham, B. Marmo, and B. Carruthers. “Monitoring and mitigation of low frequency noise from wind turbines to protect Cmprehensive Test Ban Seismic Monitoring station.” *Forth International Meeting on Wind Turbine Noise, 12-14 April 2011.* Rome, Italy, 2011.